Elucidating the role of unique structural features of the α_{1D}-adrenergic receptor: A tale of two tails

Eric M. Jennings Janezic

A dissertation

submitted in partial fulfillment of the

requirements for the degree of

Doctor of Philosophy

University of Washington

2020

Reading Committee:

Chris Hague, Chair

Edith Wang

Ning Zheng

Program Authorized to Offer Degree:

Pharmacology

©Copyright 2020
Eric M. Jennings Janezic

University of Washington

Abstract

Elucidating the role of unique structural features of the α_{1D}-adrenergic receptor: A tale of two tails

Eric M. Jennings Janezic

Chair of the Supervisory Committee:

Christopher Hague

Department of Pharmacology

G protein-coupled receptors (GPCRs) are seven transmembrane domain proteins accounting for ~4% of the human genome, and the predicted target of ~30% FDA approved therapeutics. Often, drugs compete with endogenous ligands for orthosteric binding sites, giving rise to off-target interactions and deleterious side-effects – thus there is a need to identify novel potential ligand binding sites with increased specificity. Recent advances in the field suggest that targeting protein:protein interaction networks, or post-translational modifications that regulate GPCR expression, trafficking, and/or function, may be the key to improving ligand selectivity and decreasing unwanted toxicities. To this end, I devoted my Ph.D. studies to studying two unique structural features that regulate the function of the α_{1D}-adrenergic receptor (α_{1D}-AR) – a GPCR vital for myriad peripheral and central nervous processes which has been implicated in the development and maintenance of hypertension, benign prostate hypertrophy, schizophrenia, and post-traumatic stress disorder – a distal C-terminal Type I PDZ (PSD95/Dlg/ZO-1) ligand and an unusual N-terminal domain.

Using yeast two-hybrid and tandem affinity MS/MS assays, the Hague lab previously identified that the α_{1D}-AR C-terminal PDZ ligand is responsible for the formation of obligate, cell-type specific, macromolecular protein complexes containing syntrophin, utrophin, α-dystrobrevin, α-catulin, liprin, phospholipase-Cβ2, and scribble. These complexes enhance receptor cell surface expression and function both *in vitro* and *in vivo*. Furthermore, a screen of 23 GPCRs containing Type I PDZ ligands revealed that these interacting partners are unique to α_{1D}-AR. Thus, these protein:protein interaction networks represent an opportunity to develop novel medications with increased specificity for α_{1D}-AR than currently available drugs. However, before this can come to fruition, a more thorough understanding of how these complexes are organized is necessary.

Towards mapping α_{1D}-AR complex architecture, biolayer interferometry revealed that scribble displays >8x binding affinity compared to other known α_{1D}-AR interactors. Complementary *in situ* and *in vitro* interaction assays revealed that scribble PDZ domains 1 and 4 are high affinity α_{1D}-AR PDZ ligand interaction sites. The development of a novel SNAP-GST pull-down assay found that scribble is able to bind multiple α_{1D}-AR C-terminal PDZ ligands via a cooperative mechanism. Structure-function analyses identified $R1110^{PDZ4}$ as a unique, critical residue dictating the α_{1D}-AR:PDZ4 interaction. A crystal structure of a non-binding mutant, PDZ4 R1110G, predicts a spatial shift of the carboxylate-binding loop prevents docking of the C-terminal PDZ ligand. Thus, these findings identify scribble PDZ1 and 4 as high affinity α_{1D}-AR interaction sites, and potential targets to treat diseases associated with aberrant α_{1D}-AR function.

Additionally, α_{1D}-ARs contain two putative *N*-glycosylation sites within the large N-

terminal domain at N65 and N82. However, determining the glycosylation state of this receptor has proven challenging. Towards understanding the role of these putative glycosylation sites, site-directed mutagenesis and lectin affinity purification identified N65 and N82 as *bona fide* acceptors for *N*-glycans. Surprisingly, it was revealed that simultaneously mutating N65 and N82 causes early termination of α_{1D}-AR between transmembrane domain 2 and 3. Label-free dynamic mass redistribution and cell surface trafficking assays revealed that single and double glycosylation-deficient mutants display limited function with impaired plasma membrane expression. Confocal microscopy imaging analysis and SNAP-tag sucrose density fractionation assays revealed the dual glycosylation mutant α_{1D}-AR is widely distributed throughout the cytosol and nucleus. Based on these novel findings, I propose α_{1D}-AR transmembrane domain 2 acts as an ER localization signal during active protein biogenesis, and that α_{1D}-AR N-terminal glycosylation is required for complete translation of nascent, functional receptor. Taken together, the results from these studies identify two promising mechanisms for the development of targeted therapeutics to treat diseases and disorders associated with α_{1D}-AR dysfunction.

TABLE OF CONTENTS

List of Figures viii

List of Tables x

Chapter 1 – Background and Introduction 1

1.1 G protein-coupled receptors 1

1.2 Adrenergic receptors 3

1.3 The α_{1D}-AR 4

1.4 PDZ domains 5

1.5 α_{1D}-AR C-terminal PDZ ligand is required for macromolecular complex formation 7

1.6 α_{1D}-AR N-terminal prevents plasma membrane localization 8

Figures 11

Tables 19

Chapter 2 – Scribble cooperatively binds multiple α_{1D}-AR C-terminal PDZ ligands 20

2.1 Introduction 20

2.2 Materials and Methods 22

2.3 Results and Discussion 26

Figures 35

Tables 41

Chapter 3 – *N*-glycosylation of α_{1D}-AR N-terminal domain is required for correct trafficking, function, and biogenesis 43

3.1 Introduction 43

3.2 Materials and Methods 45

3.3 Results and Discussion 50

Figures 59

Tables.....67

Chapter 4 – Final Conclusions.....69

4.1 Scribble PDZ domains 1 and 4 anchor multiple α_{1D}-AR homodimers.....69

4.2 Transmembrane domain 2 of α_{1D}-AR triggers ribosomal translocation.....70

4.3 α_{1D}-AR is a stress receptor.....70

Figures.....72

References.....74

Curriculum Vitae.....88

LIST OF FIGURES

Figure Number Page Number

1.1 Percent of drug targets by receptor class 11

1.2 Dendrogram of GPCRs encoded in the human genome 12

1.3 Schematic of G-protein activation 13

1.4 Signaling cascades of G-protein subtypes 14

1.5 α_{1D}-AR function disappears within 24 hours in primary culture.....15

1.6 Crystal structure of PDZ domain 3 of PSD-95 in complex with a synthetic peptide 16

1.7 PAGE NIR gel of SNAP-epitope tagged α_1-AR subtypes 17

1.8 Predicted phosphorylation sites of α_{1D}-AR N-terminal.....18

2.1 *In situ* affinity determination of α_{1D}-AR C-terminal PDZ ligand:PDZ protein interactions...35

2.2 *In situ* and *in vitro* analysis of α_{1D}-AR C-terminal PDZ ligand:SCRIB single PDZ domain interactions.....36

2.3 *In situ* and *in vitro* analysis of α_{1D}-AR C-terminal PDZ ligand:SCRIB truncation mutant interactions.....37

2.4 SNAP-α_{1D}-AR C-terminal PDZ ligand:GST-SCRIB pulldown assays indicate a co-operative binding model 38

2.5 Structure-function analysis of the α_{1D}-CT:SCRIB PDZ4 interaction.....39

2.6 Biolayer interferometry analysis of α_{1D}-AR C-terminal PDZ ligand:SCRIB H793A/H1170A interactions.....40

3.1 Site-directed mutagenesis and lectin affinity purification analyses reveal α_{1D}-AR is dually glycosylated at N65 and N82.....59

3.2 SNAP MS/MS analysis identifies distal peptides in WT, but not NQQ SNAP-α_{1D} lysates ...61

3.3 α_{1D}-AR function and plasma membrane insertion is glycosylation dependent.....62

3.4 Sucrose density centrifugation of SNAP-epitope tagged plasma membrane and endoplasmic reticulum markers 63

3.5 Sucrose density centrifugation of WT and glycosylation deficient SNAP-α_{1D} constructs 64

3.6 Confocal imaging reveals NQQ SNAP-α_{1D} is localized to cytosol and nucleus in HEK293 cells 65

4.1 Hypothetical model of the α_{1D}-AR:SCRIB:DAPC macromolecular complex.....72

4.2 Model of proposed role for N-terminal glycosylation on α_{1D}-AR biosynthesis.....73

LIST OF TABLES

Table Number Page Number

1.1 α_{1D}-AR PDZ interactors identified by TAP MS/MS in multiple cell types 19

2.1 Binding affinities as determined by BLI.....41

2.2 Data collection and refinement statistics for Scribble PDZ4 R1110G mutant (molecular replacement).....42

3.1 Previously reported α_{1D}-AR PDZ interactors identified by SNAP MS/MS.....67

3.2 Maximal phenylephrine stimulated DMR response in α_{1D}-AR glycosylation mutants 68

ACKNOWLEDGMENTS

I would like to thank Dr. Chris Hague for his superb mentorship and guidance throughout my graduate school tenure. I would also like to thank all the members of the Hague lab, past and present, with special thanks to Dorathy-Ann Harris and Kyung-Soon Lee. I want to thank my supervisory committee, Drs. Chris Hague, Ning Zheng, Edith Wang, and Alex Merz. I also want to thank Dr. Peter Hsu for all his guidance and friendship, which helped me persevere and see the finish line. I would also like to thank my parents, Anna and Mark Janezic, grandparents, John and Mary Janezic, and brother, Brian Janezic for all their continued support and encouragement. Lastly, I want to thank my wonderful wife, Miki Jennings Janezic, for her support, staying by my side throughout the many moves, and growing with me.

Chapter 1 - Background and Introduction

1.1 G protein-coupled receptors

Cells have evolved elaborate mechanisms of sending and receiving signals – both electrical and chemical – to sense changes in their environment. These signals are recognized by specialized proteins, known as receptors, which fall into four major classes: nuclear, tyrosine kinase, ion channel, and G protein-coupled receptors (GPCRs) (Blumenthal, 2017). The ligands and mechanism by which each receptor class transduces external stimuli into internal changes within the cell are varied. For example, nuclear receptors typically interact with lipophilic hormones to modulate transcription directly (McEwan, 2009). Receptor tyrosine kinases are transmembrane proteins that canonically contain intracellular kinase domains and are activated by homodimerization upon ligand binding. This subclass of receptors is heavily utilized by cell survival, migration, and proliferation pathways (Ferguson, 2008). Ion channels regulate the flow of ions – namely Na^+, K^+, Cl^-, and Ca^{2+} – in and/or out of the cell upon activation by different types of signals including chemical ligands (Jegla *et al.*, 2009), mechanical stimuli (Coste *et al.*, 2010), or voltage changes (Catterall, 2017).

GPCRs are the largest class of receptors with >800 unique genes in the human genome (Lander *et al.*, 2001), and are targets for ~30% of approved therapeutics (Figure 1.1) (Overington *et al.*, 2006; Sriram and Insel, 2018). GPCRs respond to myriad endogenous ligands including neurotransmitters, peptides, hormones, and lipids. These cell-surface receptors can be phylogenetically classified into sub-classes using the GRAFS system: Glutamate, Rhodopsin-like, Adhesion, Frizzled, and Secretin (Figure 1.2; Fredriksson *et al.*, 2003; Blumenthal, 2017). A majority of GPCRs are within the Rhodopsin-like class (Bjarnadóttir *et al.*, 2006). Though there is great diversity in the primary structures, receptors within the Rhodopsin-like class share

a conserved tertiary structure containing an extracellular N-terminal domain (NTD), seven transmembrane alpha helices (TM1-7), three extracellular and three intracellular loops (ECL1-3 and ICL1-3, respectively), and a cytosolic C-terminal tail (CT) containing an eighth alpha helix (Langerström and Schiöth, 2008).

Some of the first crystal structures within this class of GPCRs have provided invaluable insights into the conserved features that confer stability and function (Palczewski *et al.*, 2000; Cherezov *et al.*, 2007; Rasmussen *et al.*, 2011a). Namely, interactions of the TM helicies with the ECLs, especially a disulfide bridge between cysteine residues in ECL2 and TM3, are thought to stablize the receptor and prevent large-scale changes in stability upon ligand activation (Palczewski *et al.*, 2000; Rasmussen *et al.*, 2011a; Wheatley *et al.*, 2011). Typically, the orthosteric binding site consists of residues within TM3, TM5, TM6, and TM7 (Ring *et al.*, 2013); however in some cases (i.e. $5HT_{2B}$-R:LSD interaction) ECL2 also contributes to ligand binding (Wacker *et al.*, 2017). Upon agonist binding, the cytosolic tip of TM6 undergoes large multi-angstrom shifts (Ramussen *et al.*, 2011b).

As the name suggests, GPCRs transduce signals by coupling to heterotrimeric G proteins, consisting of α, β, and γ subunits (Gilman, 1987). The Gα subunit sits within a cytosolic facing hydrophobic pocket created by TM5 and TM6 of the GPCR, with some additional interactions with a conserved DRY motif in ICL3 (Ramussen *et al.*, 2011b). The Gα subunit is bound to GDP in the inactive state, however upon receptor activation, structural changes within the GPCR trigger a conformational change in the Gα subunit leading to decreased GDP affinity, such that it is readily displaced by GTP (Rasmussen *et al.*, 2011b; Bang and Choi, 2015). The GTP:Gα complex disassociates from the receptor and the Gβ and Gγ subunits to activate various effectors (Figure 1.3) .

The effect of GPCR activation is dependent on the Gα subtype it couples: $G\alpha_s$, $G\alpha_{i/o}$, $G\alpha_q$, or $G\alpha_{12/13}$ (Blumenthal, 2017). $G\alpha_s$ subtypes lead to increases in cAMP by stimulating adenylate cyclases (Figure 1.4A). $G\alpha_{i/o}$ activity opposes that of $G\alpha_s$ by inhibiting adenylate cyclases and reducing cAMP levels in the cells (Figure 1.4B). $G\alpha_q$ and $G\alpha_{12/13}$ are atypical G-proteins that do not interact with adenylate cyclases (Blumenthal, 2017). Instead, $G\alpha_q$ increases cytosolic Ca^{2+} by stimulating the activity of phospholipase C, which hydrolyzes PIP_2 to form DAG and IP_3. IP_3 then triggers the release of Ca^{2+} from the endoplasmic/sacroplasmic reticulum via interaction with IP_3 receptors (Figure 1.4C; Berridge, 1993). Though the signal transduction pathways of the previous three Gα subtypes are well studied, much less is known about the $G\alpha_{12/13}$ subtype, though it plays a role in cytoskeletal rearrangement (Suzuki *et al.*, 2009).

1.2 Adrenergic Receptors

Adrenergic receptors (ARs) are a family of receptors within the Rhodopsin-like class of GPCRs that respond to the endogenous ligands norepinephrine/epinephrine. This family is further divided into three subfamilies based on their structural and functional similarities (Hieble, *et al.*, 1995). The α_1-ARs, which couple to $G\alpha_q$, contain α_{1A}, α_{1B},and α_{1D}. The α_2-ARs, which couple to $G\alpha_i$, consist of the α_{2A}, α_{2B},and α_{2C} receptors. The β subfamily, which couple to $G\alpha_s$, contain the β_1, β_2, and β_3-ARs.

All three subfamilies of ARs are key regulators of central and sympathetic nervous system function, and are the targets for some of the most prescribed drugs in the US (Piascik and Perez, 2001; Fuentes *et al.*, 2018). For example, albuterol – a commonly prescribed drug for the treatment of asthma – causes bronchodilation by activating the β_2-ARs on lung bronchioles (Snider and Laguarda, 1972). β-ARs are also expressed in cardiac and smooth muscle cells

(Insel, 1996), microglia (Sugama *et al.*, 2019), and adipose tissue (Collins *et al.*, 1994). In addition to asthma, drugs targeting this family of receptors are prescribed to treat heart failure, hypertension, arrythmia, and coronary heart disease (Insel, 1996). α_2-ARs are typically found in the presynaptic terminal of noradrenergic neurons and act as auto-receptors to inhibit the release of norepinephrine in these cells (Reid, 1985). Drugs targeting these receptors are used to treat hypertension, attention-deficit/hyperactivity disorder, benzodiazepine and alcohol withdrawl symptoms, and as adjuncts with anesthetics (Giovannitti *et al.*, 2015). α_1-ARs are present in a variety of cells including vascular smooth muscle cells, neurons, and smooth muscle cells of the prostate (Docherty, 2010). Medications that target the α_1-ARs – including the α_1-AR antagonists, prazosin – are prescribed for the treatment of benign prostate hypertrophy (Fusco *et al.*, 2016), hypertension (Perez and Doze, 2011), cardiac hypertrophy (Cotecchia *et al.*, 2015), bladder obstruction (Hampel *et al.*, 2002), and post-tramuatic stress disorder (Olson *et al.*, 2011). Unfortunately, the use of these medications often times results in deleterious side-effects due to off-target interactions (ALLHAT, 2002). Thus, there is a need to develop medications with greater receptor subtype specificity.

1.3 The α_{1D}-AR

The α_{1D}-AR is expressed throughout the central and peripherial nervous systems (Piascik *et al.*, 1995; Tanoue *et al.*, 2002; Nalepa *et al.*, 2013; da Silva *et al.*, 2014), thus abberant expression and dysfunction of this receptor has been implicated in hypertension (Sever, 1999), benign prostate hypertrophy (Walden *et al.*, 1999; Kojima *et al.*, 2011), bladder obstruction (Hampel *et al.*, 2002), post-tramuatic stress disorder (Hendrickson and Raskind, 2016; Raskind *et al.*, 2018), and schizophrenia (Liu *et al.*, 2015). Unfortunately – though clinically relevant –

the α_{1D}-AR remains poorly understood due to technical challenges, namely (A) a cell line endogenously expressing functional α_{1D}-AR has yet to be identified; (B) a lack of α_1-AR subtype selective antibodies (Jensen *et al.*, 2009); (C) functional α_{1D}-ARs are undetectable within 24-48 after culturing of primary aortic vasuclar smooth muscle cells (Figure 1.5; Fan *et al.*, 2009); and (D) ectopic expression of α_{1D}-AR results in intracellular sequesteration (Hague *et al.*, 2004; Petrovska *et al.*, 2005; Garcia-Cazarin *et al.*, 2008).

Interestingly, the α_{1D}-AR contains two distinct structural features that make it unique amongst the other α_1-AR subtypes: (A) the presence of a distal C-terminal Type I PSD95/Dlg/ZO1 (PDZ) ligand (-RETDI-COOH), and (B) an NTD that is twice as long as the average Rhodopsin-like GPCR at 95 amino acids (Wallin and von Heijne, 1995). With the over-arching goal of identifying potential therapuetic targets, the Hague lab is interested in how these structural features affect α_{1D}-AR function and trafficking.

1.4 PDZ domains

Protein trafficking and function can be controlled by modular, conserved protein:protein interaction domains (Langeberg and Scott, 2015). PDZ domains, found in >350 proteins throughout the human genome, are one such interface typically found in proteins involved in scaffolding transmembrane proteins (Letunic *et al.*, 2012; Manjunath *et al.*, 2018). There are three major subtypes of PDZ domains: Type I, Type II, and Type III – classisified by the sequence of the ligands they recognize. Type I PDZ domains canonically interact with C-terminal PDZ ligands containing the sequence X-[S/T]-X-[Φ]-COOH, Type II domains recognize X-[Φ]-X-[Φ]-COOH, and Type III PDZ domains interact with ligands of sequence X-[D/E]-X-[Φ]-COOH, where Φ is any hydrophobic amino acid and X is any amino acid

(Marchese *et al.*, 2008). Typically, PDZ ligands are numbered with the C-terminal amino acid as 0, and the upstream residues -1, -2, -3, etc (Mamonova *et al.*, 2017). PDZ ligands are characteristically C-terminal ligands, though internal, non-C-terminal ligands have been identified (Hillier *et al.*, 1999).

Though the three PDZ domain subtypes recognize distinct peptidic ligands, they share structural homology. PDZ domains are small, globular domains of ~90 residues in length, and contain six β-strands and two α-helicies (Harris and Lim, 2001). Crystal structures (Doyle *et al.*, 1996) and large peptide library screens (Songyang *et al.*, 1997) have identified a conserved ligand binding pocket created by βB, αB, and a flexible loop termed the carboxylate-binding loop with a conserved R/K-X-X-X-G-L-G-F sequence motif (Figure 1.6; Doyle *et al.*, 1996). Upon interacting with the PDZ domain, the PDZ ligand forms a β-strand, with extensive hydrogen bonding between the peptide backbone and the binding pocket (Doyle *et al.*, 1996; Lim *et al.*, 2017).

Though they share conserved structures, the three subtypes diverge in a key residue found within αB. This key amino acid interacts with residue -2 of cognate ligands. In Type I PDZ domains, this amino acid is a histidine residue (Doyle *et al.*, 1996); Type II domains substitute this histidine for a methionine or leucine residue (Daniels *et al.*, 1998); and Type III domains contain a tyrosine residue (Stricker *et al.*, 1997). Ligand specificity of individual PDZ domains is largely dictated by a network of hydrogen bonds between the carboxylate-binding loop and the distal C-terminal residue of the ligand (Stricker *et al.*, 1997; Harris and Lim, 2001). However, recent evidence suggests that hydrophobic interactions outside the orthosteric binding pocket may also contribute to differences in ligand binding affinities (Lim *et al.*, 2017).

1.5 α_{1D}-AR C-terminal PDZ ligand is required for macromolecular complex formation

Due to their high level of specificity for their ligands, PDZ domains have emerged as promising targets for the development of novel therapuetics (Ritter and Hall, 2009). For example, disruption of the nNOS:NMDAR:PSD95:NOS1AP protein complex with small molecules has proven to be efficacious in preclinical models for the treatment of neuropathic pain (Carey *et al*., 2017; Lee *et al.*, 2018a; 2018b), depression (Doucet *et al.*, 2013), neuronal excitotoxicity (Li *et al.*, 2013), and neuroprotection following cerebral ischemia (Zhou *et al.*, 2010). Thus, disruption of α_{1D}-AR:PDZ protein interactions has the potential to overcome the deleterious side-effects that caused to the early termination of the doxazosin arm of the ALLHAT study (ALLHAT, 2002). However, a better understanding of how the α_{1D}-AR C-terminal PDZ ligand interacts with PDZ proteins is needed before theraputeics can be developed.

The importance of the α_{1D}-AR C-terminal PDZ ligand was first reported after a yeast two-hybrid screen identified the PDZ domain containing protein, α-syntrophin, as a selective interacting partner (Chen *et al.*, 2006). Preventing this interaction decreases α_{1D}-AR binding site density and IP_3 accumulation in cultured cells (Chen *et al.*, 2006). Further studies revealed that co-expressing α_{1D}-AR and α-syntrophin in cultured cells increases plasma membrane localization and receptor pharmacological properties (Lyssand *et al.*, 2008). This study also found that the α_{1D}-AR:syntrophin interaction is necessary for blood pressure regulation *in vivo* using a pan-syntrophin knockout mouse line (Lyssand *et al.*, 2008). Subsequent Tandem Affinity Purification MS/MS (TAP MS/MS) experiments found that syntrophins enhance α_{1D}-AR function by recruiting the Dystrophin Associated Protein Complex (DAPC) and other signaling effectors, such as α-catulin and phospholipase-Cβ (Lyssand *et al.*, 2010; 2011). Advances in MS/MS technology allowed for the discovery of a number of features of the α_{1D}-AR:syntrophin

complex: (A) Scribble (SCRIB) – a protein containing multiple PDZ domains – is a member of the α_{1D}-AR:syntrophin:DAPC complex in multiple human cell lines; (B) α_{1D}-ARs are expressed as homodimers with one protomer interacting with SCRIB, and the other interacting with syntrophin; (C) the composition of the α_{1D}-AR complex is cell-type specific (Camp *et al.*, 2015; Table 1.1); and (D) this large, macromolecular complex is unique to α_{1D}-AR when compared to 23 of the 30 GPCRs containing Type I PDZ ligands (Camp *et al.*, 2016).

As shown in Table 1.1, α_{1D}-AR interacts with SCRIB and syntrophins in all human cell lines examined, however, in SW480 cells, Discs Large 1 (DLG1), LIN7A, and calcium/calmodulin-dependent serine protein kinase (CASK) are also recruited to this complex (Camp *et al.*, 2015). Interestingly, all of these proteins, with the exception of syntrophins, are involved in the establishment of cell polarity in polarized cells (Stephens *et al.*, 2018), suggesting that these complexes are regulating the trafficking of α_{1D}-AR to the correct membrane. Furthermore, a unique structural characteristic of SCRIB is the presence of four Type I PDZ domains within its C-terminal. Thus, SCRIB may be anchoring multiple α_{1D}-AR at lumenal membranes to form 'microdomains' of α_{1D}-AR signaling.

1.6 α_{1D}-AR NTD prevents plasma membrane localization

Another unique structural feature of the α_{1D}-AR is the extralong 95 amino acid extracellular NTD, which is >2x the size of the average NTD of Rhodopsin-like GPCRs (Wallin and Heijne, 1995). Our lab and others have shown that the α_{1D} NTD is an ER retention signal in cultured human cell lines, and full and partial truncation of this domain enhances α_{1D}-AR pharmacological properties and plasma membrane insertion (Pupo *et al.*, 2003; Hague *et al.*, 2004; Kountz *et al.*, 2016). However, why and how this domain retains nascent polypeptide in

the ER membrane remains unknown.

Though still a mystery, few reports provide insight into the mechanism by which this occurs. For example, the addition of an N-terminal signal peptide increases the binding site density and function of the receptor, presumably due to enhanced exocytosis of α_{1D}-AR from the ER or increased protein expression (Petrovska *et al.*, 2005). Other studies found that truncation of amino acids 1-79 increases binding site density, IP_3 accumulation, and surface expression with no change in protein levels (Pupo *et al.*, 2003; Hague *et al.*, 2004). Surprisingly, chimeric receptors containing the α_{1D} NTD are also sequestered to the ER and display reduced functionality (Hague *et al.*, 2004). Thus, ER sequesteration is a transferable and intrisic property of the α_{1D} NTD.

Recently by harnessing the power of cutting-edge SNAP-epitope tag technology, which allows for increased sensitivity and direct visualization of tagged proteins in polyacrylamide gels, the Hague lab found that α_{1D}-AR undergoes an endogenous N-terminal domain cleavage event between Leu^{90}/Val^{91} (Kountz *et al.*, 2016). Truncated receptors display enhanced pharmacological properties and decreased ER retention. Though, the mechanisms that regulate this event were not determined, it is interesting to note that chimeric receptors do not undergo this cleavage, suggesting that the cleavage is controlled by sequences downstream of the N-terminal.

Another interesting observation from this study (Kountz *et al.*, 2016) was that the N-terminus consistently migrates as three distinct bands on SDS PAGE electrophoresis (Figure 1.7, *red square*). Discovering if this band pattern represents multiple cleavage products or post-translational modification states is essential to understand the mechanisms that regulate this event. Of note, the α_{1D}-NTD contains nine predicted phosphorylation sites (Figure 1.8) and two

putative *N*-glycosylation sites at N65 and N82 (Perez *et al*, 1991). Additionally, multiple bands are observed even in α_{1D}-AR mutants with truncations upstream of the cleavage site (Kountz *et al*, 2016). Thus, these data support the hypothesis that this band pattern is due to differential post-translational modification states of the α_{1D} NTD.

Abbreviations: GPCR, G protein-coupled receptor; NTD, N-terminal domain; TM, transmembrane; ECL, extracellular loop; ICL, intracellular loop; CT, C-terminal tail; AR, adrenergic receptor; PDZ, PSD95/Dlg/ZO1; TAP MS/MS, Tandem Affinity Purification Mass spectrometry/Mass spectrometry; DAPC, Dystrophin Associated Protein Complex; SCRIB, scribble; DLG1, Discs Large 1; CASK, calcium/calmodulin-dependent serine protein kinase; ER, endoplasmic reticulum

Figures for Chapter 1

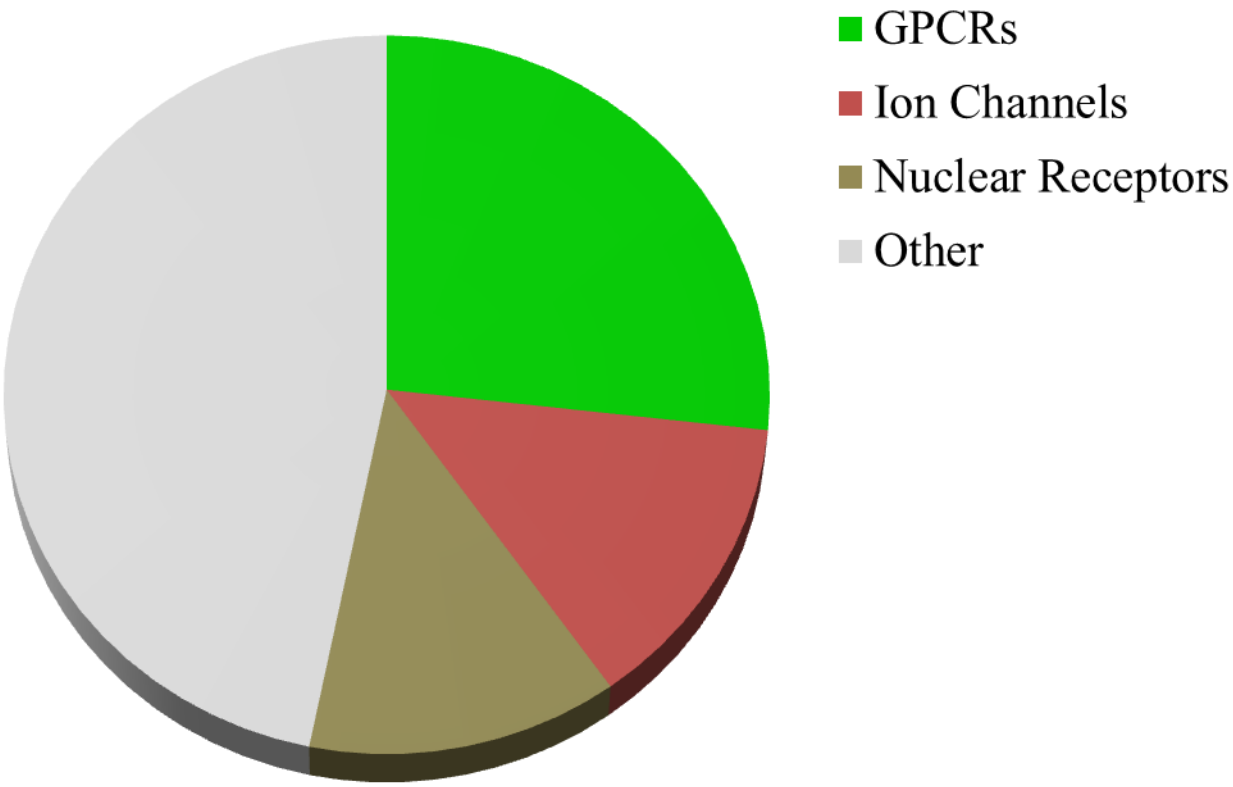

Figure 1.1. Percent of drug targets by receptor class. Modified from Overington et al., 2006.

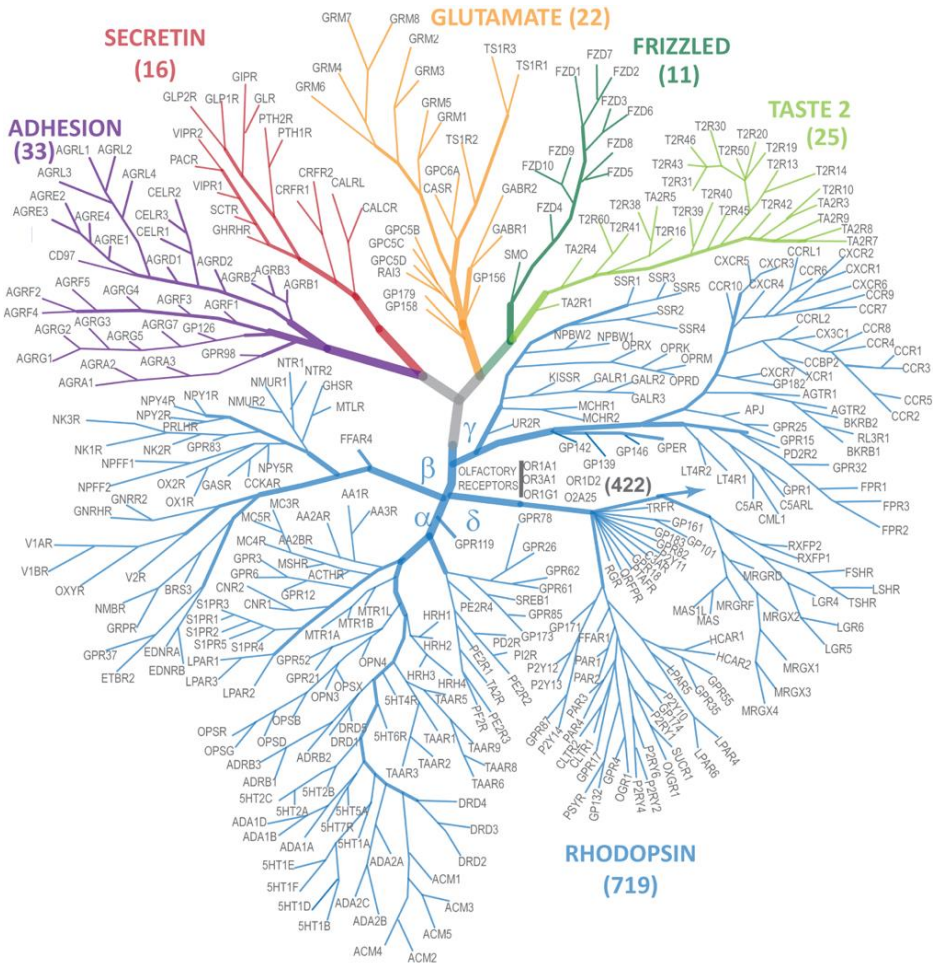

Figure 1.2. Dendrogram of GPCRs encoded in the human genome. Branches are color coded to denote class of GPCR accordin to GRAFS system. Taste 2 is often considered part of the Rhodopsin-like class. Figure is reproduced from Blumenthal, 2017.

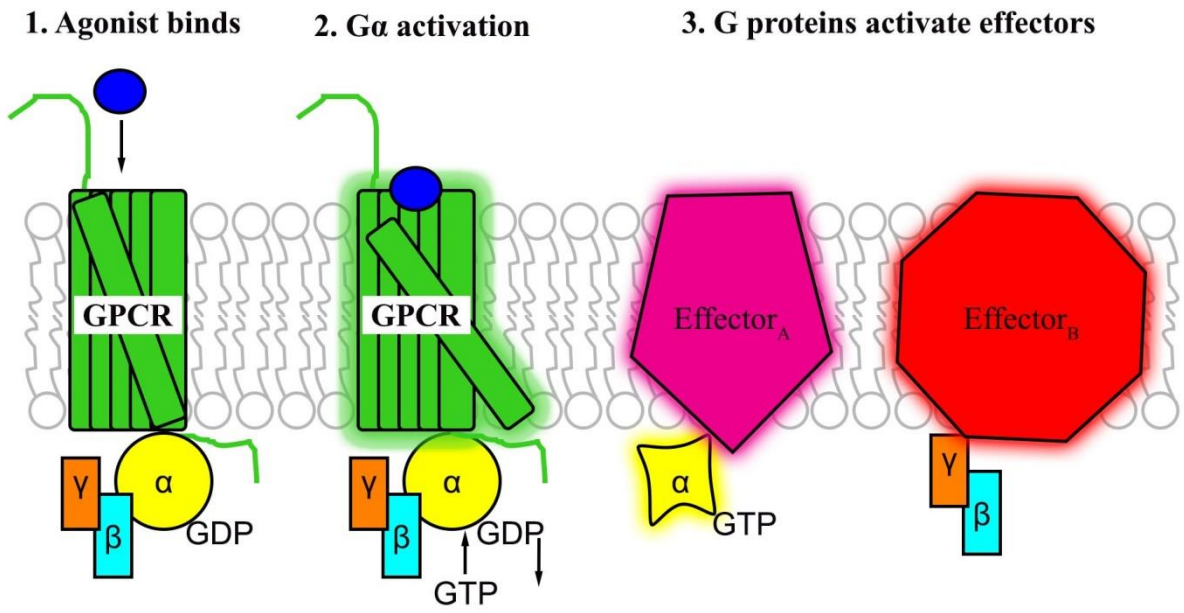

Figure 1.3. Schematic of G-protein activation. The GPCR:heterotrimeric G protein complex is in the inactive state with GDP bound to the Gα subunit (yellow). The GPCR is activated upon agonist binding which causes a conformational change in the GPCR and Gα subunit. The Gα subunit structural changes promote the GDP → GTP exchange, activating the Gα protein. The GTP bound Gα dissociates from the GPCR and Gβ and Gγ subunits and the G proteins interact with downstream effector proteins.

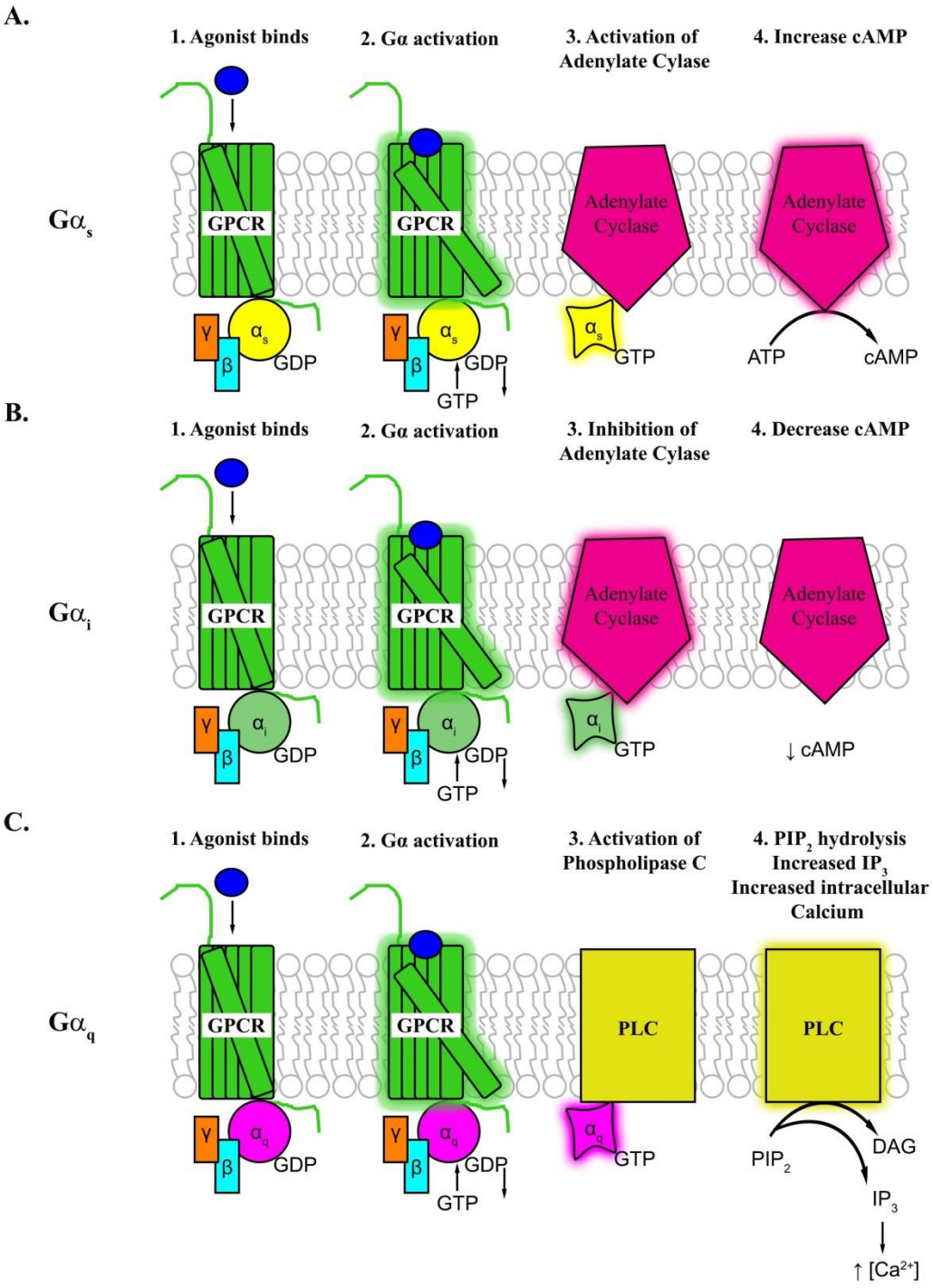

Figure 1.4. Signaling cascades of G-protein subtypes. A. Upon G-protein activation, $G\alpha_s$ activates adenylate cyclase to increase cAMP levels in the cell. B. $G\alpha_i$ subunits inhibit adenylate cyclases to prevent the production of more cAMP. C. $G\alpha_q$ subunits activate phosopholipase C to hydrolyze PIP_2 to DAG and IP_3. IP_3 triggers the release of Ca^{2+} stores within the endoplasmic/sarcoplasmic reticulum.

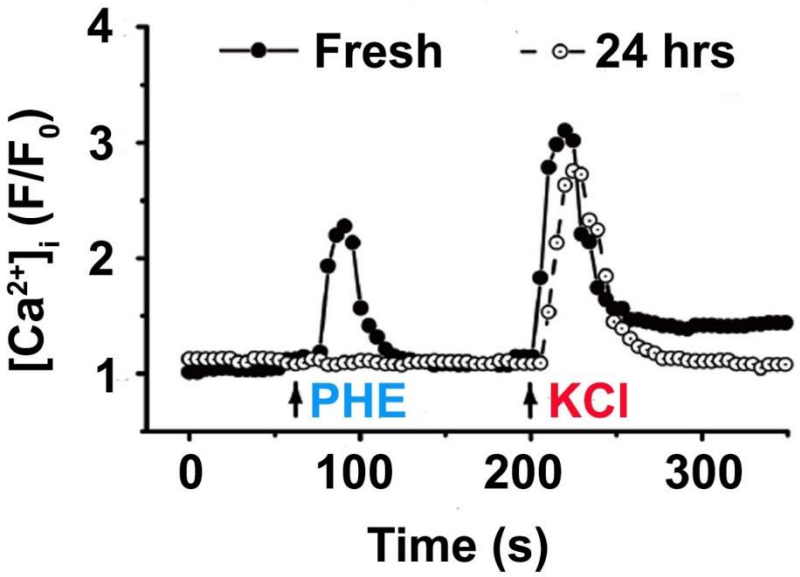

Figure 1.5. α_{1D}-AR function disappears within 24 hours in primary culture. Calcium imaging data from primary vascular smooth muscle cells from mouse aortia. Freshly dissociated cells (black trace), but not the same cells after 24 hrs in culture (white trace), show increased intracellular calicum levels in response to the α_1-AR agonist, phenylephrine (PHE). KCl causes intracellular calcium increases in a receptor independent mechanism and is used to show the cells are still viable. Modified from Fan *et al.*, 2009.

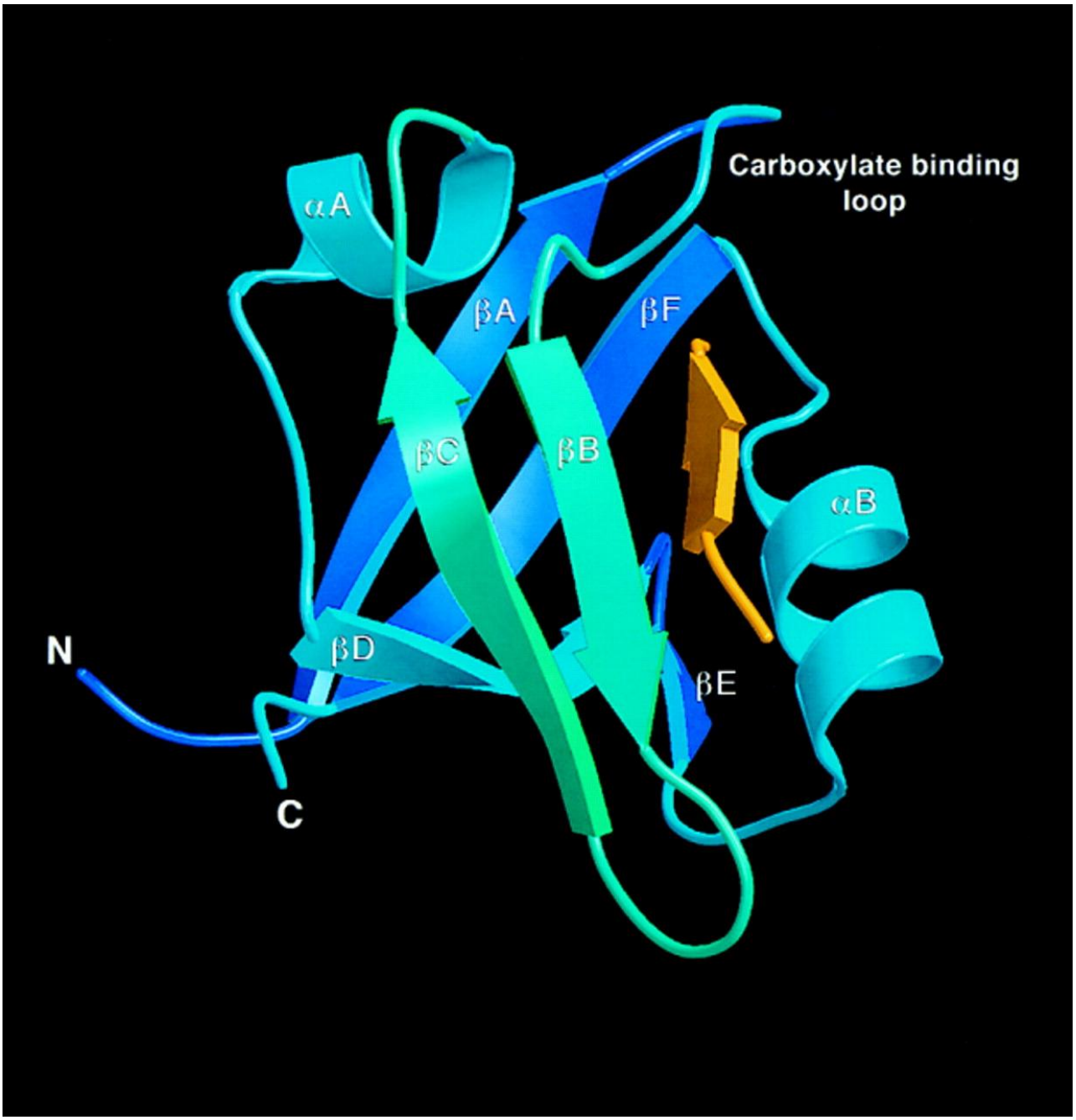

Figure 1.6. Crystal structure of PDZ domain 3 of PSD-95 in complex with a synthetic peptide. PDZ domain 3 of PSD-95 (in blue and green) contains 6 β strands (A-F) and 2 α helicies (A-B). The binding pocket consists of βB, αB, and the carboxylate binding loop. In yellow is a synthetic peptide ligand, which forms a β strand upon binding to the PDZ domain. PBID: 1BE9, from Doyle *et al.*, 1996.

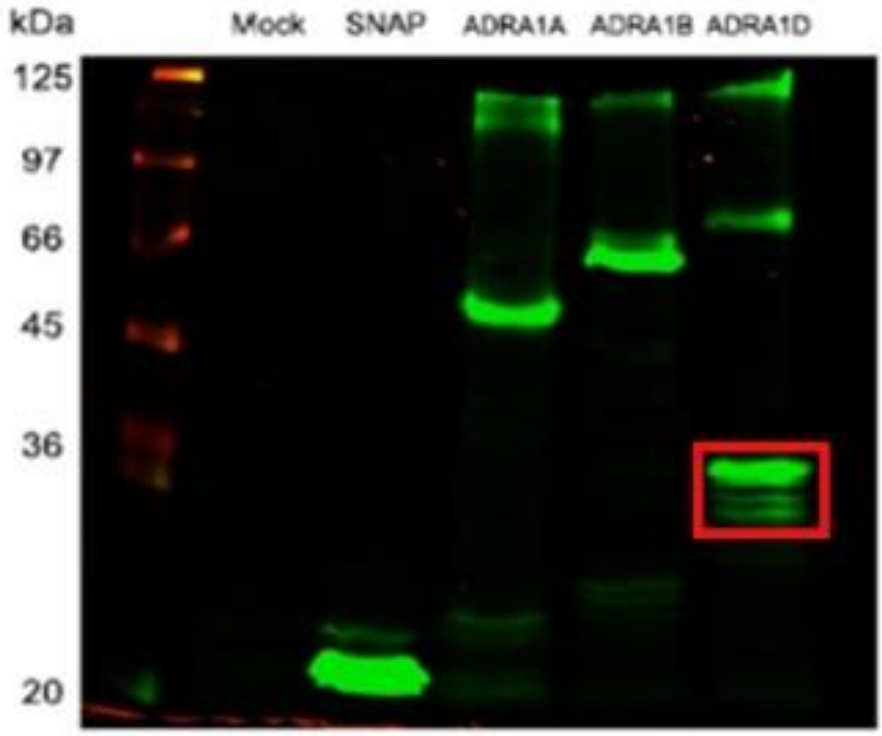

Figure 1.7. PAGE NIR gel of SNAP-epitope tagged α_1-AR subtypes. HEK293 cells were transfected with empty vector (SNAP) or indicated SNAP-epitope tagged α_1-AR receptor subtype. Lysates were labeled with SNAP substrate, BG-782, subjected to SDS PAGE electrophoresis, and imaged using a LI-COR imager. Red square indicated α_{1D}-AR N-terminal cleavage products. Image modified from Kountz *et al.*, 2016.

```
##gff-version 2
##source-version netphos-3.1b
##date 2019-03-25
##Type Protein Sequence
##Protein Sequence
##MTFRDLLSVSFEGPRPDSSAGGSSAGGGGGSAGGAAPSEGPAVGGVPGGAGGGGGVVGAG
##SGEDNRSSAGEPGSAGAGGDVNGTAAVGGLVVSAQ
##end-Protein
# seqname            source        feature      start   end   score  N/A   ?
# ------------------------------------------------------------------------------
Sequence             netphos-3.1b  phos-PKC         8     8   0.744  . .  YES
Sequence             netphos-3.1b  phos-unsp       10    10   0.956  . .  YES
Sequence             netphos-3.1b  phos-unsp       18    18   0.977  . .  YES
Sequence             netphos-3.1b  phos-unsp       19    19   0.857  . .  YES
Sequence             netphos-3.1b  phos-cdc2       31    31   0.572  . .  YES
Sequence             netphos-3.1b  phos-unsp       38    38   0.568  . .  YES
Sequence             netphos-3.1b  phos-unsp       61    61   0.997  . .  YES
Sequence             netphos-3.1b  phos-unsp       67    67   0.577  . .  YES
Sequence             netphos-3.1b  phos-unsp       68    68   0.995  . .  YES
```

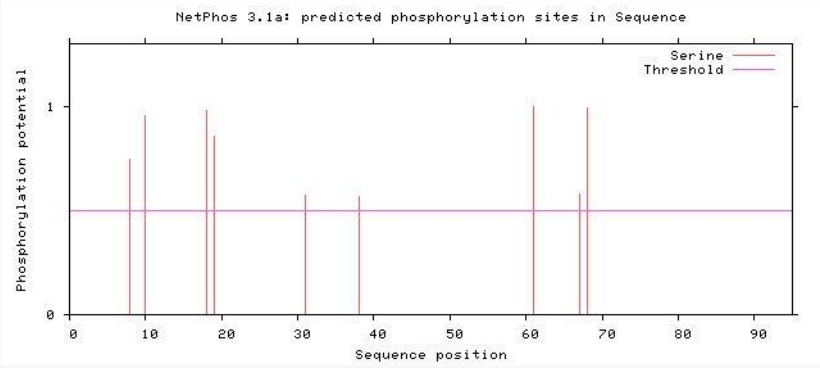

Figure 1.8. Predicted phosphorylation sites of α_{1D}-AR N-terminus. The α_{1D}-AR N-terminal sequence was analyzed for potential phosphorylation potential using NetPhos 3.1 (Blom *et al.*, 1999).

Tables for Chapter 1

Cell Type	α_{1D}-AR		PDZ proteins			Non-PDZ proteins		
Tissue	**% Cov**	**#UP**	**Name**	**% Cov**	**#UP**	**Name**	**% Cov**	**#UP**
HEK293T	15.4	9	SCRIB	10.7	12	CTNNAL1	1.1	1
Kidney			SNTB1	27.9	11	DMD	3	10
			SNTB2	42.4	19	DTNA	17.6	50
						UTRN	17	50
HeLa	10.0	4	SCRIB	13.5	8	CTNNAL1	13.6	8
Cervix			SNTA	6.3	4	DTNA	4	9
			SNTB1	27.7	13	DTNB	17.3	8
			SNTB2	37.6	26	UTRN	20.3	62
A549	2.6	2	SCRIB	2.3	2	DMD	8.5	4
Lung			SNTB2	32.4	17	DTNB	6.3	4
						MAPK1	4.7	2
						UTRN	11.3	36
MCF-7	9.8	3	SCRIB	4.9	6	DMD	7.4	4
Breast			SNTB2	27.4	15	DTNA	26.1	9
						DTNB	7.9	5
						MAPK1	9.2	4
						MAPK3	9.8	3
						UTRN	15.7	48
A375	2.6	2	SCRIB	2.8	2	DMD	4.5	2
Skin			SNTB2	9.6	28	DTNA	8.7	4
						DTNB	5	3
						UTRN	9.6	28
SW480	8.6	5	CASK	5.1	4	CTNNAL1	10.9	7
Colon			DLG1	7.2	5	DTNA	11	3
			LIN7A	7.7	1	DTNB	17.1	9
			SCRIB	8.8	12	PPFIA1	11.1	8
			SNTB1	37	20	PPFIBP1	12.9	9
			SNTB2	43.9	26	UTRN	22.5	76

Table 1.1. α_{1D}-AR PDZ interactors identified by TAP MS/MS in multiple cell types. Data shown include cell type and source tissue; % Cov = percent peptide coverage; #UP = number of unique peptides. Data from Camp *et al.*, 2015.

Chapter 2 – Scribble cooperatively binds multiple α_{1D}-AR C-terminal PDZ ligands

2.1 Introduction

G protein-coupled receptors (GPCRs) account for ~4% of the human genome and are targets for ~30% of FDA approved drugs (Overington *et al.*, 2006). Typically these medications compete with endogenous ligands for orthosteric binding sites, hindering drug selectivity due to the similarity of binding pockets amongst closely related GPCRs. Thus, there is great interest in identifying novel sites to modulate GPCR signaling. To this end, a growing body of research has focused on identifying and characterizing the functional roles of GPCR interacting proteins. Two prominent examples are the β-arrestins (Shukla *et al.*, 2011); and PDZ (PSD95/Dlg/ZO-1) domain containing proteins, which typically interact with C-terminal PDZ ligands (Ritter and Hall, 2009; Romero *et al*., 2011). Since the discovery that rhodopsin interacts with inaD (Tsunoda *et al.*, 1997) and β_2-adrenergic receptor (AR) with NHERF (Hall *et al.*, 1998), significant effort has been put forth to understand GPCR:PDZ protein interactions and their potential as drug targets (Xu *et al.*, 2001; Gage *et al.*, 2005; Guillaume *et al.*, 2008; Lauffer *et al.*, 2010; Dunn and Ferguson, 2015). For example, pharmacological disruption of the nNOS:NOS1AP:PSD95:NMDAR protein complex provides an alternative approach to NMDAR antagonists for treating neuropathic pain (Carey *et al.*, 2017; Lee *et al.*, 2018a; 2018b) and neuronal excitotoxicity (Li *et al.*, 2013), demonstrating the therapeutic potential of targeting PDZ protein interactions to selectively modulate membrane protein function.

Of the three α_1-AR GPCR subtypes (α_{1A}, α_{1B}, α_{1D}) that respond to the endogenous catecholamines epinephrine and norepinephrine, only the α_{1D}-AR subtype contains a C-terminal Type I PDZ ligand. Yeast 2-hybrid (Chen *et al.*, 2006) and tandem-affinity purification/mass spectrometry (Lyssand *et al.*, 2010) screens initially revealed the α_{1D}-AR PDZ ligand interacts

with the syntrophin family of PDZ domain containing proteins. Syntrophins enhance α_{1D}-AR function via recruiting the Dystrophin Associated Protein Complex (DAPC) and signaling effectors, α-catulin, liprin and phospholipase-Cβ (Lyssand *et al.*, 2011). Improved proteomic analyses subsequently revealed that, in addition to syntrophins, α_{1D}-ARs also interact with the multi-PDZ domain containing protein scribble (SCRIB); and that α_{1D}-ARs are expressed as modular homodimers, with one α_{1D}-AR protomer bound to SCRIB, the other to syntrophin, in all human cell lines examined to date (Camp *et al.*, 2015). Strikingly, the α_{1D}-AR:SCRIB:syntrophin complex is highly unique – no other GPCRs containing C-terminal Type I PDZ ligands have been shown to interact with both SCRIB and syntrophins (Camp *et al.*, 2016). Without significant expression of necessary PDZ proteins, α_{1D}-ARs are retained intracellularly and produce weak functional responses (Hague *et al.*, 2004; Petrovska *et al.*, 2005; Garcia-Cazarin *et al.*, 2008), suggesting this protein:protein interaction site has the potential for pharmacological modulation. Indeed, numerous diseases are associated with aberrant α_1-AR function, including hypertension (Server, 1999), benign prostate hypertrophy (Walden *et al.*, 1999), bladder obstruction (Hampel *et al.*, 2002), schizophrenia (Liu *et al.*, 2015), and post-traumatic stress disorder (Olson *et al.*, 2011; Raskind *et al.*, 2018). Unfortunately, deleterious side effects (i.e. orthostatic hypotension, reflex tachycardia) are frequently observed with chronic use of non-selective α_1-AR antagonists. For example, the doxazosin portion of the ALLHAT anti-hypertensive study was prematurely halted due to increased morbidity (Miller, 2011). Thus, selectively targeting the α_{1D}-AR:SCRIB:syntrophin complex may provide therapeutic benefit, minus the toxicities associated with non-selective α_1-AR ligands.

Herein, we employed a combination of biophysical, biochemical and cell-based approaches to acquire structural insights into the α_{1D}-AR:PDZ protein complex. Together, our data implicate

SCRIB PDZ domains 1 and 4 as the primary anchor sites for the α_{1D}-AR. We further highlight differences in α_{1D}-AR:PDZ1 versus α_{1D}-AR:PDZ4 interactions by identifying unique residues in PDZ4 that are critical for α_{1D}-AR binding.

2.2 Materials and Methods

Plasmids and Chemicals. Molecular cloning was performed using inFusion HD cloning technology (Clontech/Takara Biotech, Mountain View, CA). Constructs used for bacterial expression were sub-cloned into a modified pGEX vector to add GST-tags. For mammalian expression, constructs were inserted into pGLUE to add streptavidin binding protein/TEV/calmodulin binding protein tags; or pSNAPf to add SNAP-epitope tags; or pcDNA3.1 to fuse MYC tags. BG-782 SNAP substrate was from New England Biolabs (Ipswich, MA). PageRuler Prestained NIR Protein Ladder was used for all PAGE NIR (Thermo Fisher Scientific, Waltham, MA).

Cell Culture. Human embryonic kidney (HEK) 293 cells were grown in Dulbecco's modified Eagle's medium (DMEM) supplemented with 10% fetal bovine serum and 2 mM L-glutamine. Cells were transfected with 1 mg/ml polyethyleneimine (PEI) and used ~48h post-transfection. For the development of the SNAP-α_{1D}-AR stable cell line, G418 was added to the media 24h post-transfection. [^{3}H]-Prazosin saturation radioligand binding (data not shown) and PAGE NIR (Kountz *et al.*, 2016) were used to verify SNAP-α_{1D}-AR protein expression.

Label-free Dynamic mass redistribution (DMR) assays. DMR assays were performed in 384 well Corning Epic sensor microplates (Corning, Corning, NY) using the protocol described

previously (Kountz *et al*, 2016). Data were analyzed with GraphPad Prism software (La Jolla, CA).

Recombinant Protein Expression & Purification. Recombinant proteins were expressed in Rosetta™ (DE3) competent cells (EMD Millipore, Burlington, MA) in Miller LB supplemented with 100 μg/mL Ampicillin and 34 μg/mL Chloramphenicol at 37°C until an OD_{600} = 0.6 – 1.0 was reached; followed by induction with IPTG (1 mM) at 18°C for 18h. Cells were harvested by centrifugation and lysed (20 mM Tris-HCl pH 8.0, 200 mM NaCl, 5 mM DTT, Protease inhibitors). GST-tagged protein was immobilized on Pierce® glutathione agarose beads (Thermo Scientific, Waltham, MA) and washed (20 mM Tris-HCl pH 8.0 and 200 mM NaCl). Bound protein was eluted from the beads in wash buffer supplemented with 10 mM glutathione and concentration was determined using Bradford assay. Immobilized protein for crystallography was incubated with TEV at 4°C for 18h and subjected to size exclusion chromatography using a Superdex 75 Increase 10/300 GL (GE Healthcare, Chicago, IL) on an AKTA FPLC (GE Healthcare, Chicago, IL) in lysis buffer. The peak 215 nm fractions were collected. SDS-PAGE analysis was employed to determine purity, and protein was flash frozen and stored at -80°C until needed.

SNAP GST-pulldown Assay. SNAP-α_{1D}-C terminal domain (SNAP-α_{1D}-CT) was created by subcloning cDNA encoding the distal 16 amino acids of the human α_{1D}-C terminal domain into the 3' MCS of pSNAP. SNAP and SNAP-α_{1D}-CT were then subcloned into a modified pGEX vector to add N-terminal GST tags, expressed in, and purified from *E.* coli using the previously described method (Figure 2.4B). Following TEV cleavage and ion exchange chromatography,

SNAP-α_{1D}-CT was reacted with BG-782 (1 μM) for 30 min @ 37°C in the dark. Serial dilutions of BG-782:SNAP-α_{1D}-CT were subjected to SDS-PAGE and near infrared fluorescence (NIR: λ = 800 nm) was quantified with the LI-COR Odyssey CLx (Figure 2.4C; LI-COR, Lincoln, NE). Fluorescence intensity standard curves for SNAP-α_{1D}-CT were generated to calculate protein concentrations (Figure 2.4D). For GST-pulldown, 25 μL of 1 μM GST-tagged SCRIB proteins and 25 μL of BG-782:SNAP-α_{1D}-CT were incubated with 25 μL of packed Pierce® glutathione agarose beads and rotated in the dark for 1 h at 4°C. Samples were centrifuged @ 500 RPM at 4°C for 5 min. Supernatant was discarded and beads were washed 3x (20 mM Tris-HCl pH 8.0, 200 mM NaCl, and 0.05% NP-40). Samples were boiled in SDS-sample buffer, and 10 μL aliquots were subjected to PAGE NIR.

Affinity Purification/Co-immunoprecipitation. TAP purification was performed using the protocol described previously (Camp *et al.*, 2015; 2016). 5 μL of 25 μM BG-782 was included in the 1st overnight solubilization step with 0.5% digitonin to label SNAP-α_{1D}-ARs. PAGE NIR was used to observe SNAP-α_{1D}-AR protein levels. Gels were then transferred to nitrocellulose and blotted for anti-HA (#2367, Cell Signaling Technology, Danvers, MA) or anti-MYC (#9B11, Cell Signaling Technology, Danvers, MA), then anti-mouse Alexa-Fluor 2° antibodies in the 700-800 nm range (Invitrogen, Carlsbad, CA). Gels and blots were imaged with the LI-COR Odyssey CLx.

Biolayer interferometry (BLI). BLI was performed using the Octet Red 96 system (Pall Forte Bio, Fremont, CA). All steps were performed in 20 mM Tris-HCl pH 8.0, 200 mM NaCl, and 0.1% bovine serum albumin. 50 nM of biotin labeled peptide containing the last 20 amino acids

of the α_{1D}-CT (BioMatik, Cambridge, ON) was immobilized to streptavidin coated probes, followed by biocytin. The immobilized peptide was incubated in serial dilutions of target proteins until steady-state binding was reached. Biocytin was used to determine non-specific binding. For reverse BLI, GST-SCRIB was immobilized using anti-GST probes, and then incubated in serial dilutions of biotin labeled α_{1D}-CT.

Cell Surface Assay. HEK293 cell surface expression of SNAP-α_{1D}-AR was quantified with cell impermeable SNAP-substrate BG-782 using the method described previously (Kountz *et al.*, 2016). TO-PRO-3 nuclear stain was used to normalize samples according to cell number. Data were analyzed with GraphPad Prism software.

X-ray crystallography. SCRIB PDZ4 R1110G was concentrated to 11 mg/mL in 20 mM Tris at pH 8.0, 200 mM NaCl, and 5 mM DTT and screened against crystallization conditions using a Mosquito Liquid Handler (TTP Labtech, Cambridge, MA). Final crystals were obtained in 21% PEG 3,350 and 0.25 M Ammonium Nitrate. Crystals were flash frozen in mother liquor supplemented with 15% glycerol. All diffraction data was collected at the Advanced Light Source at Berkeley on beam line 8.2.1, integrated with XDS (Kabsch, 2010), and scaled with AIMLESS (Evans, 2006; Winn *et al.*, 2011). Phases were determined by molecular replacement using *Phaser* (McCoy *et al.*, 2007) and SCRIB PDZ4 (Ren *et al.*, 2015; PDB ID: 4WYT) as a search model. The *Phaser* solution was manually rebuilt over multiple cycles using Coot (Emsley and Cowtan, 2004) and refined using *PHENIX* (Adams *et al.*, 2010). All images were generated using the PyMOL Molecular Graphics System, Version 1.74 Schrödinger, LLC. Coordinate files have been deposited in the Protein Data Bank under the accession code 6EEY.

Molecular Docking. The distal 6 amino acids of the α_{1D}-AR C-terminus, LRETDI, was modeled into the canonical βB and αB binding pocket of Scribble PDZ4 (Ren *et al.*, 2015) using PyMOL and submitted to FlexPepDock server (Raveh *et al.*, 2010; London *et al.*, 2011). Models with scores greater than -131 were analyzed for hydrogen bonding (1.5-2.5Å) between peptide and PDZ4. Only interactions identified in greater than 5 models are reported**.**

2.3 Results and Discussion

α_{1D}-AR preferentially binds SCRIB PDZ domains 1 and 4

We previously discovered the α_{1D}-AR interacts with multiple PDZ proteins with cell-type specificity: scribble (SCRIB), α_1-syntrophin (SNTA), human discs large MAGUK scaffold protein 1 (DLG1), and calcium/calmodulin-dependent serine protein kinase (CASK) (Camp *et al.*, 2015). With the goal of elucidating the molecular architecture of this unique, modular GPCR:PDZ protein complex, we employed BioLayer Interferometry (BLI) to quantify equilibrium dissociation constants (K_D) for α_{1D}-AR PDZ ligand:PDZ protein interactions (Table 2.1). cDNAs encoding for the PDZ domains of these proteins were subcloned into a modified pGEX vector (pCOOL), expressed in *E. coli* and purified. Immobilized biotin-labeled peptides containing the distal 20 amino acids of α_{1D}-AR (α_{1D}-CT) were incubated with purified PDZ proteins and subjected to BLI analysis (Figure 2.1A). We first compared α_{1D}-CT binding to SCRIB and α_1-syntrophin (SNTA), as α_{1D}-ARs were found to interact with both PDZ proteins in all human cell lines examined (Camp *et al.*, 2015). Remarkably, α_{1D}-CT bound SCRIB (K_D = 70 ± 20 nM; Figure 2.1B) with ~8 higher affinity than SNTA (K_D = 0.56 ± 0.14 μM; Figure 2.1C). DLG1 (K_D = 0.79 ± 0.21 μM; Figure 2.1D) and CASK (K_D = 1.15 ± 0.21 μM; Figure 2.1E),

similar to SNTA, bind α_{1D}-CT with lower affinity than SCRIB. MPP7, a known interactor of DLG1 and CASK (Stucke *et al.*, 2007), displayed negligible α_{1D}-CT binding (Figure 2.1F). The combined rank order of affinity for α_{1D}-CT interactions with known PDZ proteins is SCRIB >>> SNTA > DLG1 > CASK >>> MPP7 (Figure 2.1G). α_{1D}-CT:SCRIB binding affinity was validated by performing reverse BLI on GST-SCRIB probes incubated in serial dilutions of biotinylated α_{1D}-CT (K_D = 76 ± 20 nM; Figure 2.1H).

A defining structural characteristic of SCRIB includes the presence of four clustered PDZ domains in the C-terminal portion of the polypeptide. Thus, we questioned if α_{1D}-CT selectively associates with targeted PDZ domains on SCRIB. Individual PDZ domains were purified as GST-fusion proteins from *E.coli* and subjected to BLI analysis. SCRIB PDZ1 (K_D = 1.93 ± 0.49 μM; Figure 2.2A) and SCRIB PDZ4 (K_D = 1.14 ± 0.23 μM; Figure 2.2D) bind α_{1D}-CT with the highest affinity, followed by SCRIB PDZ2 (K_D = 14.9 ± 5.44 μM; Figure 2.2B) and SCRIB PDZ3 (K_D = 44.16 ± 13.52 μM; Figure 2.2C).

Next, SCRIB containing all 4 PDZ domains (WT), SCRIB mutants containing single-PDZ domains (PDZ1, PDZ2, PDZ3, PDZ4), and SCRIB lacking all 4 PDZ domains (ΔPDZ) were subcloned into the pGlue vector to add N-terminal tandem affinity purification (TAP) epitope tags. Next, constructs were transiently transfected into HEK293 cells stably expressing SNAP-α_{1D}-AR. Cell lysates were affinity purified with streptavidin beads. Samples were labeled with BG-782 to detect SNAP-α_{1D}-AR and imaged with PAGE NIR. As shown in Figure 2.2E, SNAP-α_{1D}-AR co-immunoprecipitated robustly with SCRIB WT, PDZ1, PDZ4, and to a lesser extent, with PDZ3. As expected SCRIB ΔPDZ produced no significant SNAP-α_{1D}-AR binding. Thus, *in vitro* analysis of α_{1D}-AR:SCRIB interactions concurs with prior *in situ* BLI results.

Taken together, these data implicate SCRIB PDZ1 and PDZ4 as the central scaffolds of the

α_{1D}-AR complex. Based on our discovery that CASK and DLG1 bind with relatively low affinity to the α_{1D}-AR PDZ ligand, and that previous studies have reported SCRIB can interact with additional PDZ proteins (Stephens *et al.*, 2018), we suspect CASK and DLG1 are recruited to the α_{1D}-AR complex indirectly by SCRIB. For example, DLG1 can be indirectly recruited to SCRIB via GUKH, which interacts with SCRIB PDZ2 in *Drosophila* synaptic boutons (Mathew *et al.*, 2002), or LGL – a known interactor with both DLG1 and SCRIB (Kallay *et al.*, 2006; Zhu *et al.*, 2014). Additionally, DLG1, CASK, and LIN-7A are expressed as a tripartite complex *in vitro* and *in vivo* (Butz *et al.*, 1998; Borg *et al.*, 1998; Lee *et al.*, 2002), suggesting DLG1 may be recruiting CASK and LIN-7A to the α_{1D}-AR complex via indirect interactions with SCRIB.

α_{1D}-CT:SCRIB binding is co-operative

A key finding from BLI studies was the notable difference in α_{1D}-CT binding affinity for SCRIB containing all 4 PDZ domains (70 nM) relative to each individual SCRIB PDZ domain (1.14 - 44.16 μM). The divergent α_{1D}-CT:SCRIB binding affinities are suggestive of a co-operative binding mechanism, in that the binding of a single α_{1D}-CT PDZ ligand to SCRIB enhances the affinity of subsequent intramolecular α_{1D}-CT:SCRIB PDZ binding events. We tested this model by quantifying the affinity of SCRIB C-terminal truncation mutants missing PDZ4 (ΔPDZ4) or PDZ3 and PDZ4 (ΔPDZ34) with BLI. α_{1D}-CT bound SCRIB ΔPDZ4 (K_D = 0.14 ± 0.02 μM; Figure 2.3A) and SCRIB ΔPDZ34 (K_D = 0.16 ± 0.01 μM; Figure 2.3B) with ~2x lower affinity than SCRIB WT (not significant, One-way ANOVA with Tukey's post-hoc test), but ~6x higher affinity than SCRIB PDZ1 ($p = 0.001$, One-way ANOVA with Tukey's post-hoc test) or PDZ4 alone ($p = 0.07$, One-way ANOVA with Tukey's post-hoc test). In the reverse experiment, α_{1D}-CT bound SCRIB PDZ3 and PDZ4 (PDZ34) with substantially lower

affinity ($K_D = 0.34 \pm 0.09$ μM; Figure 2.3C; not significant, One-way ANOVA with Tukey's post-hoc test) than SCRIB WT, but greater than SCRIB PDZ4 (not significant, One-way ANOVA with Tukey's post-hoc test). Thus, these findings are suggestive of a co-operative α_{1D}-CT:SCRIB binding modality, and provide additional support for previous studies suggesting SCRIB PDZ34 forms a "supramodule" binding site for PDZ ligands (Ren *et al.*, 2015).

We then tested the ability of SCRIB truncation mutants to co-immunoprecipitate with full length α_{1D}-AR in mammalian cell culture. TAP-SCRIB mutants were co-transfected with myc-α_{1D}-AR into HEK293 cells, digitonin-solubilized as cell lysates, immunoprecipitated with streptavidin beads and probed for anti-HA (TAP-SCRIB; Figure 2.3D, *upper panel*) and anti-myc (α_{1D}-AR; Figure 2.3D, *lower panels*). As shown, successive C-terminal SCRIB deletions produced progressive decreases in α_{1D}-AR monomer (Figure 2.3D, *bottom panel*, 68 kDa) and multimer (Figure 2.3D, *middle panel*, ~250 kDa) signal, whereas SCRIB ΔPDZ produced no detectable α_{1D}-AR interaction. Of note, the most dramatic decrease in α_{1D}-AR binding was observed with SCRIB containing only PDZ1 (Figure 2.3D, lane PDZ1).

Next, SNAP GST-tag pulldown assays were used to test the proposed co-operative model of α_{1D}-AR:SCRIB binding. The experimental approach involved the creation of a novel reporter construct: a SNAP-epitope tag adjacent to the N-terminus of the distal 16 amino acids of the α_{1D}-CT (SNAP-α_{1D}-CT). PAGE near infrared (NIR) analysis of HEK293 cell lysates transfected with SNAP-α_{1D}-CT displayed protein bands of expected size 21.7 kDa (Figure 2.4A). Next, GST-SNAP-α_{1D}-CT was expressed in and purified from *E. Coli*, then eluted via TEV cleavage (Figure 2.4B). SNAP-α_{1D}-CT was pre-labeled with 1 μM SNAP-substrate BG-782 and subjected to PAGE NIR/LICOR Odyssey NIR imaging (Figure 2.4C) to generate a standard curve (Figure 2.4D). Glutathione agarose beads were incubated with previously described GST-SCRIB

constructs, mixed with serial dilutions of labeled SNAP-α_{1D}-CT, eluted, and analyzed with PAGE NIR. 10 μM BG-782 pre-labeled SNAP-α_{1D}-CT was included in each gel as a normalization control (Figure 2.4E, F, G, denoted as INPUT). In accordance with previous BLI experiments, SCRIB WT bound SNAP-α_{1D}-CT in a concentration-dependent manner (Figure 2.4E), with higher avidity than PDZ4 (Figure 2.4F; $p < 0.0001$, One-way ANOVA with Tukey's post-hoc test) or PDZ1 (Figure 2.4G; $p < 0.0001$, One-way ANOVA with Tukey's post-hoc test). Interestingly, SCRIB ΔPDZ4 (~48% of SCRIB WT; $p < 0.0001$, One-way ANOVA with Tukey's post-hoc test) and ΔPDZ34 (~34% of SCRIB WT; $p < 0.0001$, One-way ANOVA with Tukey's post-hoc test) produced maximal SNAP-α_{1D}-CT binding responses that were less than SCRIB WT, yet greater than single SCRIB PDZ domain constructs (<10% of SCRIB WT, Figure 2.4H; $p < 0.0001$, One-way ANOVA with Tukey's post-hoc test). Taken together, our findings support the model that multiple α_{1D}-AR CT PDZ ligands bind a single molecule of SCRIB via a co-operative mechanism.

A similar model has been proposed for numerous proteins containing multiple PDZ domains (Grootjans *et al.*, 2000; Long *et al.*, 2003; Grembecka *et al.*, 2006; Dicks *et al.*, 2019). For example, PDZ domains 1 and 2 of PSD-95 exhibit greater affinity for binding partners Kv1.4, NR2B, and CRIPT when expressed in tandem (Long *et al.*, 2003). The PDZ domains of syntenin also work co-operatively to bind syndecan dimers – syntenin PDZ2:syndecan interaction is a pre-requisite for syntenin PDZ1:syndecan binding (Grootjans *et al.*, 2000; Grembecka *et al.*, 2006). A recent study similarly found that PDZ domains 2 and 3 of PTPN13 show enhanced binding for the PDZ ligand of APC when expressed together compared to individual domain constructs (Dicks *et al.*, 2019). These previously characterized interactions further support our findings that the α_{1D}-CT:SCRIB interaction is co-operative.

Structure-function analyses identify R1110^{PDZ4} as a selectivity determinant for α_{1D}-CT binding

We next compared α_{1D}-CT:SCRIB binding parameters to previously identified SCRIB PDZ1 and PDZ4 interactors. SCRIB PDZ1 interacts with >20 proteins (Stephens *et al.*, 2018), whereas PDZ4 interacts with NOS1AP (Richier *et al.*, 2010), APC (Takizawa *et al.*, 2006), p22phox (Zheng *et al.*, 2016), NMDA receptor subunits GluN2A and GluN2B (Piguel *et al.*, 2014), and DLC3 (Hendrick *et al.*, 2016). Remarkably, α_{1D}-CT has the highest reported affinity to date of all reported SCRIB PDZ4 interactors. For example, the PDZ ligand of p22phox binds SCRIB PDZ4 with K_D = 40 μM (Zheng *et al.*, 2016), whereas the NMDA receptor PDZ ligands bind SCRIB PDZ4 with K_D > 150 μM (Piguel *et al.*, 2014). Thus, targeting SCRIB PDZ4 may provide the highest opportunity to disrupt α_{1D}-AR function without perturbing other SCRIB complexes.

We first investigated the impact of SCRIB PDZ4 on α_{1D}-AR functional responses. Label-free dynamic mass redistribution (DMR) signaling assays were performed using HEK293 cells stably expressing SNAP-α_{1D}-AR alone or transiently co-expressing SCRIB WT, SCRIB PDZ4 or SCRIB ΔPDZ4. Concentration-response curves were generated for the selective α_1-AR agonist phenylephrine to facilitate efficacy comparison between transfection conditions. As shown, phenylephrine efficacy was enhanced by all SCRIB constructs with rank order WT > PDZ4 > ΔPDZ4 > pGLUE vector control (Figure 2.5A). Next, the ability of SCRIB mutants to promote α_{1D}-AR plasma membrane trafficking were assessed using a 96-well plate near infrared imaging cell surface assay. The rank order of SCRIB constructs for promoting α_{1D}-AR plasma membrane trafficking was WT > PDZ4 > ΔPDZ4 > pGlue (Figure 2.5B, C). We have previously reported that α-syntrophin interacts with α_{1D}-AR in the endoplasmic reticulum (Lyssand *et al.*, 2008), and

that SCRIB and syntrophin co-localize and compete for the PDZ ligand of α_{1D}-CT (Camp *et al.*, 2015). Therefore, we propose the α_{1D}-AR:SCRIB interaction occurs in the endoplasmic reticulum to facilitate trafficking to the plasma membrane. However, further studies are warranted to determine the precise mechanism and machinery by which this complex formation is regulated.

Functional studies indicate targeting SCRIB PDZ4 alone may be a useful approach to modulate α_{1D}-AR processes *in vivo*. However, this requires a thorough understanding of the structural determinants governing selectivity of the α_{1D}-CT PDZ ligand for SCRIB PDZ4. Molecular docking that employed the solved crystal structure of SCRIB PDZ4 (PDB ID: 4WYT; Raveh *et al.*, 2010; London *et al.*, 2011; Ren *et al.*, 2015) was used to predict α_{1D}-CT:SCRIB PDZ4 interactions. Our model identified $D571^{\alpha 1D\text{-}AR}$:$R1110^{PDZ4}$ of the carboxylate binding loop and $T570^{\alpha 1D\text{-}AR}$:$H1170^{PDZ4}$ of α-helix B as possible α_{1D}-CT PDZ ligand interaction sites within SCRIB PDZ4 (Figure 2.5D). SCRIB PDZ domain sequence alignment revealed that R1110, but not H1170, is unique to PDZ4, suggesting that this residue may be responsible for the specificity of α_{1D}-AR to PDZ4 (Figure 2.5E). In support of our structural prediction, purified PDZ4 harboring either R1110G or H1170A mutations ablates α_{1D}-CT binding (Figure 2.5F).

Previous structural and biophysical studies have identified homologous histidine residues within Type I PDZ domains that control ligand specificity (Doyle *et al.*, 1996; Songyang *et al.*, 1997; Babault *et al.*, 2011; Mamonova *et al.*, 2017). However, the structural role of R1110 is unknown. To resolve the mechanistic underpinnings of this interaction, the crystal structure of PDZ4 R1110G was solved to 1.15 Å resolution (Figure 2.5G; Table 2.2). A superposition of the R1110G mutant with WT PDZ4 reveals a 4.5 Å shift of the carboxylate binding loop (Figure 2.5H). We predict this shift creates steric hindrance that prevents the interaction between

I572$^{\alpha 1D\text{-}AR}$ and PDZ4. Previous studies have found PDZ ligand:PDZ domain interactions are dictated by interactions of the C-terminal residue of the PDZ ligand (Doyle *et al.*, 1996; Stricker *et al.*, 1997; Babault *et al.*, 2011). For example, *in situ* peptide library screens revealed 89% of peptides interacting with the PDZ domain of nNOS contain a C-terminal valine (Stricker *et al.*, 1997). Thus, we propose that preventing I572$^{\alpha 1D\text{-}AR}$ from interacting with PDZ4 is sufficient to inhibit α_{1D}-CT binding.

Finally, we leveraged the information gathered from our structural studies to understand how mutations in either PDZ1 and/or PDZ4 affect the α_{1D}-CT interaction in context of the core binding protein, SCRIB. This involved introducing H793A PDZ1 and H1170A PDZ4 mutations into GST-SCRIB (Figure 2.6A, schematic) and subjecting to α_{1D}-CT BLI analysis. As shown, SCRIB H1170A retains significant α_{1D}-CT binding with affinity ($K_D = 0.32 \pm 0.08$ μM; Figure 2.6A) similar to the SCRIB PDZ34 construct (Figure 2.3D). Mutating the equivalent amino acid in SCRIB PDZ1, H793A, produced a species that retains α_{1D}-CT binding, with ~20x lower affinity ($K_D = 7.34 \pm 4.53$ μM; Figure 2.6B) than SCRIB PDZ4 H1170A. Strikingly, introducing both H793A and H1170A mutations into SCRIB abolished α_{1D}-CT binding as measured by BLI (Figure 2.6C).

Previous studies have identified a large, macromolecular complex containing PDZ proteins and non-PDZ proteins (Chen *et al.*, 2006; Lyssand *et al.*, 2008; Lyssand *et al.*, 2010; Camp *et al.*, 2015). However, the presence of a PDZ ligand on the distal C-terminal of α_{1D}-AR is essential for complex formation. Thus, the purpose of this study was to identify the primary PDZ domain interaction which anchors this complex. Using Octet BLI, we were able to identify Scribble, specifically PDZ domains 1 and 4, as the primary interface for the α_{1D}-AR PDZ ligand. We also developed a novel semi-quantitative *in vitro* GST pulldown assay by harnessing the power and

sensitivity of the SNAP-epitope tag. From this assay, we were able to establish a relative stoichiometry which suggests that Scribble is able to anchor multiple α_{1D}-AR PDZ ligands in a cooperative mechanism. Using structural modeling and x-ray crystallography, we identified a unique side-chain interaction at $D571^{\alpha 1D\text{-}AR}$:$R1110^{PDZ4}$. We further show that mutating R1110 to disrupt this interface inhibits α_{1D}-CT binding. Therefore, we posit that disrupting this interaction is a potential drug target to specifically modulate α_{1D}-AR signaling in disease.

Abbreviations: GPCR, G protein-coupled receptor; FDA, Food and Drug Administration; PDZ, PSD95/Dlg/ZO-1; AR, adrenergic receptor; NHERF, Na^+/H^+ exchanger regulatory factor; nNOS, neuronal nitric oxide synthase; NOS1AP, nitric oxide synthase 1 adaptor protein; PSD95, post-synaptic density 95; NMDAR, N-methyl-D-aspartate receptor; DAPC, dystophin associated protein complex; SCRIB, scribble; ALLHAT, Antihypertensive and Lipid-Lowering Treatment to Prevent Heart Attack Trial; GST, glutathione S-transferase; HEK, human embryonic kidney; DMR, dynamic mass redistribution; BLI, biolayer interferometry; SNTA, α_1-syntrophin; DLG1, human discs large MAGUK scaffold protein 1; CASK, calcium/calmodulin-dependent serine protein kinase; K_D, equilibrium dissociation constants; α_{1D}-CT; C-terminal of α_{1D}-AR; MPP7, Membrane Palmitoylated Protein 7; TAP, tandem affinity purification; GUKH, GUK holder; LGL, lethal giant larvae

Figures for Chapter 2

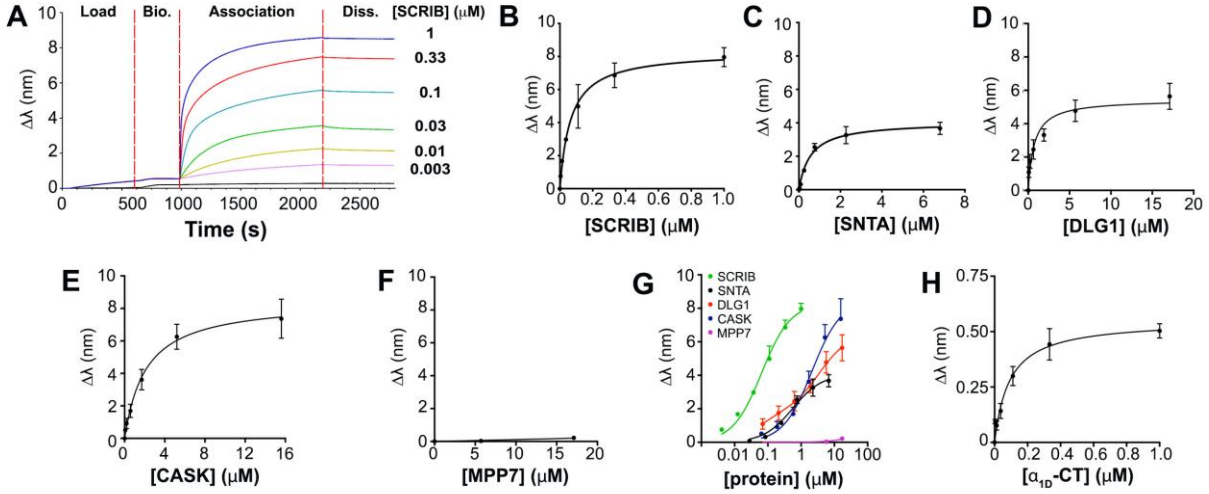

Figure 2.1. *In situ* affinity determination of α_{1D}-adrenergic receptor C-terminal PDZ ligand:PDZ protein interactions. (A) Real-time biolayer interferometry (BLI) association/dissociation curve measuring binding of α_{1D} C-terminus (α_{1D}-CT) to purified scribble (SCRIB). Biotin-labeled α_{1D}-CT was immobilized to streptavidin probes. Indicated concentrations of SCRIB were used as analytes. (Bio. = Biocytin, Diss. = Dissociation). (B-F) Quantified BLI binding data for biotin labeled α_{1D}-CT binding to (B) SCRIB, (C) α_1-syntrophin (SNTA), (D) human discs large MAGUK scaffold protein 1 (DLG1), (E) calcium/calmodulin dependent serine protein kinase (CASK), and (F) membrane palmitoylated protein 7 (MPP7). (G) Comparative analysis of BLI concentration-response curves for α_{1D}-CT:PDZ protein association binding. (H) Reverse BLI assay of purified α_{1D}-CT (analyte) bound to immobilized biotin-labeled SCRIB (probe). Data are presented as mean ± SEM, n = 3.

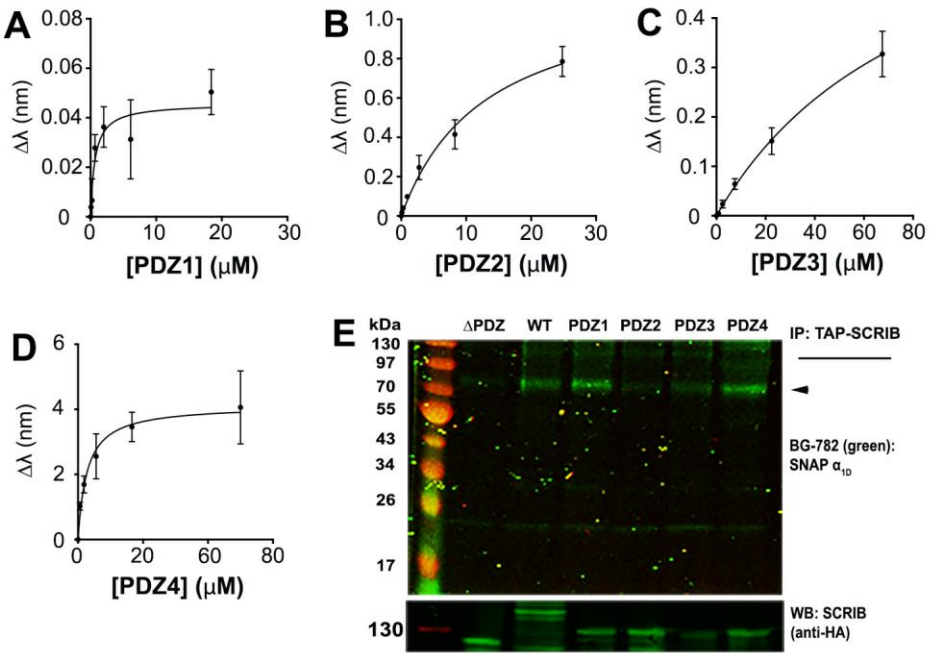

Figure 2.2. *In situ* and *in vitro* analysis of α_{1D}-adrenergic receptor C-terminal PDZ ligand:SCRIB single PDZ domain interactions. (A-D) Biolayer interferometry (BLI) analyses of immobilized biotin-labeled α_{1D}-CT binding to (A) SCRIB PDZ domain 1 (PDZ1), (B) SCRIB PDZ domain 2 (PDZ2), (C) SCRIB PDZ domain 3 (PDZ3) and (D) SCRIB PDZ domain 4. BLI data are presented as mean ± SEM, n = 3. (E) *Top panel*, PAGE NIR of BG-782 labeled SNAP-α_{1D}-AR co-immunoprecipitated with TAP-SCRIB containing all 4 PDZ domains (WT), PDZ domain 1 (PDZ1), 2 (PDZ2), 3 (PDZ3) or 4 (PDZ4), or no PDZ domains (ΔPDZ) from HEK293 cell lysates. *Bottom panel*, Anti-HA western blot of upper gel for listed TAP-SCRIB constructs. ◄ indicates SNAP-α_{1D}-AR monomer band.

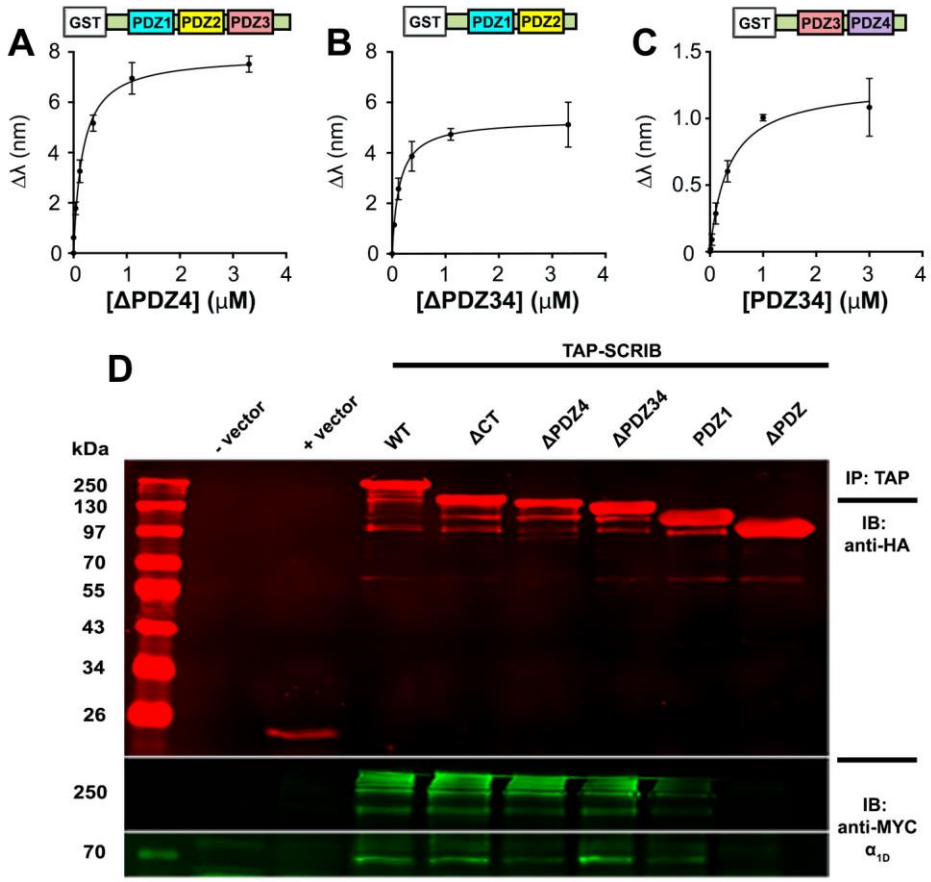

Figure 2.3. *In situ* and *in vitro* analysis of α_{1D}-AR C-terminal PDZ ligand:SCRIB truncation mutant interactions. (A-C). Biolayer interferometry (BLI) analyses of α_{1D}-CT binding to SCRIB ΔPDZ4 (A), SCRIB ΔPDZ34 (B) and SCRIB PDZ34 (C). BLI data are presented as mean ± SEM, n = 3. (D) Co-immunoprecipitation of myc-α_{1D}-AR with transfection vehicle (- vector), empty pGlue vector (+ vector), TAP-SCRIB containing all 4 PDZ domains (WT), or sequentially truncated at the C-terminus (CT), PDZ domain 4 (ΔPDZ4), PDZ domain 3 (ΔPDZ34), PDZ domain 2 (PDZ1) or PDZ domain 1 (ΔPDZ) from HEK293 cell lysates. Shown are western blots of TAP-SCRIB constructs (*top panel*), myc-α_{1D}-AR multimers (*middle panel*) and monomers (*bottom* panel).

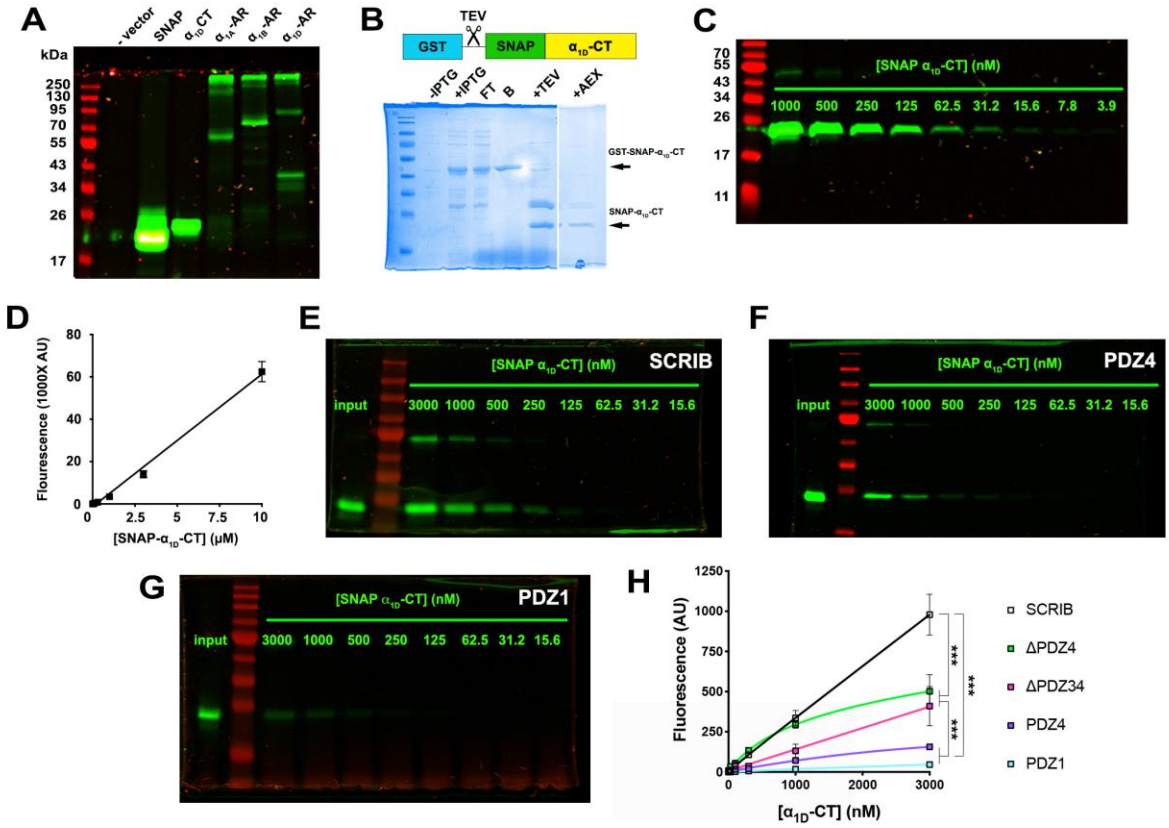

Figure 2.4. SNAP-α_{1D}-AR C-terminal PDZ ligand:GST-SCRIB pulldown assays indicate a co-operative binding model. (A) PAGE NIR of HEK293 cell lysates transfected with vehicle alone (- vector), pSNAP vector (SNAP), N-terminal SNAP-tagged α_{1D}-AR C-terminus (α_{1D}-CT), α_{1A}, α_{1B} and α_{1D}-AR. (B) Coomassie stain of GST-SNAP-α_{1D}-CT purification ± IPTG induction, unbound (FT), bound to beads (B), following TEV cleavage (+TEV) and anion exchange chromatography (AEX). (C) PAGE NIR of purified SNAP-α_{1D}-CT pre-labeled with BG-782. (D) SNAP-α_{1D}-CT standard curve plotting concentration of BG-782 labeled SNAP-α_{1D}-CT versus fluorescence quantified at λ = 800 nm. (E-G) Representative PAGE NIR gels of SNAP-α_{1D}-CT pulldowns with GST-SCRIB (E), GST-PDZ4 (F), or GST-PDZ1 (G). (H) Concentration-response curves quantifying SNAP-α_{1D}-CT bound to GST-SCRIB, SCRIB truncated before PDZ domain (ΔPDZ4), before PDZ domain 3 (ΔPDZ34), SCRIB PDZ1, or SCRIB PDZ4 (mean ± SEM, n = 3-4). *** = $p < 0.001$, One-way ANOVA with Tukey's post-hoc test.

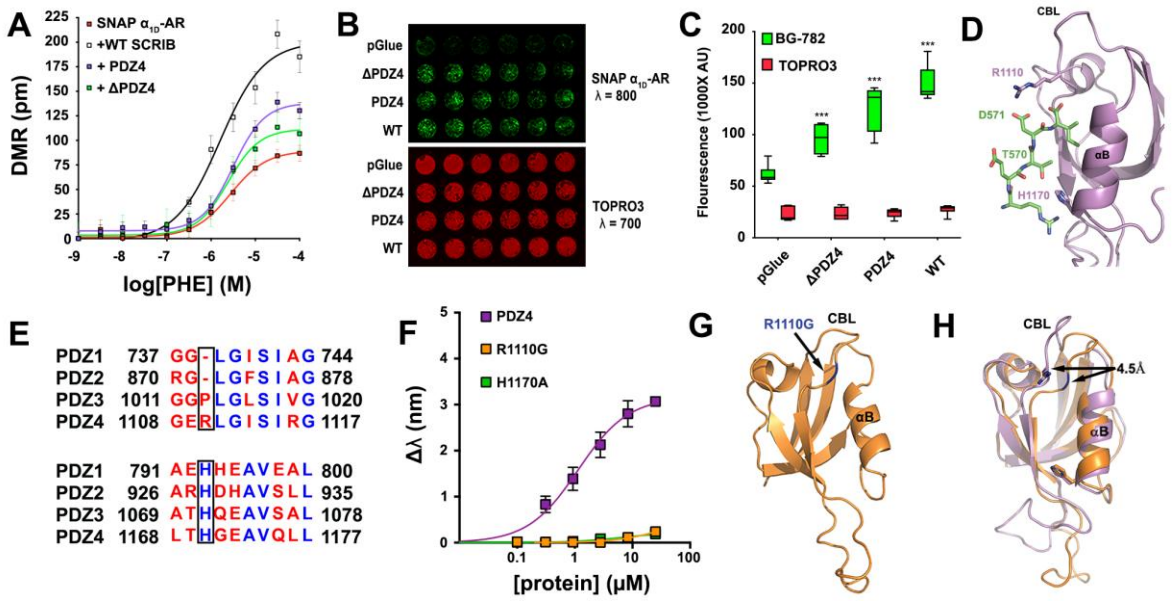

Figure 2.5. Structure-function analysis of the α_{1D}-CT:SCRIB PDZ4 interaction. (A) Dynamic mass redistribution assays quantifying phenylephrine efficacy in HEK293 cells stably expressing SNAP-α_{1D}-AR alone, or transfected with SCRIB WT, PDZ4, or SCRIB containing only PDZ domains 1, 2 and 3 (ΔPDZ4). Data are the mean of 12 replicates ± SEM. (B) Cell surface expression of SNAP-α_{1D}-AR in HEK293 cells transfected with vector control (pGlue), ΔPDZ4, PDZ4, or SCRIB WT (*top panel, green*); nuclear stain TO-PRO-3 was used to normalize for cell number (*bottom panel, red)*. (C) Quantification of data from B (mean ± SEM, n = 3, 6 replicates; *** = $p < 0.001$ from pGLUE, One-way ANOVA with Tukey's post-hoc tests). (D) Molecular docking model of α_{1D}-CT:SCRIB PDZ4 interaction (purple = PDZ4, green = α_{1D}-CT, PDB ID = 4WYT used for model). (E) Sequence alignment of SCRIB PDZ domains (boxes indicate residues identified in D). (F) Biolayer interferometry (BLI) analysis of SCRIB mutations H1170A and R1110G on α_{1D}-CT binding (mean ± SEM, n = 3). (G) X-ray crystallography structure of SCRIB PDZ4 R1110G (mutation highlighted in blue; PDB ID = 6EEY). (H) R1110G (orange) causes a 4.5 Å shift in carboxylate binding loop, as determined by superposition with WT PDZ4 (purple).

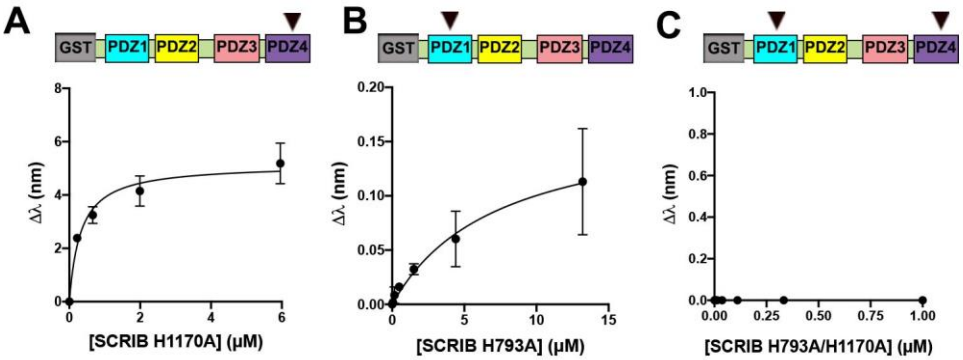

Figure 2.6. Biolayer interferometry analysis of α_{1D}-AR C-terminal PDZ ligand:SCRIB H793A/H1170A interactions. Biolayer interferometry (BLI) was used to quantify α_{1D}-CT binding to full length SCRIB containing point mutations H1170A (A), H793A (B), or both H793A and H1170A (C). ▼ indicate the SCRIB PDZ domain harboring the denoted H→A mutation. Data are presented as mean ± SEM, n = 3.

Tables for Chapter 2

Analyte	**K_D (uM)**	**SEM**
SCRIB	0.07	0.024
PDZ1	1.93	0.49
PDZ2	14.9	5.44
PDZ3	282.7	543
PDZ4	1.144	0.2332
Δ34	0.16	0.01
Δ4	0.1399	0.016
α_{1D}-CT	0.076	0.02
H1170A	NB	NB
R1110G	NB	NB
hDLG1	0.79	0.21
Syntrophin	0.5644	0.14
Cask	1.151	0.212
MPP7	NB	NB
Lin7a	75.19	42.36
Scrib PDZ34	0.3475	0.09245
SCRIB H793A/H1170A	NB	NB
SCRIB H793A	7.34	4.53
SCRIB H1170A	0.32	0.08

Table 2.1. Binding affinities as determined by BLI. Data represents average of 2-3 experiments.

	SCRIB PDZ4 R1110G
Data collection	
Space group	P 1 21 1
Cell dimensions	
a, *b*, *c* (Å)	27.29, 40.24, 32.26
α, β, γ (°)	90, 97.85, 90
Resolution (Å)	31.96 - 1.145 (1.186 - 1.145)*
R_{merge}	0.06674 (0.07563)*
$I / \sigma I$	12.82 (3.48)*
Completeness (%)	82.58 (3.40)*
Redundancy	4.4 (1.0)*
Refinement	
Resolution (Å)	31.96 - 1.145 (1.186 - 1.145)*
No. reflections	20613 (85)*
R_{work} / R_{free}	0.1571 (0.1385)/ 0.1818 (0.1574)*
No. atoms	1646
Protein	692
Ligand/ion	--
Water	131
B-factors	
Protein	7.36
Ligand/ion	--
Water	16.20
R.m.s. deviations	
Bond lengths (Å)	0.008
Bond angles (°)	1.35

Table 2.2. Data collection and refinement statistics for Scribble PDZ4 R1110G mutant (molecular replacement).

Chapter 3 - *N*-glycosylation of α_{1D}-AR N-terminal domain is required for correct trafficking, function, and biogenesis

3.1 Introduction

G protein-coupled receptors (GPCRs) are essential membrane proteins that regulate the vast majority of physiological functions in the human body. As a result, GPCRs have been estimated to be targeted by approximately one third of all currently approved medications (Overington *et al.*, 2006). Adrenergic receptors (ARs) are a clinically relevant subfamily of GPCRs. Activated by the endogenous sympathetic neurotransmitters epinephrine and norepinephrine, adrenergic GPCRs consist of three major subtypes: α_1, α_2, and β. The α_1 sub-family – containing α_{1A}, α_{1B}, and α_{1D} subtypes (Docherty, 2010) – are targets for medications that regulate blood pressure (Tanoue *et al.*, 2002; Lyssand *et al.*, 2008), bladder (Hampel *et al.*, 2002; Bouchelouche *et al.*, 2005), prostate (Walden *et al.*, 1991; Kojima *et al.*, 2011), and central nervous system function (Olson *et al.*, 2011; Perez and Doze, 2011; Raskind *et al.*, 2013). Thus, understanding the molecular and cellular mechanisms regulating α_1-AR function will help spur the development of new medications associated with aberrant α_1-AR signaling, such as hypertension, PTSD, schizophrenia and benign prostatic hypertrophy (Cotecchia *et al.*, 2015; Fusco *et al.*, 2016; Hendrickson and Raskind, 2016; Akinaga *et al.*, 2019).

Among the three α_1 subtypes, the α_{1D}-AR remains poorly understood due to technical challenges. Relative to the closely related α_{1A} and α_{1B}-AR subtypes, α_{1D}-AR displays limited functional responses and minimal plasma membrane expression when expressed in heterologous cell culture (Hague *et al.*, 2004; Petrovska *et al.*, 2005; Garcia-Cazarin *et al.*, 2008). Although pharmacologically detectable in intact isolated aortae in organ-tissue bath assays (Piascik *et al.*, 1995), α_{1D}-AR functional expression rapidly disappears in primary vascular smooth muscle cell

cultures within 24-48 hours (Fan *et al.*, 2009). Also, immortalized cell lines that endogenously express α_{1D}-ARs have yet to be discovered. Combined, these experimental clues indicate the molecular and cellular mechanisms governing α_{1D}-AR functional expression in cells are unique amongst the α_1-AR subtypes, and thus may be targeted by novel drugs to exogenously regulate α_{1D}-AR signaling in human disease.

Important clues towards solving why α_{1D}-ARs are poorly expressed in cell culture include two structural features distinct to the α_{1D}-AR: (A) a C-terminal PSD-95/Dlg/ZO-1 (PDZ) ligand that ensures the formation of a modular, homodimeric macromolecular complex via binding to PDZ-domain containing proteins Scribble and syntrophin (Chen *et al.*, 2006; Lyssand *et al.*, 2010; Lyssand *et al.*, 2011; Camp *et al.*, 2015; Janezic *et al.*, 2019); and (B) an atypical extracellular N-terminal domain (NTD). The average NTD for class A GPCRs is 40 amino acids (Wallin and von Heijne, 1995), making the 95 amino acid α_{1D} NTD unusually long. We, and others, have previously demonstrated the α_{1D}-AR NTD contains an endoplasmic reticulum (ER) retention signal (Pupo *et al.*, 2003; Hague *et al.*, 2004; Petrovska *et al.*, 2005), and that the NTD undergoes an endogenous cleavage event that enhances α_{1D}-AR plasma membrane trafficking and agonist-stimulated functional responses (Kountz *et al.*, 2016). Unfortunately, the mechanisms by which the NTD regulates α_{1D}-AR trafficking and function are unknown.

GPCR trafficking is a highly complex process that is regulated in part by multiple factors, including Rab GTPases (Wu, 2012; Li *et al.*, 2017), TBC domain-containing proteins (Wei *et al.*, 2019), GPCR oligomerization (Balasubramanian *et al.*, 2004; Uberti *et al.*, 2005), N-terminal cleavage (Nordström *et al.*, 2006; Dunham *et al.*, 2009; Hakalahti *et al.*, 2010; Mattila *et al.*, 2016), and N-terminal translocation and glycosylation in the ER lumen (Petäjä-Repo *et al.*, 2000; Andersson *et al.*, 2003; Van Craenenbroeck *et al.*, 2005; Chitwood *et al.*, 2018). Previous studies

employed WGA lectin and deglycosylating enzymes to demonstrate endogenous α_1-ARs are glycosylated in rat brain (Sawutz *et al.*, 1987), but were unable to determine if individual α_1-AR subtypes were glycosylated due to technical limitations (Jensen *et al.*, 2009). Subsequent studies have produced conflicting results (Björklöf *et al.*, 2002; Vicentic *et al.*, 2002; Pupo *et al.*, 2003; Lopez-Gimenez *et al.*, 2007), and as a result, it remains unclear how NTD glycosylation regulates α_1-ARs physiological function. Interestingly, the α_{1D}-AR NTD contains two putative *N*-glycosylation sites located at N65 and N82 (Perez *et al.*, 1991). In this study, we leverage SNAP-epitope tag labeling and label-free dynamic mass redistribution technology to show, for the first time, that the α_{1D}-AR NTD is dual glycosylated, thereby ensuring proper biosynthesis and trafficking of nascent receptors.

3.2 Materials and Methods

Plasmids and Chemicals. Molecular cloning was performed using inFusion HD cloning technology (Clontech/Takara Biotech, Mountain View, CA). The $pSNAP_f$ and pCLIP vector, as well as SNAP substrates, BG-782 and Alexa Fluor 488, and CLIP substrate, BC-680 were purchased from New England Biolabs (Ipswich, MA). PageRuler Prestained NIR Protein Ladder was used for all PAGE NIR analyses (Thermo Fisher Scientific, Waltham, MA).

Cell culture. Human Embryonic Kidney (HEK) 293 cells were grown in Dulbecco's Modified Eagle's Medium (Corning, Corning, NY) supplemented with 10% fetal bovine serum and 2 mM L-glutamine at 37°C in 5% CO_2. Cells were used ~48 hrs post-transfection with polyethyleneimine.

Lentil Lectin Affinity Purification. Cells were lysed in 20 mM Tris-HCl (pH 8), 200 mM NaCl, 5 mM DTT, and 1% NP-40 on ice for 20 min. with vortexing every 5 min, followed by 14K RPM centrifugation at 4°C for 10 min. The soluble fraction was incubated with Lentil Lectin Sepharose 4B beads (GE Healthcare, Chicago, IL) and 1 μL of 25 μL BG-782 for 1 hr at room temperature. Beads were pelleted and washed 3X in excess lysis buffer. Bound protein was eluted with lysis buffer supplemented with 200 mM methyl-α-D-mannopyranoside at 37°C shaken at 300 RPM for 10 min. Elutant was collected and subjected to SDS-PAGE electrophoresis, followed by PAGE NIR analysis using a Li-COR Odyssey CLx (LI-COR, Lincoln, NE; Kountz *et al.*, 2016; Camp *et al.*, 2016; Janezic *et al.*, 2019).

Tunicamycin Treatment. HEK293 cells were transfected with WT SNAP-α_{1D}. 24 hr after transfection, cells were washed 3X with PBS, and incubated with media containing 5 ug/mL of tunicamycin or 95% EtOH vehicle for 16 hr. Following incubation, cells were washed 3X with ice cold PBS, lysed, subjected to SDS PAGE, and analyzed by PAGE NIR as described above.

Bortezomib Treatment. HEK293 cell were transfected with either S-WT-C or S-NQQ-C. 24 hr after trransfections, cells were treated with 1 μM of bortezomib or DMSO vehicle for 24 hr. Following treatment, cells were lysed and lysate analyzed via PAGE NIR.

Protease Inhibitor Treatment. HEK293 cell were transfected with either S-WT-C or S-NQQ-C. 24 hr after trransfections, cells were treated with of Pierce™ Protease Inhibitor cocktail (Thermo Scientific, Rockford, IL) using a 1:200 dilution or vehicle for 24 hr. Cells were then lysed and lysates were analyzed using PAGE NIR analysis.

SNAP MS/MS. HEK293 cells were transiently transfected with either WT or NQQ SNAP-α_{1D} for 48 hrs. Cells were collected and lysed as above, with the addition of end-over-end rocking for 2 hrs. at 4°C prior to centrifugation to remove insoluble fraction. Each condition was divided into 4 1.5 mL tubes for 16 hr. incubation with 20 µL of packed SNAP-Capture pull-down resin (New England Biolabs, Ipswich, MA) at 4°C with end-over-end rocking. Beads were washed 3X with lysis buffer, transferred to new 1.5 mL tubes and washed 3X with 20 mM Tris-HCl pH 8.0 and 2 mM $CaCl_2$. After the final wash the saturated beads were incubated with 20 mM Tris-HCl pH 8.0 supplemented with 5 mM DTT for 30 min at 60°C with agitation, followed by incubation with 15 mM iodoacetamide for 10 min at RT. Denatured protein was then incubated with 1.5 µg of Trypsin (Sigma, St. Louis, MO) and 1.5 µg of Glu-C endoprotease (Thermo Fisher Scientific, Waltham, MA) for 16 hr at 37°C with vigorous agitation. Peptides were collected and acidified using formic acid (FA) to a final concentration of 1% FA and desalted using StageTips (Schindelin *et al.*, 2012). Peptides were eluted from StageTips using elution buffer (40% acetonitrile, 1% FA), dried down and re-suspended in 8% acetonitrile, 1% FA. Samples were then loaded on a self-pulled 360 µm OD x 100 µm ID 15 cm column with a 7 µm tip packed with 3 µm Reprosil C18 resin (Dr. Maisch, Germany). Peptides were analyzed by nanoLC-MS in a 90 minutes linear gradient from 6% to 38% buffer B (buffer A: 0.1% acetic acid; buffer B: 0.1% acetic acid, 80% acetonitrile) (Thermo EASY nLC 1200) on an Orbitrap Fusion Lumos Tribrid Mass Spectrometer. Orbitrap FTMS spectra (R = 60 000 at 200 m/z; m/z 350–1600; 7e5 target; max 20ms ion injection time) and Top Speed data-dependent acquisition with 3 second cycle time; HCD MS/MS spectra (R = 30 000 at 200 m/z; 31% CE; 5e4 target; max 100 ms injection time) were collected with an intensity filter set at 2.5e4 and dynamic exclusion for 45

second. Mass spectra were searched against the UniProt human reference proteome downloaded on February 20th, 2020 with the addition of SNAP-tag-ADRA1D sequence using MaxQuant v1.6.10.43. Detailed MaxQuant settings: samples were set to fraction 1 and 5 for NQQ mutant and WT, respectively, to allow within-group "match between run"; Trypsin/P and Glu-C were selected in digestion setting. Other settings were kept as default.

Label free dynamic mass redistribution (DMR) assay. DMR assays were performed in 384-well Corning Epic microsensor plates (Corning, Corning, NY) using previously described protocols (Camp *et al.*, 2016; Kountz *et al.*, 2016; Harris *et al.*, 2017; Janezic *et al.*, 2019). Data were analyzed using GraphPad Prism (La Jolla, CA).

Cell surface assay. Cell surface assay was performed as described previously (Kountz *et al.*, 2016; Camp *et al.*, 2016; Janezic *et al.*, 2019).

Sucrose Density Centrifugation. Cells (~6.7M cells/mL) were suspended in detergent-free lysis buffer (1 mM Tris-HCl pH 7.4, 140 mm NaCl, 10% sucrose) on ice for 20 min with vortexing every 5 min. 19 μL of lysate (~125,000 cells) was labeled with BG-782 at 37°C. Reacted lysate was gently layered on top of a discontinuous sucrose gradient. Gradient consisted of equal volumes of 65%, 62.5%, 60%, 57.5%, 55%, 52.5%, 50%, and 15% sucrose dissolved in 1 mM Tris-HCl pH 7.4 and 140 mM NaCl. Samples were centrifuged at 134,633 x *g* at 4°C for 65 min using a TH-660 rotor (Thermo Fisher Scientific, Waltham, MA). 400 μL fractions were collected and subjected to PAGE NIR analysis. Fluorescence of each fraction was quantified (NIR: λ = 800 nm) using Image Studio software (LI-COR, Lincoln, NE) and analyzed using area under the

curve (AUC) analysis with a cut-off of 10% and minimum change in height of 5% from minimum to maximum in GraphPad Prism (La Jolla, CA).

Confocal Microscopy. 48 hours after transfection, cells were fixed with 4% paraformaldehyde/PBS solution for 10 min at room temperature, washed with PBS, and permeabilized in 0.1% TritonX-100/PBS for 1 min. Cells were incubated with 1 μM of SNAP Surface Alexa Fluor 488 (New England BioLabs #S9129S) and 1:1000 ER Staining Kit-Red Fluorescence- Cytopainter (Abcam #139482, Cambridge, MA) at 37°C for 30 minutes protected from light. Hoechst 33342 was used for nuclear staining. Cover slips were mounted using ProLong Glass antifade reagent (ThermoFisher #P36982). Confocal fluorescence microscopy was performed using Leica SP8X laser scanning confocal microscope equipped with a 40x oil immersion objective (Leica Camera, Wetzlar, Germany). The detection pinhole was set to 1 Airy unit, light collection configuration was optimized according to the combination of chosen fluorochromes (Alexa Fluor 488, Texas Red, and Hoechst), and sequential channel acquisition was performed to minimize the risk of bleed-through. The intensity gain was adjusted for each channel before capture in order to avoid saturated pixels. 8 bit, 1024x1024 pixel images were collected as Z-stack acquisition. All microscopy was performed in collaboration with the W.M. Keck Microscopy center on the University of Washington School of Medicine campus.

Colocalization analysis. The Alexa Fluor 488 (SNAP) and Texas Red (ER) channels were analyzed for colocalization using Coloc2 plugin for Fiji (Schindelin *et al.*, 2012). Pearson's coefficients for a cell were averaged over each slice in a Z-stack. Data were analyzed using GraphPad Prism (La Jolla, CA).

3.3 Results and Discussion

N-terminal glycosylation is required for complete α_{1D}-AR biogenesis

The α_{1D}-AR N-terminal contains two putative *N*-glycosylation sites (N65, N82) with both serving as theoretical acceptors for *N*-glycans within the ER lumen (Perez *et al.*, 1991). *N*-glycosylation is the covalent attachment of an *N*-glycan sugar moiety to an asparagine residue within the consensus sequence N-X-S/T, where X is any amino acid except proline (Helenius *et al.*, 1994; Imperiali *et al.*, 1999). Thus, we first sought to examine the glycosylation state of full length α_{1D}-AR using lentil lectin affinity purification. Lentil lectin recognizes complex glycans containing α-(1→6)-linked fucose on the core GalNAc as well as glucose and/or α-mannose residues (Kornfeld *et al.*, 1981; Debray *et al.*, 1981). To test this possibility, HEK293 cells were transiently transfected with N-terminal SNAP-epitope tagged α_{1D}-AR cDNA constructs (SNAP-α_{1D}). We have previously demonstrated the SNAP epitope-tag facilitates visual analysis of GPCR protein bands directly within polyacrylamide gels, and do not require nitrocellulose paper transfer or antibody staining, thus removing all potential false positive bands (Kountz *et al.*, 2016; Camp *et al.*, 2016; Janezic *et al.*, 2019). Incorporating this powerful technology, HEK293 cell lysates expressing SNAP-α_{1D} were incubated with lentil lectin sepharose beads. Samples were eluted and subjected to polyacrylamide gel electrophoresis, followed by near infrared imaging (PAGE NIR). Shown in Figure 3.1 are the results. In agreement with our previous studies (Kountz *et al.*, 2016; Janezic *et al.*, 2019), the input lane demonstrates full length SNAP-α_{1D} is robustly expressed as a monomeric band at ~80 kDa, a larger, more intense band at ~90 kDa (Figure 3.1A, *arrow*), as higher order oligomers (MW > 180 kDa), and as multiple NTD cleavage products (MW = ~30-35 kDa). Remarkably, the larger ~90 kDa monomeric and

multimeric SNAP-α_{1D} species were detected in the lectin bound lane (Figure 3.1A, bound). Although faint, the largest α_{1D} NTD cleavage product (Kountz *et al.*, 2016) was also observed in the lectin-bound sample. Thus, this experiment clearly demonstrates, for the first time, that the α_{1D} NTD is *N*-glycosylated.

Towards our goal of addressing the importance of each NTD glycosylation site for α_{1D}-AR function, we created single (N65Q or N82Q) and double (NQQ) glycosylation deficient SNAP-α_{1D} mutants using PCR site-directed mutagenesis (see Figure 3.1B for schematic). To ensure each α_{1D}-AR NTD mutant was expressed as protein, cDNA constructs were transfected into HEK293 cells and subjected to PAGE NIR analysis. Both the N65Q and N82Q SNAP-α_{1D} NTD mutants display equivalent protein band patterns as SNAP-α_{1D} (Figure 3.1C). Unexpectedly, the NQQ SNAP-α_{1D} double mutant did not produce monomeric or higher order oligomeric bands. Instead, NQQ SNAP-α_{1D} was primarily expressed as a single, robust band of ~43 kDa in size. Subtracting the size of the SNAP-epitope tag plus linker (25 kDa) yields a polypeptide of 18 kDa, – roughly equivalent in size to the α_{1D} NTD, transmembrane domain (TM) 1, intracellular loop 1, and TM2. To ensure this unexpected NQQ product was due to inhibition of glycosylation, and not a by-product of mutation, cells expressing WT SNAP-α_{1D} were treated with tunicamycin – an inhibitor of *N*-glycosylation (Guillemette *et al.*, 2011). 24 hours after transfection with WT SNAP-α_{1D}, HEK293 cells were treated with fresh media supplemented with 5μg/mL tunicamycin or EtOH vehicle followed by PAGE NIR (Figure 3.1D). Interestingly, though faint, the same ~43 kDa species observed in the NQQ SNAP-α_{1D} is also present in the tunicamycin treated samples (Figure 3.1D; *circle*). Thus, this initial round of experiments demonstrates that (A) α_{1D}-AR is glycosylated at N65 and N82; (B) only a single glycosylation

site needs to be available for the NTD to become glycosylated and full length α_{1D} protein processing to occur; and (C) removal of both α_{1D} NTD glycosylation sites not only prevents glycosylation, but produces an abnormally short, previously unreported α_{1D}-AR peptide species.

We next tested two potential explanations for this serendipitous, intriguing result: (A) the NQQ double mutation introduces a destabilizing effect, causing the α_{1D}-AR to be targeted for degradation, with the observed 43 kDa band representing the major degradation product; or (B) NQQ is inhibiting proper translation of α_{1D}-AR, causing an early termination after TM2. These hypotheses were tested using a dual epitope-tagging approach. InFusion PCR was used to add C-terminal CLIP-epitope tags to WT SNAP-α_{1D} (S-WT-C) and NQQ SNAP-α_{1D} (S-NQQ-C). CLIP is a homolog of SNAP that covalently interacts with benzylcytosine conjugates, displaying no cross-reactivity for the SNAP substrate, benzylguanine (Schultz and Köhn, 2008). We reasoned that if A is true, CLIP substrate fluorescence in the 700 channel (red) would be observed in both the S-WT-C and S-NQQ-C PAGE NIR lanes. Conversely, we would expect to detect no 700 signal in the S-NQQ-C lane if B were true, as the CLIP tag would not be transcribed if α_{1D}-AR translation was halted at TM2. Thus, S-WT-C and S-NQQ-C α_{1D}-AR cDNA constructs were expressed in HEK293 cells and subjected to PAGE NIR analysis. Figure 3.1E shows that overlapping CLIP (red) and SNAP (green) substrate signals are detectable in the S-WT-C lane (left). Contrarily, no CLIP signal is observed in the S-NQQ-C lane, and only the previously observed 43 kDa SNAP-α_{1D} species.

As an orthogonal approach, HEK293 cells expressing either S-WT-C or S-NQQ-C were incubated with bortezomib (BTZ) – a proteasomal inhibitor (Figures 3.1F,G) – or protease inhibitor (PI) cocktail (Figures 3.1I, J) for 24 hours followed by PAGE NIR analysis. As expected, significant increases of S-WT-C and S-NQQ-C protein bands were observed with BTZ

treatment (Figure 3.1H; S-WT-C = 166.3 ± 4.3%, mean ± SEM of vehicle; S-NQQ-C = 186.3 ± 6.0% mean ± SEM of vehicle; Unpaired t test; $p < 0.001$), but not with PI cocktail treatment (Figure 3.1K; S-WT-C = 96.7 ± 0.3%, mean ± SEM of vehicle; S-NQQ-C = 97.0 ± 2.5%, mean ± SEM of vehicle; Unpaired t test, $p > 0.05$). However, neither BTZ nor PI cocktail had any discernable effect on the molecular weight of the NQQ band; nor were CLIP signals observed in either condition. Taken together, these findings indicate that the NQQ α_{1D}-AR species is not created by proteolytic cleavage and/or degradation of full-length α_{1D}-AR.

To further confirm the identity of this unexpected NQQ species, HEK293 cells were transiently transfected with either WT SNAP-α_{1D} or NQQ SNAP-α_{1D}, lysed, and SNAP-fusion proteins were isolated with SNAP-Capture beads. Due to the covalent nature of the SNAP-Capture:SNAP-tag, an on-bead digest was performed using Trypsin and Glu-C proteases. Samples were subjected to MS/MS analysis (SNAP MS/MS). As shown in Figure 3.2A, identified peptides spanned the entirety of the WT SNAP-α_{1D} (Figure 3.2A, *underlined*). Contrarily, only peptides in the N-terminal domain were identified in NQQ SNAP-α_{1D} samples (Figure 3.2B, *underlined*). Furthermore, previously reported α_{1D}-AR interactors syntrophin (Chen *et al.*, 2006; Lyssand *et al.*, 2011; Camp *et al.*, 2015), members of the dystrophin-associated protein complex (Lyssand *et al.*, 2010), and scribble (Camp *et al.*, 2015; Janezic *et al.*, 2019) were identified in the WT, but not NQQ samples (Table 3.1). Together, these data provide compelling evidence that glycosylation of both N65 and N82 are necessary for proper biogenesis of full-length α_{1D}-AR, and disruption of these essential glycosylation sites results in early termination of α_{1D}-AR processing after TM2.

Glycosylation imparts α_{1D}-AR function and plasma membrane insertion

The effects of NTD glycosylation on GPCR function and trafficking are highly divergent. Mutating N-terminal glycosylation sites decreases functional responses of the FSH (Davis *et al.*, 1995), dopamine D2 (Cho *et al.*, 2012), and neurokinin 1 receptor subtypes (Tansky *et al.*, 2007), while loss of glycosylation has no effect on the function of the histamine H2 receptor (Fukushima *et al.*, 1995). Conversely, blocking N-terminal glycosylation increases binding site density of the human oxytocin receptor (Kimura *et al.*, 1997), and signaling efficacy of the vasopressin 1A receptor (Hawtin *et al.*, 2001). To understand how *N*-glycosylation impacts α_{1D}-AR function, label-free dynamic mass redistribution (DMR) assays were used to quantify the efficacy of the α_1-AR agonist phenylephrine for stimulating α_{1D} NTD glycosylation site mutants. HEK293 cells expressing WT, N65Q, N82Q, or NQQ SNAP-α_{1D} were seeded in 384-well DMR plates and incubated with increasing concentrations of phenylephrine to facilitate concentration-response curve analysis (Figure 3.3A; Table 3.2). Surprisingly, phenylephrine maximal responses for N65Q (24.99 ± 11.35 pm, mean ± SEM; Table 3.2), N82Q (46.64 ± 9.96 pm, mean ± SEM), and NQQ (45.20 ± 8.35 pm, mean ± SEM) were significantly lower than WT SNAP-α_{1D} (112.5 ± 9.27, mean ± SEM; $p < 0.01$, One-way ANOVA with Tukey's multiple comparisons post-hoc test).

Glycosylation has been shown to facilitate plasma membrane trafficking of the angiotensin II type 1 (Lanctôt *et al.*, 1999), GPR30 (Gonzalez de Valdivia *et al.*, 2019), rhodopsin 1 (Webel *et al.*, 2000), δ-opioid receptor (Petäjä-Repo *et al.*, 2000; Markkanen *et al.*, 2008; Lackman *et al.*, 2014), and $P2Y_2$ receptor subtypes (Nakagawa *et al.*, 2007). Therefore, one possible explanation for the reduced function of α_{1D} NTD glycosylation mutants may be aberrant cellular trafficking, leading to a decrease in cell surface expression. This was examined by quantifying WT, N65Q,

N82Q and NQQ SNAP-α_{1D} plasma membrane expression levels in fixed HEK293 cells treated with the cell-impermeable SNAP substrate, BG-782 (Figure 3.3B, C; Camp *et al.*, 2016; Kountz *et al.*, 2016; Janezic *et al.*, 2019). Cells were also treated with nuclear stain TO-PRO-3 to normalize for cell number. We observed significant reductions in N65Q (13.40 ± 4.65%, mean ± SEM change from SNAP), N82Q (9.49 ± 5.95%, mean ± SEM change from SNAP), and NQQ (13.64 ± 5.76%, mean ± SEM change from SNAP) cell surface expression in comparison to WT SNAP-α_{1D} (46.13 ± 5.61%, mean ± SEM change from SNAP; $p < 0.01$, One-way ANOVA with Tukey's multiple comparisons post-hoc test). Combined, these data strongly indicate both N65 and N82 must be glycosylated to facilitate α_{1D}-AR plasma membrane insertion and agonist-stimulated functional responses in cultured human cells.

TM2 of α_{1D}-AR triggers ER translocation during protein synthesis

TM1 domain is thought to provide the ER localization signal for myriad polytropic integral membrane proteins – including GPCRs – during protein synthesis (Chitwood *et al.*, 2018). Though, synthesis of TM2 has also been shown to trigger ribosomal translocation to the ER for some multi-pass transmembrane proteins, such as Cig30 (Monné *et al.*, 1999; Monné *et al.*, 2005) and ProW (Nilsson *et al.*, 2000). Because the α_{1D}-AR NQQ mutant appears to cause early termination after TM2 (Figure 3.1C, E, G, J, Figure 3.2), we hypothesized that TM2 acts as the ER localization signal for α_{1D}-ARs. To test this, we utilized two orthogonal, but complementary, approaches: sucrose density gradient and confocal imaging.

Previous studies examining α_1-AR subcellular localization used cell fractionation/sucrose density gradient to sequester distinct cellular compartments, and then radioligand binding to quantify the number of receptors present in each compartment sample (Hague *et al.*, 2004).

Although useful, this method is only able to detect properly folded, functional receptors that are able to bind ligand; and has non-optimal signal-to-noise ratios (Hague *et al.*, 2004). Thus, sucrose density centrifugation protocols were modified to incorporate the sensitivity of SNAP-epitope tag PAGE NIR imaging analysis. This novel experimental approach allows accurate detection of poorly expressing α_{1D}-AR peptide species, regardless of their structural or functional state. Furthermore, the use of the SNAP epitope tag displays increased sensitivity compared to traditional immunoblotting techniques, which can be limited by the inability of antibodies to detect low expression levels of endogenous protein markers (Cole, 2013). Thus, HEK293 cells were transfected with SNAP-α_{1A}-AR, which we have previously shown expresses readily at the plasma membrane (Hague *et al.*, 2004), or SNAP-Sec61β, an ER integral membrane protein (Kopito, 1997). Cells were lysed in detergent free buffer then conjugated to SNAP substrate BG-782. Labelled lysates were then fractionated in a discontinuous gradient, collected, and subjected to PAGE NIR analysis. In each case, the detectable SNAP signal from each isolated fraction was normalized to input. Data were analyzed by area under curve (AUC) to quantify the distribution of each SNAP protein in specific fractions. Figure 3.4 displays the PAGE NIR band pattern for SNAP-α_{1A} (Figure 3.4A) and SNAP-Sec61β (Figure 3.4B). Subsequent AUC analysis revealed SNAP-Sec61β to be primarily distributed in fractions 1 through 4 with a peak in fraction 2 (91.50% total AUC; Figure 3.4C), which is considered to be the ER fraction (Hague *et al.*, 2004). Conversely, SNAP-α_{1A} is significantly concentrated in fractions 6 through 9 with the maximum signal in fraction 7 (100% total AUC).

Next, WT, N65Q, N82Q and NQQ SNAP-α_{1D} cDNA constructs were examined (Figure 3.5A-D). As expected based on the findings of previous studies performed by us and others (Hague *et al.*, 2004; Petrovska *et al.*, 2005; Garcia-Cazarin *et al.*, 2008), WT SNAP-α_{1D} (Figure

3.5A) displayed a similar distribution pattern as SNAP-Sec61β, with a major peak spanning from fractions 1 to 4 (92.47% total AUC; Figure 3.5E) and a minor peak in fractions 6 to 8 (7.53% total AUC). Similarly, N65Q SNAP-α_{1D} (Figure 3.5B) was bi-modally distributed, with peaks in fractions 1 to 3 (46.33% total AUC) and fractions 5 to 7 (53.67% total AUC; Figure 3.5E). N82Q SNAP-α_{1D} (Figure 3.5C) was largely concentrated in fractions 1 through 4 with the maximum signal in fraction 2 (89.13% total AUC). A minor peak was also observed in fractions 6 to 7 (10.87% AUC; Figure 3.5E). Remarkably, NQQ SNAP-α_{1D} (Figure 3.5D) formed a single, strong peak spanning fractions 1 to 3, with the majority of the protein concentrated to the first fraction (100% total AUC; Figure 3.5E), which corresponds with a primarily cytosolic localization.

These findings were subsequently corroborated with confocal microscopy imaging analysis. HEK293 cells were transiently transfected with WT (Figure 3.6A-D), N65Q (Figure 3.6E-H), N82Q (Figure 3.6I-L), NQQ (Figure 3.6M-P) SNAP-α_{1D}, or empty pSNAP vector (SNAP; Figure 3.6Q-T). Cells were fixed with paraformaldehyde and detergent-permeabilized, then incubated with SNAP substrate Alexa Fluor 488 to label SNAP proteins and red fluorescence-Cytopainter stain to label the ER. Visual analysis reveals robust puncta of WT (Figure 3.6D), N65Q (Figure 3.6H), and N82Q (Figure 3.6L) SNAP-α_{1D} within the ER. Contrarily, both NQQ SNAP-α_{1D} (Figure 3.6P) and SNAP (Figure 3.6T) are diffuse throughout the cell cytosol and nucleus. Colocalization quantification analysis (Figure 3.6U) revealed a significant correlation between WT (Pearson's coefficient = 0.72 ± 0.03, mean ± SEM, $p < 0.001$ from SNAP, $p < 0.01$ from NQQ), N65Q (Pearson's coefficient = 0.70 ± 0.04, mean ± SEM, $p < 0.001$ from SNAP, $p < 0.01$ from NQQ), and N82Q (Pearson's coefficient = 0.53 ± 0.07, mean ± SEM, $p < 0.001$ from SNAP, $p < 0.01$ from NQQ) SNAP-α_{1D} constructs with ER stain CytoPainter, when

compared with NQQ SNAP-α_{1D} (Pearson's coefficient = 0.19 ± 0.03, mean ± SEM, p = 0.12 from SNAP) and SNAP (Pearson's coefficient = 0.03 ± 0.05, mean ± SEM). Together, our cell fractionation and confocal microscopy data support the hypothesis that α_{1D}-AR requires the synthesis of TM2 prior to ER localization, where the N-terminal translocates into lumen, becomes glycosylated, and translation continues. If this does not occur, translation is prematurely terminated and the non-functional polypeptide is likely degraded via the ER-associated degradation (ERAD) pathway (Kopito, 1997; Huang *et al.*, 2006; Brodsky, 2012; Neal *et al.*, 2018). Further studies are necessary to determine the extent to which this mechanism is involved in the turnover of nascent α_{1D}-AR and other GPCRs.

Abbreviations: GPCR, G protein-coupled receptor; AR, adrenergic receptor; PTSD, post-traumatic stress disorder; PDZ, PSD-95/Dlg/ZO-1; NTD, N-terminal domain; ER, endoplasmic reticulum; WGA, Wheat germ agglutinin; HEK, human embryonic kidney; RPM, rotations per minute; DMR, dynamic mass redistribution; PBS, phosphate buffered solution; WT, wild-type; TM, transmembrane domain; FSH, follicle stimulating hormone; AUC, area under the curve; ERAD, endoplasmic reticulum-associated degradation

Figures for Chapter 3

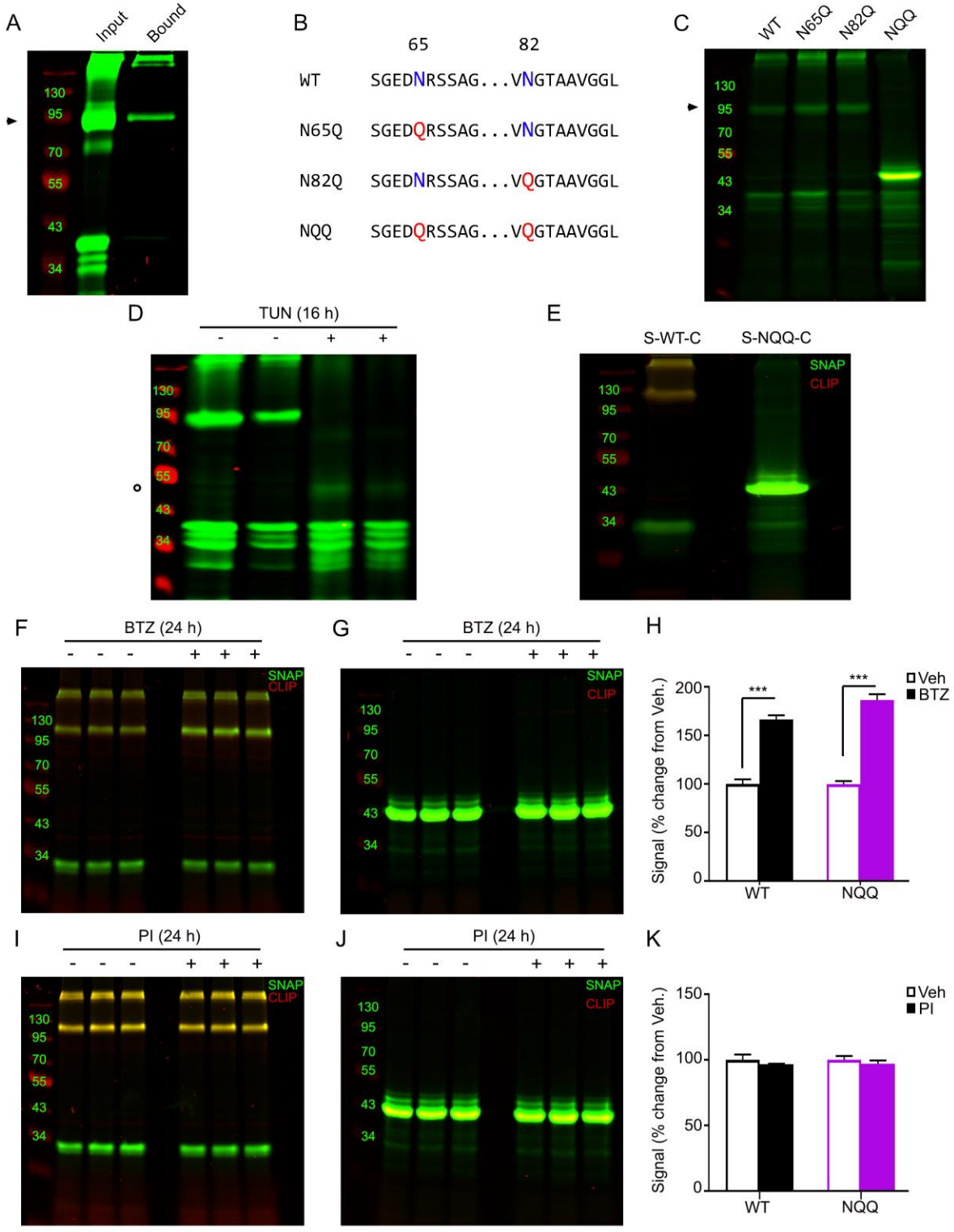

Figure 3.1. Site-directed mutagenesis and lectin affinity purification analyses reveal α_{1D}-AR is dually glycosylated at N65 and N82. (A) Lysate from HEK293 cells expressing WT SNAP-

α_{1D} (*input*) was incubated with lentil lectin sepharose beads to isolate glycosylated proteins. Bound protein was eluted with methyl-α-D-mannopyranoside (*bound*), and analyzed using PAGE NIR. SNAP-α_{1D} monomers (►) and higher order oligomers, as well as the previously described N-terminal cleavage product, are present in the elutant. (B) Schematic and (C) PAGE NIR of HEK293 cell lysate expressing WT, single glycosylation mutants (N65Q and N82Q), and double glycosylation mutant (NQQ) SNAP-α_{1D} species. (D) HEK293 cells expressing WT SNAP-α_{1D} were incubated for 16 hr with vehicle (-) or tunicamycin (TUN, +), and analyzed with PAGE NIR. A signal at 43 kDa was observed in the tunicamycin treated samples (○). (E) PAGE NIR of HEK293 cell lysate transfected with N-terminal SNAP-epitope ($\lambda = 800$ *nm, green*) and C-terminal CLIP-epitope ($\lambda = 700$ *nm, red*) dual tagged WT (S-WT-C) and NQQ (S-NQQ-C) α_{1D}-AR constructs. (F, I) PAGE NIR of HEK293 cell lysate expressing S-WT-C or (G, J) S-NQQ-C following 24 hr bortezomib (BTZ) (F, G) or protease inhibitor (PI) treatment (I, J). (H) Quantitation of signals from F and G normalized to vehicle. (K) Quantitation of fluorescent signals from I and J normalized to vehicle. All gels are representative images from n = 3 experiments. For F and G, data are represented as mean ± SEM; Unpaired t tests, *** = $p < 0.001$.

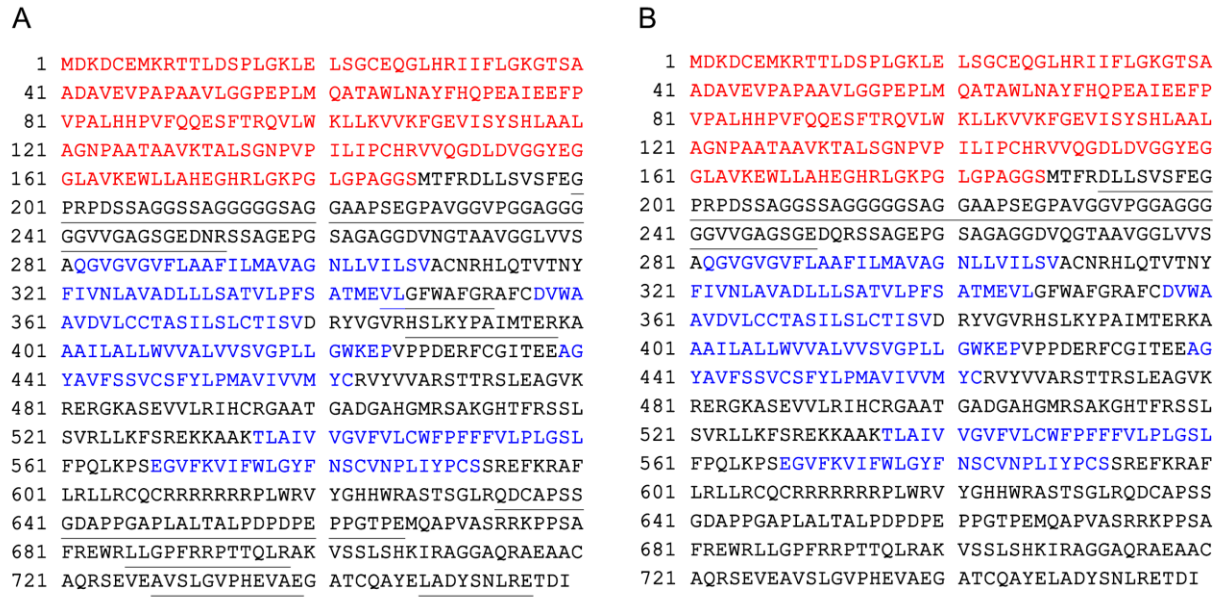

Figure 3.2. SNAP MS/MS analysis identifies distal peptides in WT, but not NQQ SNAP-α_{1D} lysates. (A) WT or (B) NQQ SNAP-α_{1D} was purified from HEK293 lysate using SNAP-Capture pull-down resin, then subjected to on-bead double-enzymatic digestion, and MS/MS analysis. Red text indicates SNAP-epitope tag. Blue text indicates transmembrane domains. Peptides identified in MS/MS analysis are underlined.

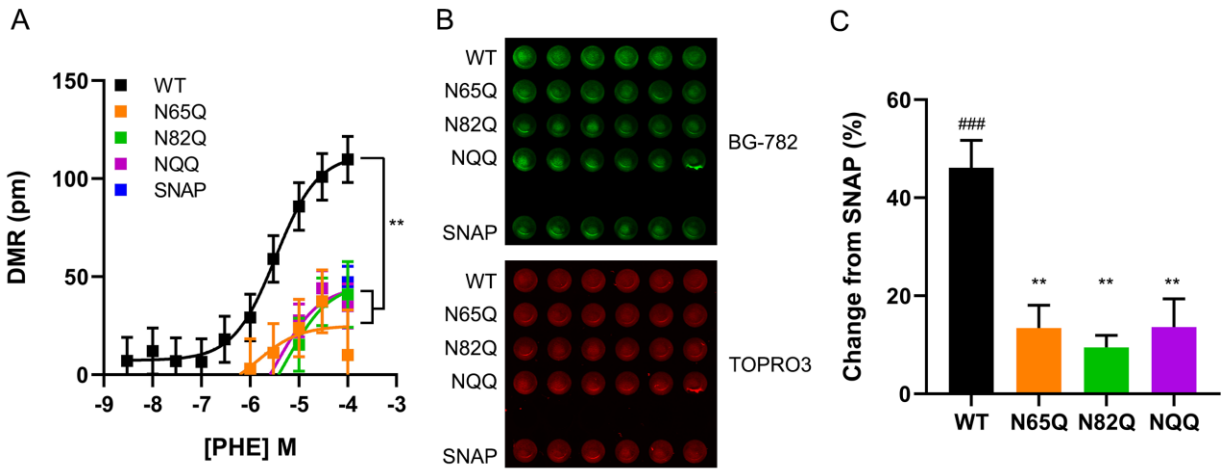

Figure 3.3. α_{1D}-AR function and plasma membrane insertion is glycosylation dependent. (A) Dynamic mass redistribution assays quantifying phenylephrine efficacy in HEK293 cells transfected with WT, N65Q, N82Q, or NQQ SNAP-α_{1D}. Data are the mean of 8 replicates ± SEM; ** = $p < 0.01$ E_{max} from WT. (B) Cell surface expression of WT, N65Q, N82Q, or NQQ SNAP-α_{1D} in fixed HEK293 cells labeled with the cell impermeable SNAP substrate, BG782 (*top panel*, *green*); nuclear stain, TO-PRO-3 was used to normalize for cell numbers (*bottom panel*, *red*). (C) Fluorescence intensity of data from B was normalized to cells expressing SNAP alone. Data are mean of 6 replicates ± SEM; One-way ANOVA with Tukey's multiple comparisons post-hoc tests, ** = $p < 0.01$ from WT SNAP-α_{1D}; ### = $p < 0.001$ from empty SNAP.

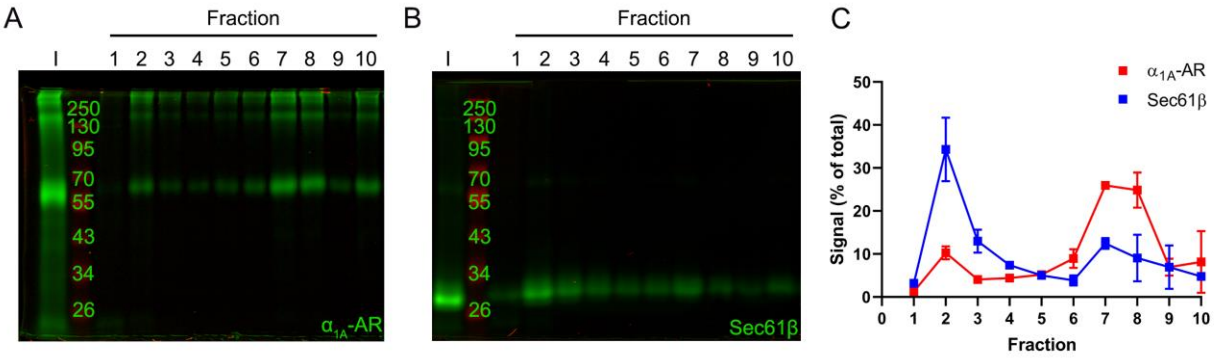

Figure 3.4. Sucrose density centrifugation of SNAP-epitope tagged plasma membrane and endoplasmic reticulum markers. HEK293 cell lysates expressing (A) SNAP-α_{1A}-AR (*plasma membrane)* or (B) SNAP-Sec61β (*endoplasmic reticulum*) were labeled with SNAP substrate, BG-782, fractionated by discontinuous sucrose density gradient centrifugation, and analyzed using PAGE NIR. I = input. (C) Quantification of fluorescence signal from A and B normalized to respective inputs. Data are mean of 2 experiments ± SEM.

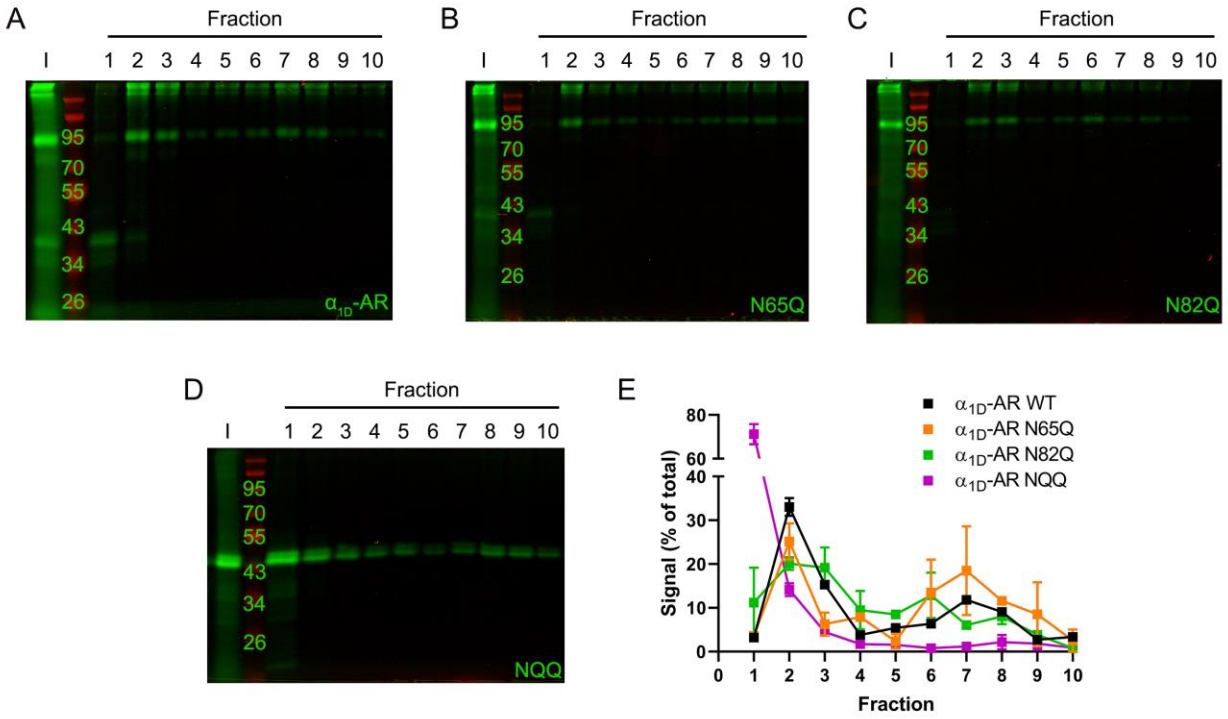

Figure 3.5. Sucrose density centrifugation of WT and glycosylation deficient SNAP-α_{1D} constructs. Representative PAGE NIR of HEK293 cell lysates transfected with (A) WT, (B) N65Q, (C) N82Q, or (D) NQQ SNAP-α_{1D} following sucrose density centrifugation. I = input. (E) Quantification of band intensity from A-D normalized to respective inputs. Data are presented as mean of 3 experiments ± SEM.

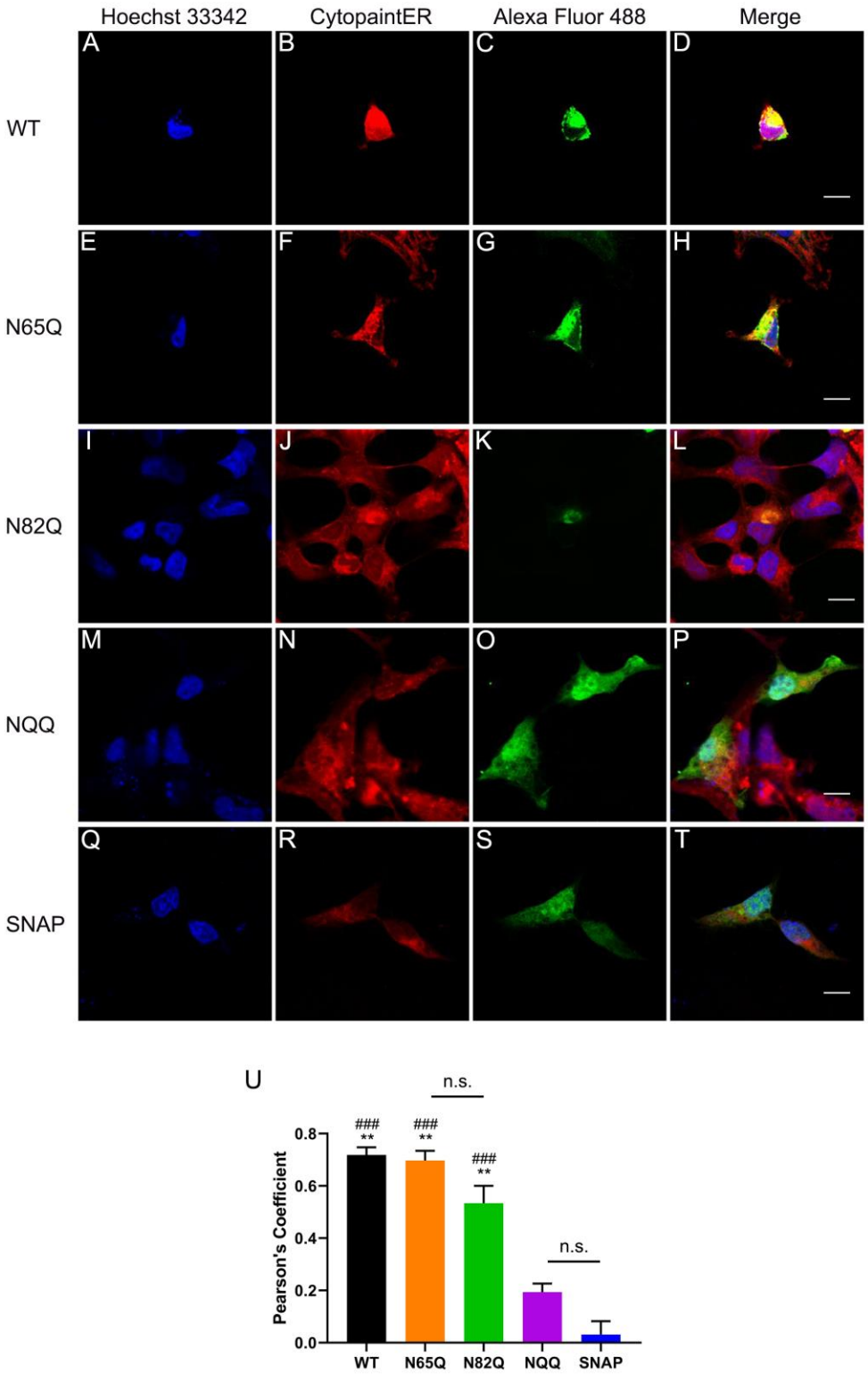

Figure 3.6. Confocal imaging reveals NQQ SNAP-α_{1D} is localized to cytosol and nucleus in HEK293 cells. HEK293 cells transfected with (A-D) WT, (E-H) N65Q, (I-L) N82Q, (M-P)

NQQ SNAP-α_{1D}, or (Q-T) empty pSNAP vector were fixed, stained for Hoechst 33342 (*blue*), fluorescence-Cytopainter stain (*red*), and SNAP-epitope tag (*BG-488; green*), and imaged using confocal microscopy. Right panels are merged images of three channels. Scale bar = 10 μm. (U) Pearson's coefficients of SNAP and ER fluorescence signals were computed to measure the extent of colocalization. Data are mean of 5-6 cells ± SEM; One-way ANOVA with Tukey's multiple comparisons post-hoc tests, ### = $p < 0.001$ compared to empty SNAP; ** = $p < 0.01$ compared to NQQ SNAP-α_{1D}, n.s = $p > 0.05$.

Tables for Chapter 3

Protein	NQQ 1	NQQ 2	NQQ 3	WT 1	WT 2	WT 3
DMD	--	--	--	9385000	20429000	7117900
DLG1	--	--	--	573890	896640	457710
SCRIB	--	--	--	1.44E8	1.55E8	93057000
SNTB1	--	--	--	12735000	41530000	17520000
DTNB	--	--	--	15780000	24201000	6457700
UTRN	--	--	--	5873000	89238000	46644000
SNTB2	--	--	--	87584000	1.25E8	66987000
CTNNAL1	--	--	--	1037700	1612800	726370
DTNA	--	--	--	2523400	4069500	1048900

Table 3.1. Previous reported α_{1D}-AR PDZ interactors identified by SNAP MS/MS. Data shown include protein gene name and intensity for each replicate.

α_{1D}-AR Construct	Maximal DMR Response (pm)
WT	112.5 ± 9.27
N65Q	24.99 ± 11.35
N82Q	46.64 ± 9.96
NQQ	45.20 ± 8.35

Table 3.2. Maximal phenylephrine stimulated DMR response in α_{1D}-AR glycosylation mutants. Data is shown as the average of 8 replicates ± SEM.

Chapter 4 – Final Conclusions

4.1 Scribble PDZ domains 1 and 4 anchor multiple α_{1D}-AR homodimers

The data presented in Chapter 2 strongly suggests that α_{1D}-CT is capable of binding each SCRIB PDZ domain, but preferentially interacts with SCRIB PDZ1 and PDZ4. Also, the α_{1D}-CT:SCRIB interaction appears to be co-operative, potentially driving multiple α_{1D}-AR PDZ ligands to bind one molecule of SCRIB. Though further studies are necessary, we predict that binding to PDZ1 increases the affinity of PDZ2 for the α_{1D}-AR PDZ ligand. Similarly, we hypothesize that interacting with PDZ4 of Scribble increases the ability of PDZ3 to bind α_{1D}-AR. We previously reported α_{1D}-ARs can be expressed as modular homodimers in human cells, with one α_{1D}-AR protomer bound to SCRIB, the other to syntrophin and the DAPC (Camp *et al.*, 2015). Based on the results of the present study, it is possible that α_{1D}-AR homodimers interact simultaneously with both SCRIB PDZ1 and PDZ4, with at least one α_{1D}-AR protomer interacting with the syntrophin:DAPC via the non-SCRIB bound PDZ ligand, and the other bound to a second syntrophin:DAPC module, or the DLG:CASK:LIN-7A tripartite complex (Butz *et al.*, 1998; Borg *et al.*, 1998; Lee *et al.*, 2002; hypothetical schematic of α_{1D}-AR:SCRIB:DAPC shown in Figure 4.1). Alternatively, an α_{1D}-AR protomer may bind another SCRIB, anchoring interconnected α_{1D}-AR:SCRIB:DAPC complexes at the plasma membrane in human cells. If true, this would mean Scribble can potentially anchor up to four α_{1D}-AR homodimers at the cell membrane creating a ‘micro-domain’ of α_{1D}-AR signaling. Finally, we demonstrate that SCRIB $R1110^{PDZ4}$ serves as a unique α_{1D}-CT interface site that could be targeted to modulate α_{1D}-AR pharmacodynamics.

4.2 Transmembrane domain 2 of α_{1D}-AR triggers ribosomal translocation

Our findings presented in Chapter 3 support a model in which TM2, not TM1, triggers ribosomal translocation to the ER during α_{1D}-AR synthesis (Monné *et al.*, 1999; Nilsson *et al.*, 2000; Monné *et al.*, 2005; Öjemalm *et al.*, 2012). Upon docking with the ER, the N-terminus is translocated into the ER lumen – possibly via the ER protein complex (Chitwood *et al.*, 2018; Guna and Hegde, 2018; Guna *et al.*, 2018; Chitwood and Hegde, 2019) – where glycosylation occurs. This event prevents the N-terminus from retrotranslocating back to the cytosol, which anchors the nascent peptide in the ER membrane in the proper membrane topology, such that the N-terminal will be within the extracellular matrix upon plasma membrane insertion. This event is required before complete translation of the nascent polypeptide continues. However, if glycosylation is prevented, the immature receptor does not anchor in the ER membrane, thus terminating receptor translation after TM2 (Figure 4.2 for schematic); and presumably this degenerate polypeptide is degraded via ERAD (Brodsky, 2012) or other cytosolic degradation mechanisms (Petäjä-Repo *et al.*, 2000; 2001). Furthermore, we show that glycosylation of both N65 and N82 is required for proper function and plasma membrane expression of α_{1D}-ARs.

4.3 α_{1D}-AR is a stress receptor

The above studies provide insight into mechanisms regulating function and trafficking of the α_{1D}-AR, but why this receptor is so tightly regulated remains mysterious. However, examining the conditions in which this receptor is studied – along with diseases associated with its dysfunction – may provide some clues. For example, a seminal study identifying the role of α_{1D}-AR in aortic contractions utilized organ tissue bath experiments (Piascik *et al.*, 1995). This requires extraction of the target tissue immediately following sudden death – which is arguably a

stressful event (Tsunoda *et al.*, 1989). Furthermore, the link between hypertension – a disease of increased sympathetic nervous system activity – and stress has been known for >30 years (Heine and Weiss, 1987). Post-traumatic stress disorder arises from heightened sympathetic nervous system activity due to repeated exposure to stress, and is often treated with α_1-AR antagonists (Hendrickson and Raskind, 2016). Thus, I posit that the α_{1D}-AR is a 'stress-receptor' and the intricate regulatory mechanisms (i.e. complex formation, N-terminal cleavage, and glycosylation-dependent biogenesis) allow for a quick mobilization of α_{1D}-AR signalosomes to and from the plasma membrane in response to a stress signal.

Figures for Chapter 4

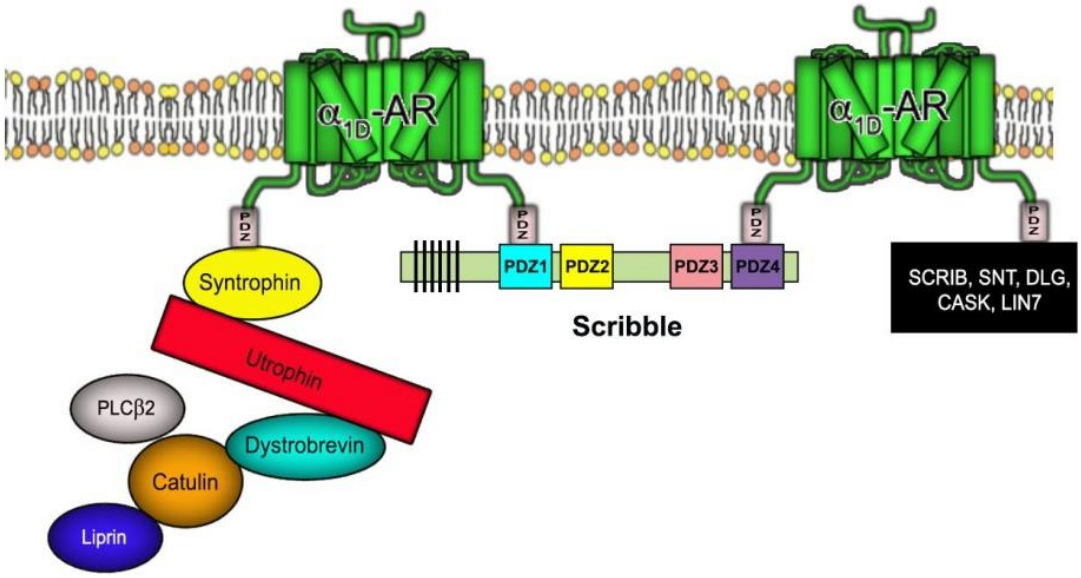

Figure 4.1. Hypothetical model of the α_{1D}-AR:SCRIB:DAPC macromolecular complex in human cells.

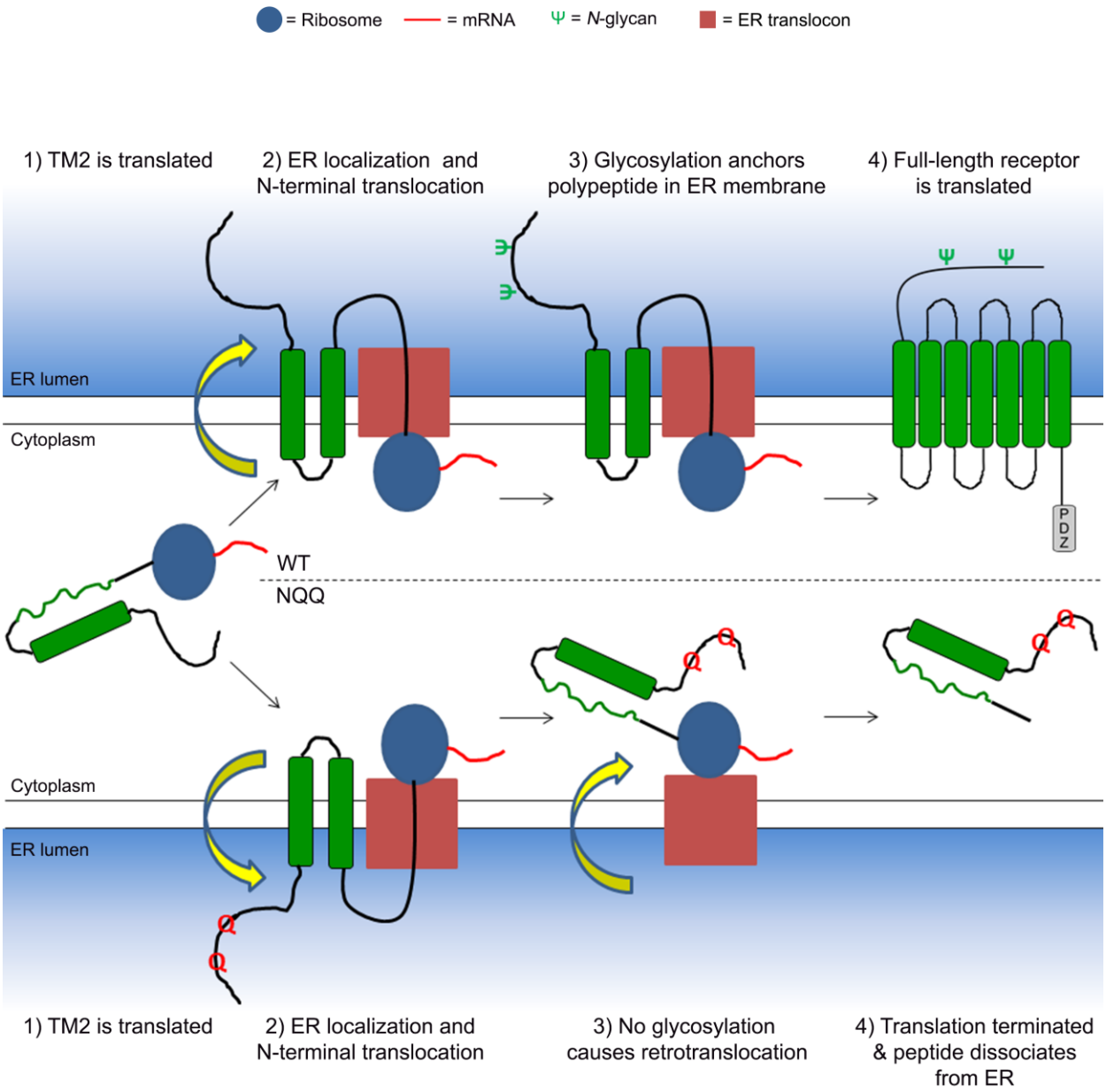

Figure 4.2. Model of proposed role for N-terminal glycosylation on α_{1D}-AR biosynthesis. *Top, WT:* (1) Nascent α_{1D}-AR peptide is translated in the cytoplasm through TM2. (2) Translation is halted as polypeptide, mRNA, and ribosomal complex translocate to the ER, where the N-terminal translocates into the ER lumen. (3) *N*-glycans anchor the immature receptor into the proper topology and ER membrane. (4) Translation continues. *Bottom, NQQ*: (1) Nascent α_{1D}-AR peptide is translated in cytoplasm through TM2. (2) The translation is halted and the ribosome, mRNA, and peptide complex translocates to ER where N-terminal enters ER lumen. (3) Lack of glycosylation causes N-terminal to retrotranslocate. (4) Translation of α_{1D}-AR is terminated and peptide dissociates from ER to likely be degraded.

References

Adams, P.D. *et al.* PHENIX: a comprehensive Python-based system for macromolecular structure solution. *Acta. Crystallogr. D Biol. Crystallogr.* **66**, 213-221 (2010).

Akinaga, J., García-Sáinz, J.A. & Pupo, A.S. Updates in the function and regulation of α_1-adrenoceptors. *Br. J. Pharmacol.* **176**, 2343-2357 (2019).

Andersson, H., D'Antona, A.M., Kendall, D.A., Von Heijne, G. & Chin, C.N. Membrane assembly of the cannabinoid receptor 1: impact of a long N-terminal tail. *Mol. Pharmacol.* **64**, 570-577 (2003).

Babault, N. *et al.* Peptides targeting the PDZ domain of PTPN4 are efficient inducers of glioblastoma cell death. *Structure* **19**, 1518-1524 (2011).

Balasubramanian, S., Teissére, J.A., Raju, D.V. & Hall, R.A. Hetero-oligomerication between GABAA and GABAB receptors regulates GABAB receptor trafficking. *J. Biol. Chem.* **279**, 18840-18850 (2004).

Bang, I. & Choi, H.J. Structural feature of β2 adrenergic receptor: Crystal structures and beyond. *Mol Cells* **38**, 105-111 (2015).

Berridge, M.J. Inositol triphosphate and calcium signaling. *Nature* **361**, 315-325 (1993).

Bjarnadóttir, T.K. *et al.* Comprehensive repertoire and phylogenetic analysis of the G protein-coupled receptors in human and mouse. *Genomics* **88**, 263-273 (2006).

Björklöf, K. *et al.* Co- and posttranslational modification of the α_{1B}-adrenergic receptor: Effects on receptor expression and function. *Biochem*. **41**, 4281-4291 (2002).

Blom, N., Gammeltoft, S. & Brunak, S. Sequence and structure-based prediction of eukaryotic protein phosphorylation sites. *J. Mol. Biol.* **294**, 1351-1362 (1999).

Blumenthal, D.K. Pharmacodynamics: molecular mechanisms of drug action in *Goodman & Gilman's: The pharmacological basis of therapeutics* (eds. Brunton, L.L., Hilal-Dandan, R., Knollmann, B.C.) Ch. 3 (McGraw-Hill, 2017)

Borg, J.P. *et al.* Identification of an evolutionarily conserved heterotrimeric protein complex involved in protein targeting. *J. Biol. Chem.* **273**, 3163-31636 (1998).

Bouchelouche, K. *et al.* Increased contractile response to phenylephrine in detrusor of patients with bladder outlet obstruction: effect of alpha1A and alpha1D-adrenergic receptor antagonist tamsulosin. *J. Urol.* **173**, 657-661 (2005).

Brodsky, J.L. Cleaning up: ER-associated degradation to the rescue. *Cell* **151**, 1163-1167 (2012).

Butz, S., Okamoto, M. & Südhof, T.C. A tripartite protein complex with the potential to couple synaptic vesicle exocytosis to cell adhesion in brain. *Cell* **94**, 773-782 (1998).

Camp, N.D. *et al.* Individual protomers of a G protein-coupled receptor dimer integrate distinct functional modules. *Cell Discov.* **1**, 15011; 10.1038/celldisc.2015.11 (2015).

Camp, N.D. *et al.* Dynamic mass redistribution reveals diverging importance of PDZ-ligands for G protein-coupled receptor pharmacodynamics. *Pharmacol. Res.* **105**, 13-21 (2016).

Carey, L.M. *et al.* Small molecular inhibitors of PSD95-nNOS protein-protein interactions suppress formalin-evoked Fos protein expression and nociceptive behavior in rats. *Neuroscience*. **349**, 303-317 (2017).

Catterall, W.A. Forty years of sodium channels: structure, function, pharmacology, and epilepsy. *Neurochem Res.* **42**, 2495-2504 (2017).

Chen, Z., Hague, C., Hall, R.A. & Minneman, K.P. Syntrophins regulate α_{1D}-adrenergic receptors through a PDZ domain-mediated interaction. *J. Biol. Chem.* **281**, 12414-12420 (2006).

Cherezov, V. *et al.* High resolution crystal structure of an engineered human β_2-adrenergic G protein-coupled receptor. *Science* **318**, 1258-1265 (2007).

Chitwood, P.J., Juszkiewicz, S., Guna, A., Shao, S. & Hegde, R.S. EMC is required to intiate accurate membrane protein topogenesis. *Cell* **175**, 1507-1519 (2018).

Chitwood, P.J. & Hegde, R.S. The role of the EMC during membrane protein biogenesis. *Trends Cell. Biol.* **29**, 371-384 (2019).

Cho, D.I. *et al.* The N-terminal region of the dopamine D2 receptor, a rhodopsin-like GPCR, regulates correct integration into the plasma membrane and endocytic routes. *Br. J. Pharmacol.* **166**, 659-675 (2012).

Collins, S. *et al*. Impaired expression and functional activity of the beta 3- and beta1-adrenergic receptors in adipose tissue of congenitally obese (C57BL/6J ob/ob) mice. *Mol. Endocrinol.* **8**, 518-527 (1994).

Coste, B. *et al.* Piezo1 and Piezo2 are essential components of distinct mechanically activated cation channels. *Science* **330**, 55-60 (2010).

Cotecchia, S., Del Vescovo, C.D., Colella, M., Caso, S., & Diviani, D. The alpha1-adrenergic receptors in cardiac hypertrophy: signaling mechanisms and functional implications. *Cell Signal.* **27**, 1984-1993 (2015)

da Silva, E.S. *et al.* Blockade of median raphe nucleus α1-adrenoceptor subtypes increases food intake in rats. *Pharmacol. Biochem. Behav.* **124**, 350-355 (2014).

Daniels, D. L., Cohen, A. R., Anderson, J. M. & Brünger, A. T. Crystal structure of the hCASK PDZ domain reveals the structural basis of class II PDZ domain target recognition. *Nat. Struct. Biol.* **5**, 317-325 (1998).

Davis, D., Liu, X. & Segaloff, D.L. Identification of the sites of N-linked glycosylation on the follicle-stimulating hormone (FSH) receptor and assessment of their role in FSH receptor function. *Mol. Endocrinol.* **9**, 159-170 (1995).

Debray, H. *et al*. Specificity of twelve lectins towards oligosaccharides and glycopeptides related to N-glycosylproteins. *Eur. J. Biochem*. **117**, 41-55 (1981).

Dicks, M. *et al.* The binding affinity of PTPN13's tandem PDZ2/3 domain is allosterically modulated. *BMC Mol. Cell. Biol.* **20;** 10.1186/s12860-019-0203-6 (2019).

Docherty, J.R. Subtypes of functional α1-adrenoceptor. *Cell. Mol. Life Sci.* **67**, 405-417 (2010).

Doucet, M.V., Levine, H., Dev, K.K. & Harkin, A. Small-molecule inhibitors at the PSD-95/nNOS interface have antidepressant-like properties in mice. *Neuropsychopharmacology.* **38**, 1575-1584 (2013).

Doyle, D.A. *et al.* Crystal structures of a complexed and peptide-free membrane protein–binding domain: molecular basis of peptide recognition by PDZ. *Cell* **85**, 1067-1076 (1996).

Dunham, J.H., Meyer, R.C., Garcia, E.L. & Hall, R.A. GPR37 surface expression enhancement via N-terminal truncation or protein-protein interactions. *Biochem.* **48**, 10286-10297 (2009).

Dunn, H.A. & Ferguson, S.S. PDZ protein regulation of G protein-coupled receptor trafficking and signaling pathways. *Mol. Pharmacol.* **88**, 624-639 (2015).

Emsley, P. and Cowtan, K. (2004) Coot: model-building tools for molecular graphics. *Acta. Crystallogr. D Biol. Crystallogr.* **60**, 2126-2132 (2007).

Evans, P. Scaling and assessment of data quality. *Acta. Crystallogr. D Biol. Crystallogr.* **62**, 72-82 (2006).

Fan, L.L *et al.* Alpha(1D)-adrenergic receptor insensitivity is associated with alterations in its expression and distribution in cultured vascular myocytes. *Acta. Pharmacol. Sin.* **30**, 1585-1593 (2009).

Ferguson, K.M. Structure-based view of epidermal growth factor receptor regulation. *Annu Rev Biophys*. **37**, 353-373 (2008).

Fredriksson, R., Lagerström, M.C., Lundin, L.G. & Schiöth, H.B. The G-protein-coupled receptors in the human genome form five main families. Phylogenetic analysis, paralogon groups, and fingerprints. *Mol. Pharmacol.* **63**, 1256-1272 (2003).

Fuentes, A.V., Pineda, M.D. & Venkata, K.C.N. Comprehension of top 200 prescribed drugs in the US as a resource for pharmacy teaching, training, and practice. *Pharmacy Basel.* **6,** 43 (2018).

Fukushima, Y. *et al.*Structural and functional analysis of the canine histamine H2 receptor by site-directed mutagenesis: N-glycosylation is not vital for its action. *Biochem. J.* **310**, 553-558 (1995).

Fusco, F. *et al.* α1-Blockers improve benign prostatic obstruction in men with lower urinary tract symptoms: a systematic review and meta-analysis of urodynamic studies. *Eur. Urol.* **69**, 1091-1101 (2016).

Gage, R.M., Matveeva, E.A., Whiteheart, S.W. & von Zastrow, M. Type I PDZ ligands are sufficient to promote rapid recycling of G protein-coupled receptors independent of binding to N-ethylmaleimide-sensitive factor. *J. Biol. Chem.* **280**, 3305-3313 (2005).

Garcia-Cazarin, M.L. *et al.* The alpha1D-adrenergic receptor is expressed intracellularly and coupled to increases in intracellular calcium and reactive oxygen species in human aortic smooth muscle cells. *J. Mol. Signal* **3**, 6; 10.1186/1750-2187-3-6 (2008).

Gilman, A.G. G proteins: transducers of receptor-generated signals. *Annu Rev Biochem.* **56**, 615-649 (1987).

Giovannitti, J.A., Jr, Thomas, S.M. & Crawford, J.J. Alpha-2 adrenergic receptor agonists: A review of current clinical applications. *Anesth. Prog.* **62**, 31-38 (2015).

Gonzalez de Valdivia, E., Sandén, C., Kahn, R., Olde, B. & Leeb-Lundberg, L.M.F. Human G protein-coupled receptor 30 is *N*-glycosylated and N-terminal domain asparagine 44 is required for receptor structure and activity. *Biosci. Rep.* **39**, BSR20182436; 10.1042/BSR20182436 (2019).

Grembecka, J. *et al.* The binding of the PDZ tandem of syntenin to target proteins. *Biochem. J.* **45**, 3674-3683 (2006).

Grootjans, J.J., Reekmans, G., Ceulemans, H., & David, G. Syntenin-syndecan binding requires syndecan-synteny and the co-operation of both PDZ domains of syntenin. *J. Boil. Chem.* **275**, 19933-19941 (2000).

Guillaume, J.L. *et al.* The PDZ protein mupp1 promotes Gi coupling and signaling of the Mt1 melatonin receptor. *J. Biol. Chem.* **283**, 16762-16771 (2008).

Guna, A. & Hegde, R.S. Transmembrane domain recognition during membrane protein biogenesis and quality control. *Curr. Biol.* **28**, R498-R511 (2018).

Guna, A., Volkmar, N., Christianson, J.C. & Hegde, R.S. The ER membrane protein complex is a transmembrane domain insertase. *Science* **359**, 470-473 (2018).

Hague, C., Uberti, M.A., Chen, Z., Hall, R.A. & Minneman, K.P. Cell surface expression of α_{1D}-adrenergic receptors is controlled by heterodimerization with α_{1B}-adrenergic receptors. *J. Biol. Chem.* **279,** 15541-15549 (2004).

Hague, C.*et al.* The N terminus of the human alpha1D-adrenergic receptor prevents cell surface expression. *J. Pharmacol. Exp. Ther*. **309**, 388-397 (2004).

Hakalahti, A.E. *et al.* Human beta1-adrenergic receptor is subject to constitutive and regulated N-terminal cleavage. *J. Biol. Chem.* **285**, 28850-28861 (2010).

Hall, R.A. *et al.* The β2-adrenergic receptor interacts with the Na+/H+-exchanger regulatory factor to control Na+/H+ exchange. *Nature* **392**, 626-630 (1998).

Hampel, C. *et al.* Modulation of bladder alpha1-adrenergic receptor subtype expression by bladder outlet obstruction. *J. Urol.* **167**, 1513-1521 (2002).

Harris, D.A. *et al*. Label-free dynamic mass redistribution reveals low-density, prosurvival α_{1B}-adrenergic receptors in human SW480 colon carcinoma cells. *J. Pharmacol. Exp. Ther.* **361**, 219-228 (2017).

Hawtin, S.R., Davies, A.R., Matthews, G. & Wheatley, M. Identification of the glycosylation sites utilized on the V_{1A} vasopressin receptor and assessment of their role in receptor signaling and expression. *Biochem. J.* **357**, 73-81 (2001).

Heine, H. & Weiss, M. Life stress and hypertension. *Eur Heart J*. **8**, B:45-55 (1987).

Helenius, A. How N-linked oligosaccharides affect glycoprotein folding in the endoplasmic reticulum. *Mol. Biol.Cell.* **5**, 253-265 (1994).

Hendrick, J. *et al.* The polarity protein Scribble positions DLC3 at adherens junctions to regulate Rho signaling. *J Cell Sci.* **19**, 3583 – 3596 (2016).

Hendrickson, R.C. & Raskind, M.A. Noradrenergic dysregulation in the pathophysiology of PTSD. *Exp. Neurol.* **284**, 181-195 (2016).

Hieble, J.P. *et al.* International union of pharmacology. X. Recommendation for nomenclature of α_1-adrenoceptors: consensus update. *Pharmacol. Rev.* **47**, 267-270 (1995).

Hillier, B. J., Christopherson, K. S., Prehoda, K. E., Bredt, D. S. & Lim,W.A. Unexpected modes of PDZ domain scaffolding revealed bystructure of nNOS-syntrophin complex. *Science* **284**, 812-815 (1999).

Huang, Y., Niwa, J., Sobue, G. & Breitwieser, G.E. Calcium-sensing receptor ubiquitination and degradation mediated by the E3 ubiquitin ligase dorfin. *J. Biol. Chem.* **281**, 11610-11617 (2006).

Imperiali, B. & O'Connor, S.E. Effect of *N*-linked glycosylation on glycopeptide and glycoprotein structure. *Curr. Opin. Chem. Biol.* **3**, 643-649 (1999).

Insel, P.A. Adrenergic receptors – evolving concepts and clinical implications. *N. Engl. J. Med.* **334**, 580-585 (1996).

Janezic, E.M. *et al.* Scribble co-operatively binds multiple α_{1D}-adrenergic receptor C-terminal PDZ ligands. *Sci. Rep.* **9**, 14073;10.1038/s41598-019-50671-6 (2019).

Jegla, T.J., Zmasek, C.M., Batalov, S. & Nayak, S.K. Evolution of the human ion channel set. *Comb Chem High Throughput Screen* **12**, 2-23 (2009).

Jensen, B.C., Swigart, P.M. & Simpson, P.C. Ten commercial antibodies for alpha-1-adrenergic receptor subtypes are nonspecific. *Naunyn Schmiedebergs Arch Pharmacol*. **379**, 409-412 (2009).

Kabsch, W. XDS. *Acta Crystallogr. D Biol. Crystallogr.* **66**, 125-132 (2010).

Kallay, L.M., McNickle, A., Brennwald, P.J., Hubbard, A.L. & Braiterman, L.T. Scribble associates with two polarity proteins, Lgl2 and Vangl2, via distinct molecular domains. *J. Cell. Biochem.* **99**, 647-664 (2006).

Kimura, T., *et al.* The role of N-terminal glycosylation in the human oxytocin receptor. *Mol. Hum Reprod.* **3**, 957-963 (1997).

Kojima, Y. *et al.* Up-regulation of α1a and α1d-adrenoceptors in the prostate by administration of subtype selective α1-adrenceptor antagonist tamsulosin in patients with benign prostatic hyperplasia. *J. Urol.* **186**, 1530-1536 (2011).

Kopito, R.R. ER quality control: The cytoplasmic connection. *Cell* **88**, 427-430 (1997).

Kornfeld, K., Reitman, M.L. & Kornfeld, R. The carbohydrate-binding specificity of pea and lentil lectins: Fucose is an important determinant. *J. Biol. Chem.* **256**, 6633-6640 (1981).

Kountz, T.S. *et al.* Endogenous N-terminal domain cleavage modulates α_{1D}-adrenergic receptor pharmacodynamics. *J. Biol. Chem.* **291**, 8210-18221(2016).

Lackman, J.J., Markkanen, P.M.H., Hogue, M., Bouovier, M. & Petäjä-Repo, U.E. *N*-glycan-dependent and –independent quality control of human δ opioid receptor N-terminal variants. *J. Biol. Chem.* **289**, 17830-17842 (2014).

Lanctôt, P.M., Leclerc, P.C., Escher, E., Leduc, R. & Guillemette, G. Role of N-glycosylation in the expression and functional properties of human AT_1 receptor. *Biochem.* **38**, 8621-8627 (1999).

Lander, E.S. *et al.* Initial sequencing and analysis of the human genome. *Nature* **409**, 860-921 (2001).

Langeberg, L.K. & Scott, J.D. Signalling scaffolds and local organizations of cellular behavior. *Nat Rev Mol Cell Biol* **16**, 232-244 (2015).

Langerström, M.C. & Schiöth, H.B. Structural diversity of G protein-coupled receptors and significance for drug discovery. *Nat Rev Drug Discov.* **7**, 339-357 (2008).

Lauffer, B.E. *et al.* SNX27 mediates PDZ-directed sorting from endosomes to the plasma membrane. *J. Cell. Biol.* **190**, 565-574 (2010).

Lee, S., Fa, S., Makarova, O., Straight, S. & Margolis, B. A novel and conserved protein-protein interaction domain of mammalian Lin-2/CASK binds and recruits SAP97 to the lateral surface of epithelia. *Mole. Cell. Biol.* **22**, 1778-1791 (2002).

Lee, W.H. *et al*. ZLcOO2, a putative small-molecule inhibitor of nNOS interaction with NOS1AP, suppresses inflammatory nociception and chemotherapy-induced neuropathic pain and synergizes with paclitaxel to reduce tumor cell viability. *Mol. Pain*. **14**, 1-17 (2018a)

Lee, W.H. *et al.* Disruption of nNOS-NOS1AP protein-protein interactions suppresses neuropathic pain in mice. *Pain*. **159**, 849-863 (2018b).

Letunic, I., Doerks, T. & Bork, P. SMART 7: recent updates to the protein domain annotation resource. *Nucleic Acids Res.* **40**, D302-305 (2012).

Li, C. *et al.* The GTPase Rab43 controls the anterograde ER-Golgi trafficking and sorting of GPCRs. *Cell Rep.* **21**, 1089-1101 (2017).

Li, L.L. *et al.* The nNOS-p38 MAPK pathway is mediated by NOS1AP during neuronal death. *J. Neurosci*. **33,** 8185-8201 (2013).

Lim, K.Y.B., Gödde, N.J., Humbert, P.O. & Kvansakul, M. Structural basis for the differential interaction of Scribble PDZ domains with the guanine nucleotide exchange factor β-PIX. *J. Biol. Chem.* **292**, 20425-20436 (2017).

Liu, J. *et al.* The association of DNA methylation and brain volume in healthy individuals and schizophrenia patients. *Schizophr. Res.* **169**, 447-452 (2015).

London, N., Raveh, B., Cohen, E., Fathi, G. & Schueler-Furman, O. Rosetta FlexPepDock web server—high resolution modeling of peptide–protein interactions. *Nucleic Acids Res.* **39**, W249-W253 (2011).

Long, J.F. *et al.* Supramodular structure and synergistic target binding of the N-terminal tandem PDZ domains of PSD-95. *J. Mol. Biol.* **327**, 203-214 (2003).

Lopez-Gimenez, J.F., Canals, M., Pediani, J.D. & Milligan, G. The α_{1b}-adrenoceptor exists as a higher-order oligomer: Effective oligomerization is required for receptor maturation, surface delivery, and function. *Mol. Pharmacol.* **71**, 1015-1029 (2007).

Lyssand, J.S. *et al.* Blood pressure is regulated by an α_{1D}-adrenergic receptor/dystrophin signalosome. *J. Biol. Chem.* **283**, 18792-18800 (2008).

Lyssand, J.S. *et al.* α-Dystrobrevin-1 recruits α-catulin to the α_{1D}-adrenergic receptor/dystrophin-associated protein complex signalosome. *Proc. Natl. Acad. Sci. U.S.A.* **107**, 21854-21859 (2010).

Lyssand, J.S., Lee, K.S., DeFino, M., Adams, M.E. & Hague, C. Syntrophin isoforms play specific functional roles in the α_{1D}-adrenergic receptor/DAPC signalosome. *Biochem. Biophys. Res. Commun.* **412**, 596-601 (2011).

Mamonova, T. *et al.* Origins of PDZ binding specificity. A computational and experimental study using NHERF1 and the parathyroid hormone receptor. *Biochemistry* **56**, 2584-2593 (2017).

Manjunath, G.P., Ramanujam, P.L. & Galande, S. Structure function relations in PDZ-domain-containing proteins: Implications for protein networks in cellular signaling. *J. Biosci.* **43**, 155-171 (2018).

Marchese, A., Paing, M.M., Temple, B.R. & Trejo, J. G protein-coupled receptor sorting to endosomes and lysosomes. *Annu Rev Pharmacol Toxicol.* **48**, 601-629 (2008).

Markkanen, P.M. & Petäjä-Repo, U.E. N-glycan-mediated quality control in the endoplasmic reticulum is required for the expression of correctly folded delta-opioid receptors at the cell surface. *J. Biol. Chem.* **283**, 29086-29098 (2008).

Mathew, D. *et al.* Recruitment of scribble to the synaptic scaffolding complex requires GUK-holder, a novel Dlg binding protein. *Curr. Biol.* **12**, 531-539 (2002).

Mattila, S.O., Tuusa, J.T. & Petäjä-Repo, U.E. The Parkinson's-diseas-associated receptor GPR37 undergoes metalloproteinase-mediated N-terminal cleavage and ectodomain shedding. *J. Cell Sci.* **129**, 1366-1377 (2016).

McCoy, A.J. *et al.* Phaser crystallographic software. *J. Appl. Crystallogr.* **40**, 658-674 (2007)

McEwan, I.J. Nuclear receptors: one big family. *Methods Mol Biol.* **505**, 3-18 (2009).

Miller, J.L. Doxazosin dropped from ALLHAT study. *Am. J. Health Syst. Pharm.* **57**, 718 (2011).

Monné, M., Gaffvelin, G., Nilsson, R. & von Heijne G. N-tail translocation in a eukaryotic polytopic membrane protein. *Eur. J. Biochem.* **263**, 264-269 (1999).

Monné, M., Hessa, T., Thissen, L. & von Heijne G. Competition between neighboring topogenic signals during membrane protein insertion into the ER. *FEBS J.* **272**, 28-36 (2005).

Nakagawa, T. *et al. N*-glycan-dependent cell-surface expression of the $P2Y_2$ receptor and *N*-glycan-independent distribution of lipid rafts. *Biochem. Biophys. Res. Commun.* **485**, 427-431 (2007).

Nalepa, I., Kreiner, G., Bielawski, A., Rafa-Zablocka, K. & Roman, A. α1-adrenergic receptor subtypes in the central nervous system: insights from genetically engineered mouse models. *Pharmacol. Rep.* **65**, 1489-1497 (2013).

Neal, S. *et al.* The Dfm1 Derlin is required for ERAD retrotranslocation of integral membrane porteins. *Mol. Cell* **69**, 306-320 (2018).

Nilsson, I.M., Witt, S., Kiefer, H., Mingarro, I. & von Heijne, G. Distant downstream sequence determinants can control N-tail translocation during protein insertion into the endoplasmic reticulum membrane. *J. Biol. Chem.* **275**, 6207-6213 (2000).

Nordström, R. & Andersson, H. Amino-terminal processing of the human cannabinoid receptor 1. *J. Recept. Signal Transduct. Res.* **26**, 259-267 (2006).

Öjemalm, K., Halling, K., Nilsson, I.M. & von Heijne, G. Orientational preferences of neighboring helices can drive ER insertion of a marginally hydrophobic transmembrane helix. *Mole. Cell* **45**, 529-540 (2012).

Olson, V.G. *et al.* The role of norepinephrine in differential response to stress in an animal model of posttraumatic stress disorder. *Biol. Psychiatry* **70**, 441-448 (2011).

Overington, J.P., Al-Lazikani, B. & Hopkins, A.L. How many drug targets are there? *Nat. Rev. Drug Discov.* **5**, 993-996 (2006).

Palczewski, K. *et al.* Crystal structure of rhodopsin: A g protein-coupled receptor. *Science* **289**, 739-745 (2000).

Perez, D.M. & Doze, V.A. Cardiac and neuroprotection regulated by α_1-adrenergic receptor subtypes. *J. Recept Signal Transduct Res* **31**, 98-110 (2011).

Perez, D.M., Piascik, M.T. & Graham, R.M. Soluiton-phase library screening for the identification of rare clones: isolation of an α_{1D}-adrenergic receptor cDNA. *Mol. Pharmacol*. **40**, 876-883 (1991).

Petäjä-Repo, U.E., Hogue, M., Laperrière, A., Walker, P. & Bouvier, M. Export from the endoplasmic reticulum represents the limiting step in the maturation and cell surface expression of the human δ opioid receptor. *J. Biol. Chem.* **278**, 13727-13736 (2000).

Petäjä-Repo, U.E *et al.* Newly synthesized human δ opioid receptors retained in the endoplasmic reticulum are retrotranslocated to the cytosol, deglycosylated, ubiquitinated, and degraded by the proteasome. *J. Biol. Chem.* **276**, 4416-4423 (2001).

Petrovska, R., Kapa, I., Klovins, J., Schiöth, H.B. & Uhlén, S. Addition of a signal peptide sequence to the α_{1D}-adrenoceptor gene increases the density of receptors, as determined by [^{3}H]-prazosin binding in the membrane. *Br. J. Pharmacol.* **144**, 651-659 (2005).

Piascik, M.T. & Perez, D.M. α1-Adrenergic receptors: new insights and directions. *J. Pharmacol. Exp. Ther.* **298**, 403-410 (2001).

Piascik, M.T. *et al.* The specific contribution of the novel alpha-1D adrenoceptor to the contraction of the vascular smooth muscle. *J. Pharmacol. Exp. Ther.* **275**, 1583-1589 (1995).

Piguel, N.H. *et al.* Scribble1/AP2 complex coordinates NMDA receptor endocytic recycling. *Cell Rep.* **9**, 712-727 (2014).

Pupo, A.S., Uberti, M.A. & Minneman, K.P. N-terminal truncation of human α_{1D}-adrenoceptors increases expression of binding sites but not protein. *Eur. J. Pharmacol.* **462**, 1-8 (2003).

Ramussen, S.G. *et al.* Structure of a nanobody-stabilized active state of the β_2 adrenoceptor. *Nature* **469**, 175-180 (2011a).

Rasmussen, S.G. *et al.* Crystal structure of the β_2 adrenergic receptor-Gs protein complex. *Nature* **477**, 549-555 (2011b).

Raskind, M.A. *et al*. A trial of prazosin for combat trauma PTSD with nightmares in active-duty soldiers returned from Iraq and Afghanistan. *Am. J. Psychiatry* **170**, 1003-1010 (2013).

Raskind, M.A. *et al.* Trial of prazosin for post-traumatic stress disorder in military veterans. *N. Engl. J. Med.* **378**, 507-517 (2018).

Raveh, B., London, N. & Schueler-Furman, O. Sub-angstrom modeling of complexes between flexible peptides and globular proteins. *Proteins* **78**, 2029-2040 (2010).

Reid, J.L. Central alpha 2 receptors and the regulation of blood pressure in humans. *J Cardiovasc Pharmacol.* **7**, S45-S50 (1985).

Ren, J. *et al.* Interdomain interface-mediated target recognition by the Scribble PDZ34 supramodule. *Biochem. J.* **468**, 133-144 (2015).

Richier, L. *et al.* NOS1AP associates with Scribble and regulates dendritic spine development. *J. Neurosci.* **30**, 4796-4805 (2010).

Ring, A.M. *et al.* Adrenaline-activated structure of the β_2-adreneroceptor stabilized by an engineered nanobody. *Nature* **502**, 575-579 (2013).

Ritter, S.L. & Hall, R.A. Fine-tuning of GPCR activity by receptor-interacting proteins. *Nat. Rev. Mol. Cell Biol.* **10**, 819-830 (2009).

Romero, G., von Zastrow, M., & Friedman, P.A. Role of PDZ proteins in regulating trafficking, signaling, and function of GPCRs: means, motif, and opportunity. *Adv. Pharmacol.* **62**, 279-314 (2011).

Sawutz, D.G., Lanier, S.M., Warren, C.D. & Graham, R.M. Glycosylation of the mammalian α_1-adrenergic receptor by complex type N-linked oligosaccharides. *Mol. Pharmacol*. **32** 565-571 (1987).

Schindelin, J. *et al.* Fiji: an open-source platform for biological-image analysis. *Nat. Methods* **9**, 676-682 (2012).

Schultz, C. & Köhn, M. Simultaneous protein tagging in two colors. *Chem. Biol.* **15**, 91-92 (2008).

Sever, P.S. Alpha 1-blockers in hypertension. *Curr. Med. Res. Opin*. **15(2)**, 95-103 (1999).

Shukla, A.K., Xiao, K. & Lefkowitz, R.J. Emerging paradigms of β-arrestin-dependent seven transmembrane receptor signaling. *Trends Biochem. Sci.* 36, 457-469 (2011).

Snider, G.L. & Laguarda, R. Albuterol and isoproterenol aerosols. A controlled study of duration of effect in asthmatic patients. *JAMA* **221**, 682-685 (1972).

Songyang, Z. *et al.* Recognition of unique carboxyl-terminal motifs by distinct PDZ domains. *Science* **275**, 73-77 (1997).

Sriram, K. & Insel, P.A. G protein-coupled receptors as targets for approved drug: How many targets and how many drugs? *Mol. Pharmacol.* **93**, 251-258 (2018).

Stephens, R. *et al.* The Scribble cell polarity module in the regulation of cell signaling in tissue development and tumorigenesis. *J. Mol. Biol.* **430**, 3585-3612 (2018).

Stricker, N.L. *et al.* PDZ domain of neuronal nitric oxide synthase recognizes novel C-terminal peptide sequences. *Nat. Biotechnol.* **15**, 336-342 (1997).

Stucke, V.M., Timmerman, E., Vandekerckhove, J., Gevaert, K. & Hall, A. The MAGUK protein MPP7 binds to the polarity protein hDlg1 and facilitates epithelial tight junction formation. *Mol. Biol. Cell* **18**, 1744-1755 (2007).

Sugama, S. *et al.* Stress-induced microglial activation occurs through β-adrenergic receptor: noradrenaline as a key neurotransmitter in microglial activation. *J Neuroinflammation.* **16**, 266; 10.1186/s12974-019-1632-z (2019).

Suzuki, N., Hajicek, N. & Kozasa, T. Regulation and physiological functions of G12/13-mediated signaling pathways. *Neurosignals* **17**, 55-70 (2009).

Takizawa, S. *et al.* Human scribble, a novel tumor suppressor identified as a target of high-risk HPV E6 for ubiquitin-mediated degradation, interacts with adenomatous polyposis coli. *Genes Cells.* **11**, 453-464 (2006).

Tanoue, A. *et al.* The α_{1D}-adrenergic receptor directly regulates atrial blood pressure via vasoconstriction. *J. Clin. Invest*. **109**, 765-775 (2002).

Tansky, M.F., Pothoulakis, C. & Leeman, S.E. Functional consequences of alteration of N-linked glycosylation sites on the neurokinin 1 receptor. *Proc. Natl. Acad. Sci. U.S.A.* **104**, 10691-10696.

The ALLHAT Officers and Coordinators for the ALLHAT Collaborative Research Group. Major outcomes in high-risk hypertensive patients randomized to angiotensin-converting enzyme inhibitor or calcium channel blocker vs diuretic: The Antihypertensive and Lipid-Lowering Treatment to Prevent Heart Attack Trial (ALLHAT). *JAMA* **288**, 2981-2997 (2002).

Tsunoda, K., Douge, K., Ming-Chang, T. & Watanabe, T. Experimental studies on stress hormones at the time of sudden death (II) – Differences is adrenocortical hormone levels of cardiac arrest-preceding type and apnea preceding type sudden death under cerebral ischemia or aortic stenosis. *Nihon Hoigaku Zasshi.* **43**, 453-459 (1989).

Tsunoda, S. *et al.* A multivalent PDZ-domain protein assembles signaling complexes in a G-protein-coupled cascade. *Nature* **388**, 243-249 (1997).

Uberti, M.A., Hague, C., Oller, H., Minneman, K.P., & Hall, R.A. Heterodimerization with beta2-adrenergic receptors promotes surface expression and functional activity of alpha1D-adrenergic receptors. *J. Pharmacol. Exp. Ther.* **313**, 16-23 (2005).

Van Craenenbroeck, K. *et al.* Folding efficiency is rate-limiting in dopamine D4 receptor biogenesis. *J. Biol. Chem.* **280**, 19350-19357 (2005).

Vicentic, A., Robeva, A., Rogge, G., Uberti, M. & Minneman, K.P. Biochemisty and pharmacology of epitope-tagged alpha(1)-adrenergic receptor subtypes. *J. Pharmacol. Exp. Ther.* **302**, 58-65 (2002).

Wacker, D. *et al.* Crystal structure of an LSD-bound human serotonin receptor. *Cell* **168**, 339-341 (2017)

Walden, P.D., Gerardi, C. & Lepor, H. Localization and expression of the α_{1A}, α_{1B} and α_{1D}-adrenoceptors in hyperplastic and non-hyperplastic human prostate. *J. Urol.* **161**, 635-640 (1999).

Wallin, E. & von Heijne, G. Properties of N-terminal tail in G-protein coupled receptors: a statistical study. *Protein Eng.* **8**, 693-698 (1995).

Webel, R., Menon, I., O'Tousa, J.E. & Colley, N.J. Role of asparagine-linked oligosaccharides in rhodopsin maturation and association with its molecular chaperone, NinaA. *J. Biol. Chem.* **275**, 24752-24759 (2000)

Wei, Z. *et al.* Specific TBC domain-containing proteins control the ER-Golgi plasma membrane trafficking of GPCRs. *Cell Rep.* **28**, 554-566 (2019).

Wheatley, M. *et al.* Lifting the lid on GPCRs: the role of extracellular loops. *Br J Pharmacol.* **165**, 1688-1703 (2012).

Winn, M.D. *et al.* Overview of the CCP4 suite and current developments. *Acta. Crystallogr. D Biol. Crystallogr.* **67**, 235-242 (2011).

Wu, G. Regulation of post-Golgi traffic of G protein-coupled receptors. *Subcell. Biochem.* **63**, 83-95 (2012).

Xu, J. *et al.* β1-adrenergic receptor association with the synaptic scaffolding protein membrane-associated guanylate kinase inverted-2 (MAGI-2). *J. Biol. Chem.* **276**, 41310-41317 (2001).

Zheng, W. *et al.* An interaction between Scribble and the NADPH oxidase complex controls M1 macrophage polarization and function. *Nat. Cell Biol.* **18**, 1244-1252 (2016).

Zhou, L. *et al.* Treatment of cerebral ischemia by disrupting ischemia-induced interaction of nNOS with PSD-95. *Nat. Med.* **16**, 1439-1443 (2010).

Zhu, J. Phosphorylation-dependent interaction between tumor suppressors Dlg and Lgl. *Cell Res.* **24**, 451-463 (2014).

Curriculum Vitae

EDUCATION

University of Washington, PhD 2016-2020
Pharmacology
Advisor: Dr. Chris Hague

Thesis: "Elucidating unique structural features that regulate α_{1D}-adrenergic receptor trafficking and function"

Delaware State University, MS 2014-2016
Molecular and Cellular Neuroscience
Advisor: Dr. Y. Hwan Kim
Thesis: "Synergistic Damage of Commercially Available Environmental Toxins: A Link to Parkinson's Disease"

University of Arizona, BS 2007-2013
Neuroscience and Cognitive Science
Minors in Mathematics and Chemistry

RESEARCH EXPERIENCE

University of Washington, Chris Hague Lab January 2017 – June 2020
Graduate Student Researcher – Utilizing a combination of *in vitro* and *in situ* biochemical and biophysical assays to determine how accessory protein complexes affect pharmacodynamics of the α_{1D}-adrenergic receptor. In part, this involved developing a novel *in situ* GST-pulldown assay to determine protein complex stoichiometry, as well using structure-based approaches to pinpoint unique determinants of PDZ protein:PDZ ligand interactions. Finally, I used pharmacological and cell-surface assays to identify the functional role of α_{1D}-adrenergic receptor:Scribble interaction. Additionally, I utilized lectin purification, sucrose density centrifugation, and dynamic mass redistribution to determine the role of N-glycosylation on α_{1D}-adrenergic receptor trafficking and function.

University of Washington, Ning Zheng Lab September – December 2016
Rotation Student – During my rotation in the Zheng Lab, I purified, crystalized, and determined the structure of the plant protein, cryptochrome 2.

Delaware State University, Y. Hwan Kim Lab August 2014 – May 2016
Graduate Student Researcher - My thesis research found that combinations of commercially available herbicides work in synergy to increase toxicity of dopaminergic-like mammalian cells *in vitro*, as well as determined a potential mechanism of action. I also used a mouse model to measure changes in motor behavior and dopaminergic cell viability via immunohistochemistry. Non-thesis related projects involved uncovering the role of DAT SUMOlyation in MPTP induced dopaminergic cell death, as well as testing novel compounds to prevent cell death.

University of Arizona, Jean-Marc Fellous Lab May 2013 – July 2014
Laboratory Manager - I worked cross-functionally with external review agencies (IACUC) to ensure the lab was meeting strict standards, assisted other researchers as needed, trained new lab members, performed trans-cranial surgeries, and acted as liaison between lab members and lab head. I was also responsible for leading my own

research project exploring the behavioral effect of long-term, sub-cutaneous oxytocin in a rodent model of post-traumatic stress disorder.

University of Arizona, Jean-Marc Fellous Lab July 2012 – May 2013

Undergraduate Researcher – Using a rodent model of post-traumatic stress disorder, I led a research project exploring the behavioral effects of acute oxytocin after trauma. Additionally, I analyzed electrophysiological data from behaving rodents using Spike2 software.

AWARDS AND FUNDING

NIMGS Award Number T32GM007750 July 2018 – Present

Delaware INBRE via NIMGS P20GM103446 August 2014 – May 2016

Undergraduate Research Mentor Nominee 2018-2019

PUBLICATIONS

Janezic EM, Lauer SML, Williams RG, Chungyoun M, Lee KS, Navaluna E, Lau HT, Ong SE, Hague C. N-glycosylation of α_{1D}-adrenergic recptor N-terminal domain is required for correct trafficking, function, and biogenesis. *Sci Rep* **10**, 7209 (2020). DOI: 10.1038/s41598-020-64102-4

Janezic EM, Harris DA, Dinh D, Lee KS, Stewart A, Hinds TR, Hsu PL, Zheng N, Hague C. Scribble co-operatively binds multiple α_{1D}-adrenergic receptor C-terminal PDZ ligands. *Sci Rep* **9**, 14073 (2019). DOI: 10.1038/s41598-019-50671-6

Cartier E, Garcia-Olivares J, Janezic EM, Viana J, Moore M, Lin M, Caplan J, Torres G, Kim YH. The SUMO-conjugase Ubc9 prevents the degradation of the Dopamine Transporter, enhacing its cell surface level and dopamine uptake. *Front Cell Neurosci* **13**, 35 (2019). DOI: 10.3389/fncel.2019.00035

Janezic EM, Caviness JE, Davis XD, Kanda SG, Kim YH. Commercially Available Pesticides Cause Synergistic or Additive Damages in Dopaminergic Cells: Relevance for Parkinson's Disease Pathology. *Annuals of Neurodegenerative Disorders* **1**, 1010-1019 (2016).

Janezic EM, Uppalapati S, Nagl S, Contreras M, French ED, Fellous JM. Beneficial effects of chronic oxytocin administration and social co-housing in a rodent model of post-traumatic stress disorder. *Behav Pharmacol* **27**, 704-717 (2016). DOI: 10.1097/FBP.0000000000000270

POSTER PRESENTATIONS

Janezic EM, Caviness JE, Kanda SG, Kim YH, *Synergistic Damage of Commercially Available Environmental Toxins in Parkinson's Disease Models*. Poster Presented at: Society for Neuroscience; 2015 Oct 17-21; Chicago, IL.

Caviness JE*, Janezic EM*, Poppana S, Lawal H, Pesyan A, Kim YH, *AurimMed's AMP-X-0079: A Potential Therapeutic for Parkinson's Disease.* Poster Presented at: Society for Neuroscience; 2015 Oct 17-21; Chicago, IL. (* = co-first author)

Cartier E, Garcia-Olivares J, Lin M, Janezic EM, Torres G, and Kim YH. *The Ubc9 SUMO conjugase enhances the function of the dopamine transporter by decreasing its ubiquitination and further degradation.* Poster Presented at: Society for Neuroscience; 2015 Oct 17-21; Chicago, IL.

Janezic EM, Nagl S, Uppalapati S, French E, Fellous JM, *Oxytocin and Social Bonding as Treatments in a Rodent Model of Post-Traumatic Stress Disorder*. Poster Presented at: Society for Neuroscience; 2014 Nov 15-19; Washington DC.

White JK, Janezic EM, Lines J, Fellous JM, *Consequences of posttraumatic stress on the reconsolidation of neutral memories: a rodent model.* Poster Presented at: UBRP 25th Annual Poster Showcase; 25 Jan 2014, Tucson, AZ.

Janezic EM, LaHood RP, Stidd D, Langevin JP, French E, Fellous JM. *Pharmacological and Deep Brain Stimulation Treatments in a Rodent Model of Post-Traumatic Stress Disorder.* Poster Presented at: Society for Neuroscience; 2013 Nov 9-13; San Diego, CA.

INVITED TALKS

Winter Conference on Brain Research, Snowmass, CO 01/28 – 02/02/2019

TEACHING AND OTHER EXPERIENCES

Student Mentor

Robert George Williams (Undergraduate – UW) July 2017- Current
Michael Chungyoun (Undergraduate – UW) May 2018 – May 2019
Sophia Lauer (Rotation Student – UW) January 2019 – March 2019
Diana Dinh (Undergraduate – UW) January 2017 – May 2018

Pharmacology Student Association Representative 2017 – 2018

Acted as liaison between students and the department chair to resolve student issues and organize student recruitment.

Teaching Assistant Autumn 2017 – Winter 2018

I led a weekly review session which included writing and administering quizzes, grading short answer test questions, and preparing teaching material covering various topics in pharmacology.

STEM Preparatory Academy Mentor Summer 2017 and Summer 2018

I trained and mentored under-represented high school juniors in molecular biology techniques and science writing.

Student Preceptor Spring 2013

I led study sessions and wrote questions for tests in “Issues and Themes in Cognitive Science”.